Nanostructuring by Templated Synthesis of Nanowires and Controlled Crystallization of Calcium Phosphate on Self-Assembled Monolayers

Dissertation

zur

Erlangung des Grades

„Doktor der Naturwissenschaften”

am Fachbereich Chemie, Pharmazie und Geowissenschaften

der Johannes-Gutenberg-Universität in Mainz

Andreas Reiber

geboren in Hamm/Westfalen

Mainz 2005

Tag der mündlichen Prüfung: 22. Juli 2005

Die vorliegende Arbeit wurde in der Zeit von Februar 2002 bis Mai 2005 am Institut für Anorganische und Analytische Chemie der Johannes-Gutenberg-Universität in Mainz angefertigt.

Dedicated to my family

Der Natur sind viele Dinge unmöglich.

Doch was sie tun kann, leistet sie meist überraschend gut.

Stephan Jay Gould

Table of Contents

1. Introduction

During the last two decades miniaturization became a general aim of development in science and technology. One of the major impacts of this field of research is the electronic industry, which made a great effort especially in the design and production of new, efficient and smaller processors and devices leading to increasingly powerful computers. Although the electronics is a main field of interest, it is not the only one. Nearly every scientific or technological area like chemistry, material science or engineering has got interest in miniaturization and all the different methods and techniques which are used for this purpose are summarized under the generic name of nanotechnology. The term „nanotechnology“ was the subject of a long discussion about the meaning of it and it can be concluded that it refers to structures in the nanometer size range which show at least in one dimension specific size-dependent properties which include magnetic, mechanic, electronic, optical, thermodynamic and thermal features [1]. At this size-range the properties of small particles depend on quantum effects like the wave character of electrons, which does not have any equivalence in the macroscopic world (Figure 1.1).

This Ph.D. thesis is divided into two parts. Both parts address synthesis, functionalization and manipulation of material at nanoscale. The first part deals with the organization of metal nanoparticles into 1-dimensional structure to obtain nanowire like structures. The second part of this work is an investigation of the crystallization behaviour of calcium phosphate on self-assembled monolayers in the presence of proteins as additives to elucidate the nucleation and crystallization process of this biomineral.

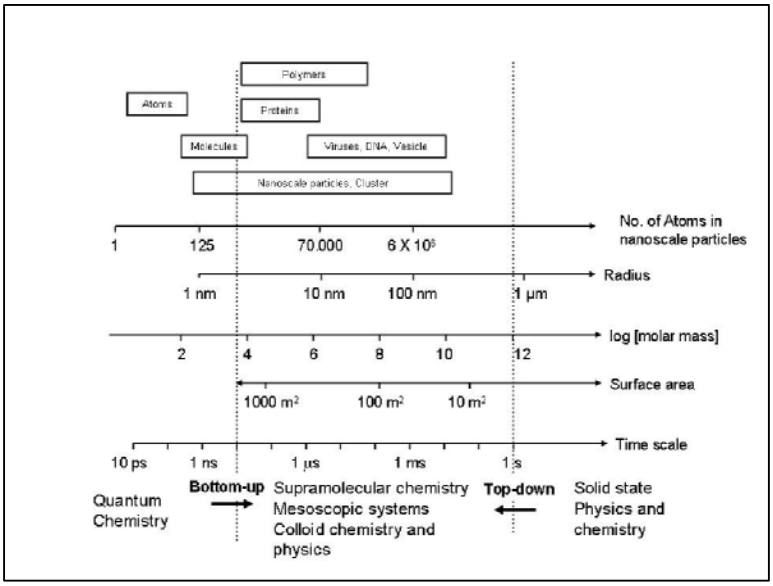

Figure 1.1: Relationship of chemistry, nanoparticles and condensed matter physics

The miniaturization without the development of sensitive analytical instruments would be unthinkable. The most important instruments for visual analysis are the different types of microscopes developed until today. It started with the construction of the first scanning

electron microscope by Max Knoll and Ernst Ruska in 1931 with a resolution of 50 nm, leading to a wide range of microscopes like the High Resolution Scanning Electron Microscope (HRSEM), the High Resolution Transmission Electron Microscope (HRTEM) with a resolution of 1-2 nm and 0,1 nm resp., along with different types of scanning probe microscopes which can reach a resolution down to the atomic size under certain circumstances [2].

The nanoscale length is an intermediate between the traditional realms of synthetic chemistry and Very Large Scale Integrated Circuit (VLSI) lithographic processing as employed in electronics. A wide range of different techniques for nanostructuring are available but they can be divided in two different main approaches. First being the "top-down"-approach which predominantly comprises physical methods like lithography with electron beam or x-ray and scan probe methods like tunnelling, force, and near-field optical microscopes to create and explore nanometer structures. Using these top-down techniques it is difficult to produce structures smaller than 200 nm. The second, "bottom-up"-approach, develops chemical synthetic self-assembly methods to create and explore such structures. In favourable cases, high quality nanocrystals with controlled surfaces can be made in gram amounts. The limit of this approach ranges from 2 to 20 nm. There are mainly two building blocks or molecules to bridge the gap between 20 and 200 nm. These are bio molecular components like proteins or nucleic acids and colloidal metal or metal chalcogenide nanoparticles or nanoclusters which can be used for further arrangement and interlinking in this size scale.

Full-shell Clusters	Total Number of Atoms	Surface Atoms (%)
1 Shell	13	92
2 Shell	55	76
3 Shell	147	63
4 Shell	309	52
5 Shell	561	45
6 Shell	1415	35

Figure 1.2: The relation between the total number of atoms in full shell clusters and the percentage of surface atoms

Though there are a lot of similarities between the theoretical background and the properties and arrangements of colloidal nanoparticles, a restriction to metallic especially, gold nanoparticles have to be made.

Metallic nanoparticles are interesting species due to their distinct properties in comparison to the bulk material. There are mainly two different characteristic effects that influence the properties of nanoparticles. One is the surface effect of the particles and the other is the volume effect. The amount of surface atoms increases with decrease in particle size (Figure

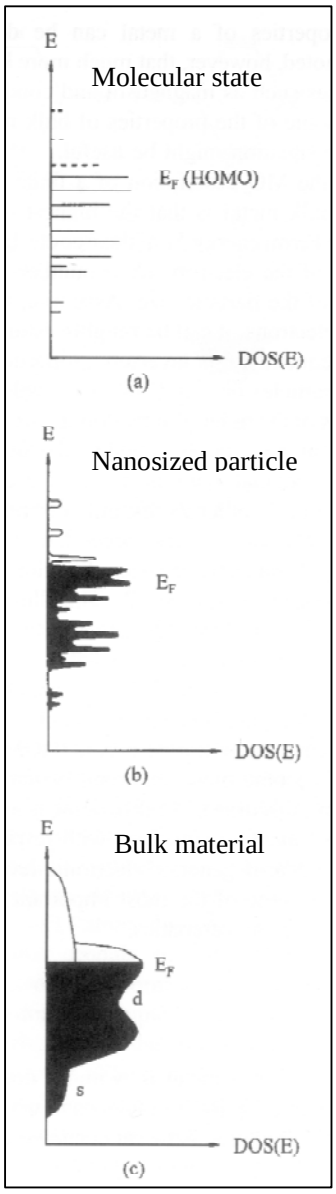

Figure 1.3: Formation of band structures in different sized gold (DOS = density of state, EF = Fermi energy)

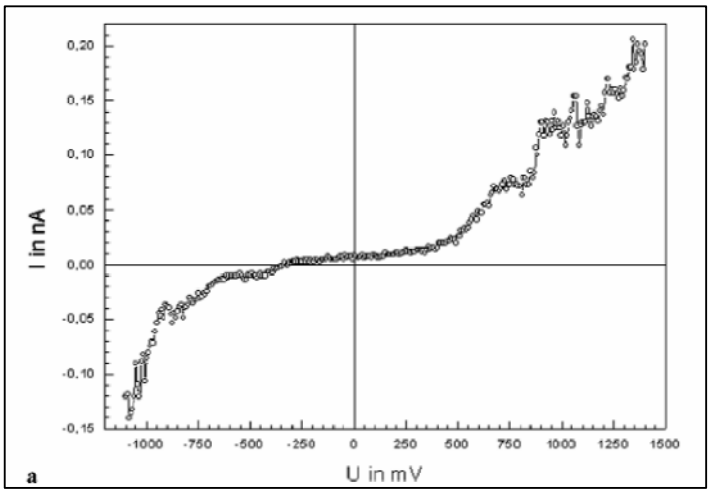

Figure 1.4: Single-electron tunnelling through a ligand-stabilized Au_{55} cluster (core diameter: 1,4 nm) at room temperature, showing a distinct Coulomb blockade

1.2). This means that the smaller the nanoparticles are the bigger are their specific surface area accompanied with a high surface energy rendering the nanoparticles highly reactive. For that reason metallic nanoparticles are ideal for heterogeneous catalysis. The reactivity of metallic nanoparticles is that high that a stabilisation by a protective shell of ligand molecules is necessary to inhibit the agglomeration of nanoparticles resulting in the bulk material. The ligation effect is a surface specific effect. It can be shown, that the inner atoms of the protected nanoparticles have the same atomic arrangement as that of a small part of the crystalline bulk material. Only the surface area of the nanoparticle is slightly disordered. Secondly, in metallic nanoparticles only a small amount of atoms are found which means that the number of electrons in comparison to the bulk material significantly decreases. Hence, a transition between the continuous band structure in the solid state and discrete energy levels in a single metal atom is observed. This volume effect causes distinct properties in the area of optoelectronic and magnetic behaviour (Figure 1.3) [3]. A

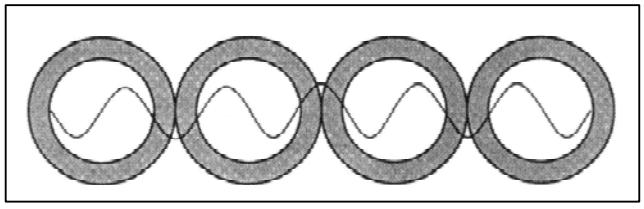

Figure 1.5: Idealized cluster wire with tunnelling conditions

conductivity measurement on a single 17 nm Pd nanoparticle shows behaviour of a good conductor at 295 K and is in accordance with Ohm's law i.e. a linear relationship between I and U. At 4,2 K its behaviour is comparable to that of a quantum dot showing a single electron transport [4].

Compared with the transportation of 10^4 electrons at present which is required to switch a silicon-based transistor, the one-electron switch being made possible by use of such quantum dots would revolutionize computer techniques. To make quantum size behaviours of small metal particles available at room temperature one has to reduce their size, as the capacitance C of the particle depends directly on their diameter. Indeed, the gold cluster compound $Au_{55}(PPh_3)_{12}Cl_6$ with a core diameter of about 1,7 nm shows typical Coulomb blockade even at room temperature (Figure 1.4) [5]. In addition to the single colloid experiment it was shown in impedance measurements with three-dimensional collectives of the colloids that due to extreme small size of these particles, discrete energy levels are formed and that exist an electronic conductivity through many clusters in a row by tunnelling processes between them through the ligand shell, leading to electronic intercluster bands by resonant tunnelling (Figure 1.5) [6]. Owing to the intercluster band structure, the electron is one-dimensionally delocalized and should therefore conduct electrons without resistance. For that reason many working groups all over the world try to achieve simple and easily reproducible one-, two- or three-dimensional arrangements of quantum dots [7].

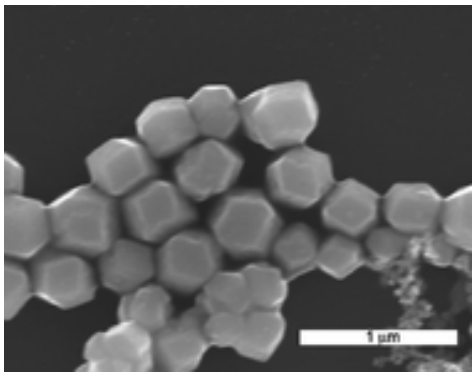

Figure 1.6: Microcrystals of bcc-structured Au_{55} clusters

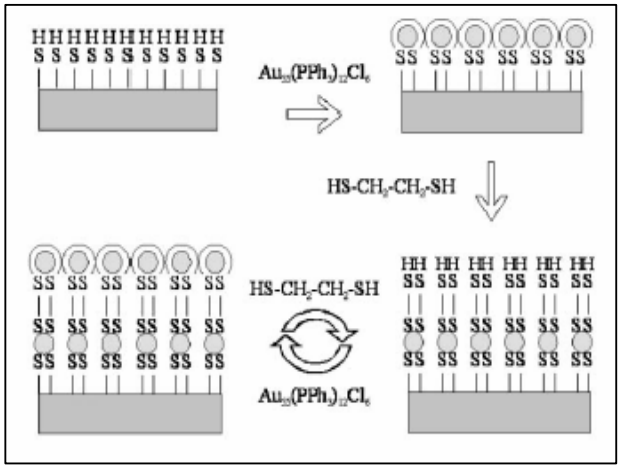

Figure 1.7: Layer-by-layer formation with linking dithiols

A three-dimensional arrangement of nanoparticles means the crystallization of quantum dots. This can often be achieved by evaporation of a solvent of the colloidal solution and was shown with nanoparticles leading to micrometer sized micro crystals like that of $Au_{55}(PPh_3)_{12}Cl_6$ cluster (Figure 1.6) [8]. Another way to produce three-dimensional arrangements represents the interlinking of metal cluster by α,ω-

alkyldithiols wherein the thiol group is forming a strong Au-S bond between vicinal gold colloids [9].

One main approach to get two-dimensionally organized mono- or multilayers of $Au_{55}(PPh_3)_{12}Cl_6$ cluster is demonstrated in figure 1.7. Self-assembled monolayer of a α,ω-alkyldithiol can bind the gold cluster from the solution caused by an easy substitution of phosphines by thiols. Further colloid layers can then be added by generating monolayers of dithiol molecules. This technique leads to non-ordered two-dimensional structures which can be observed by TEM images of sliced samples [10]. Another approach to obtain, this time, well ordered monolayers of the gold cluster can be achieved by deposition of them on thin films of appropriated polymers such as poly(ethyleneimine) (PEI), poly(phenylenealkynylenes) (PPE) or poly(vinylpyrrolidone) (PVP) [11]. A two-phase system of water-dichloromethane is used to generate a thin film of a suitable polymer at the interface. Addition of the gold cluster to the organic phase on the polymer results in a well ordered monolayer due to weak interactions between the polymer film and the ligand shell of the gold cluster. A hexagonal close-packed and a primitive square monolayer arrangement of the colloids is observed [12].

The one-dimensional arrangement of nanoparticles is difficult to achieve and needs appropriate templates or sophisticated techniques, as nature does not tend to organize in one dimension due to energetic reasons. One approach was made by the conversion of terminal CH_3 monolayers by an electrical pulse of a metallized AFM tip resulting in COOH functions in one dimension. These can be transformed in several steps to SH-functionalized patterns which can be easily decorated by Au_{55} clusters, simply by dipping into a gold cluster solution (Figure 1.8) [13]. To date different ways for the preparation of nanowires by the 1-dimensional arrangement of nanoparticles exist [14]. Still 1-dimensional arrangements are much more difficult to prepare compared to their 2- or 3-dimensional

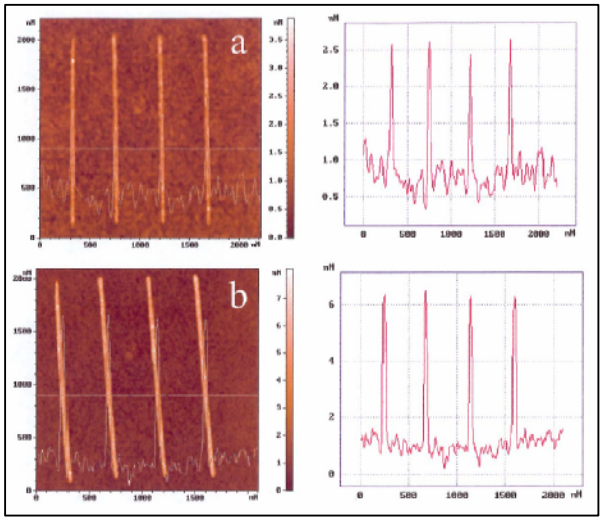

Figure 1.8: AFM micrographs of thiol-funtionalized lines (a) without and (b) with two rows of clusters on the top

counterparts and there is still no routine method to prepare 1-dimensional structures for use in a satisfying way for any technological process.

The aim of this work is to achieve the one-dimensional alignment of nanoparticles by using two different approaches. Firstly, nanochains of interlinked gold colloids within discrete vanadium oxide nanotubes were produced with results discussed in chapter 2. Secondly, collagen fibres were produced, with gold nanoparticles tagged and metallized completely by a growth step leading to gold nanowires with a diameter of few nanometers and a length of several micrometers. The results of this approach are presented in chapter 3.

Biomineralization deals with the study of formation, structures, and preparation of inorganic solids deposited in biological systems. It is an interdisciplinary field of investigation. Several million years ago, in biological systems the capability for selective extraction and uptake of elements from the local environment and their incorporation into functional structures under biological control evolved. After about 3.500 million years of evolution, biomineralization has provided organisms a variety of strong and tough building materials which are generally composed of hybrid materials formed by an inorganic mineral and an organic matrix component. This field combines the hard and stiff properties of inorganic minerals with soft and pliable but tough properties of organic materials.

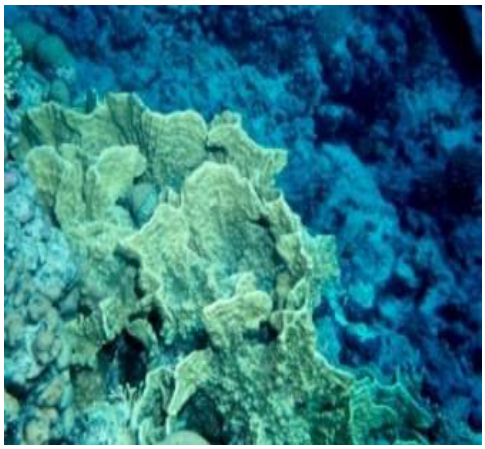

Figure 1.9: Millepora platyphylla

The biological functions of these biominerals, which show crystalline or amorphous structure, are widespread. They range from structural support, mechanical strength, protection, motion, cutting and grinding to storage and gravity sensing.

Mineralized structures as in coral reefs which are found in the tropic sea also play a role as a complete biotope which gives a habitat to a multifaceted fauna. They are formed especially by hard corals (Figure 1.9) and consist mainly of calcium carbonate which is formed by excretion of the mineral at the ectoderm of the coral building animals. The animals are sedentary and feed on micro plankton, nutrients and minerals from the sea water also from symbiotic algae which are responsible for the intensive colour of the corals and appear in corals near the water surface.

The most abundant constituents among over 60 different biological minerals are calcium, silicon, phosphorus, carbon, iron and oxygen. In this spectrum of elements calcium holds special place. It is not only widespread but also a constituent of familiar skeletal structures like bones and shells, whereas bones are preferentially made of calcium phosphate and shells of calcium carbonate. These two forms of minerals show high lattice energy and low solubility which indicate a high thermodynamic stability in biological environments.

Bones are a material with unusual mechanical properties. They consist of hydroxoapatite crystals which are embedded in an organic matrix consisting mainly of ordered nanoscale collagen fibres. The fibres are organized into a bundle forming a crystallization site for the hydroxoapatite. At the highest level of organization it is forming the macroscopic bone which is composed of a relatively dense outer side and a less dense and more porous inner side (Figure 1.10). Due to this form of construction the bone is able to support its own weight, bend without shattering and withstand acute force. It also serves as an ion reservoir for calcium and phosphate ions. Both functions depend on the size, shape chemical composition and crystal structure of the mineral phase and their arrangement inside the organic matrix. Bones are not a static organic-inorganic composite but an organ which permanently reorganizes by degradation and growth. On this account it is called “living bone”. This process of rebuilding is controlled by different cell types which are enclosed in the composite material consisting mainly of osteoblasts which account for the formation of the bone tissue and osteoclasts which are responsible for the degradation of the bone [15,16].

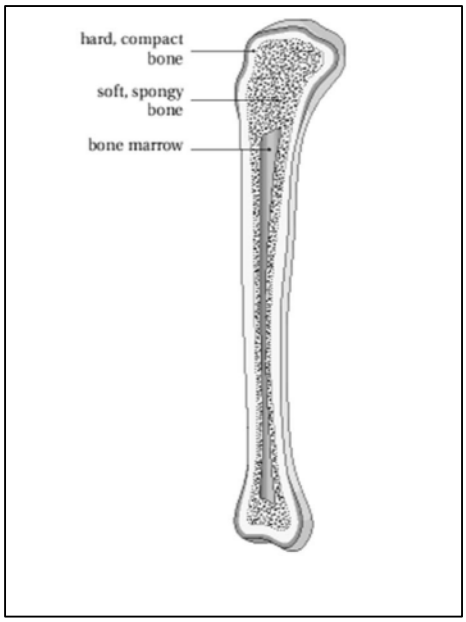

Figure 1.10: Bone structure

In magnetotactic bacteria magnetite (Fe_3O_4) crystals are found which serve as gravity or earth magnetic field sensor. They exhibit a maximal magnetic moment which means that they have a size of a simple magnetic domain of ~ 42-45 nm. These crystals are embedded mainly by a phospholipid bilayer membrane, which is synthesized de novo in the cytoplasma of those magnetobacteria [17] and organized as a chain of various crystals which are called magnetosomes. It is not completely understood how the crystallographic orientation in the magnetosome chain is controlled, but it is thought that specific proteins in the magnetosome

membrane are involved in nucleation and constrained crystal growth and thus have proteins bound to the surface of the magnetite crystals [18]. The magnetic particles are very stable, and also found in geological sediments. A selection of different magnetosomes is shown in Figure 1.11.

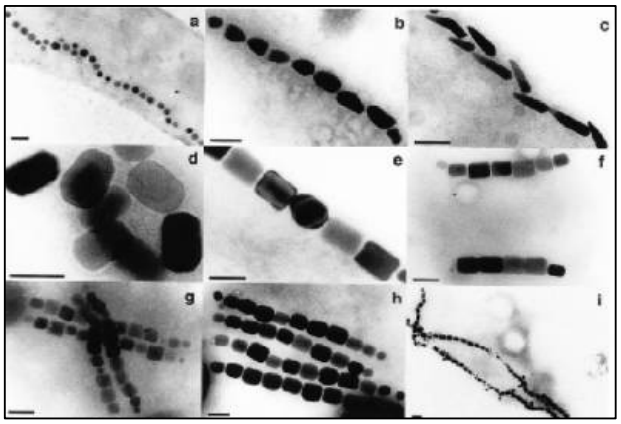

Figure 1.11: Magnetosomes found in different species of magnetotactic bacteria

The biomineralization process can be divided generally in four stages: Preorganisation of a supramolecular assembly, controlled nucleation, controlled crystal growth and cellular processes [19].

The first step is the most important where the living organism is organizing a reaction compartment wherein the crystallization zone is separated from the rest of the cellular environment. These compartments can be located on or in the membrane wall of a cell, outside the cell as in the case of the collagen induced crystallization of hydroxoapatite in bone formation or intracellular by self-assembly of enclosed protein cages or lipid vesicles and consist mainly of functionalized organic surfaces which provide the basis for the nucleation of the inorganic component by electrostatic, structural and stereo chemical recognition at the inorganic-organic interface.

The subsequent control over the crystal growth leads to a localized determination of the mineralized architecture of crystals, aggregation and texture in a biological environment. Sophisticated control mechanisms of the organism control and direct the energy transport, redox processes, selective complexation and enzymatic transport of ions, control over pH and the osmotic pressure inside the compartment.

Biomineralization does not stop with the formation of small particles but at least a cellular processing of the formed mineral takes place and continues during lifetime. This can be the rearrangement of the iron oxide nanoparticles in magnetotactic bacteria, the permanent degradation and build-up in bones or the growth of the layered calcium carbonate structure in shells such as Haliotis Rufescens.

This organized matter chemistry has a significant impact on the biomineralization related field of chemical constructions of structures with high order and with increased complexity under very mild conditions compared to usual techniques of preparative solid state chemistry [20].
Thus the modern science has growing interest in the often complex and intricate hierarchical architectures of biominerals. The development of new materials is an interdisciplinary field of investigation and biominerals represent the archetype for rigid but tough material and are the subject of research all over the world [21]. The aim is to design and synthesize biomimetic materials with specific features for medicinal applications as bone implants, for heterogeneous catalysis, for organic-inorganic hybrid materials and composites. Thus it is essential to understand the principles of the biomineralization process.
One important goal of these investigations is to investigate the structure-function relationship of biominerals and the role of the organic matrix during the biomineralization process. To date this process is not totally understood in detail due to the involvement of living cells and organisms which are controlled genetically by a harmonized complex biochemical process which cannot be observed in vivo. Thus a lack of information regarding the three-dimensional structure and cellular organization alignment of the involved proteins and other biomolecules exists[20,22]. This particular understanding of the phenomenon at the molecular level is very important. Thus appropriate in-vitro models are required to investigate the processes at the organic-inorganic interface. The nucleation process is the second and a very important step in the formation of biominerals and it can occur homogeneous or heterogeneous [23]. As the homogeneous nucleation is determined by the formation of a thermodynamically stable nuclei initiated by the super saturation of the depositing ions, the heterogeneous nucleation is induced by a template. The binding ion is lowering the surface energy resulting in a decrease of nucleation energy. The growth of the mineral occurs now in terms of epitaxial lattice matching, depending on the pattern of the substrate, which is reflected by the specific orientation and morphology of the resulting crystals. This means that it should be possible to control the nucleation by a well defined structure of the template [24]. Several model systems were used to mimic and to elucidate the phenomenon of heterogenoues nucleation. One approach is the use of isolated proteins from biological material in in-vitro experiments [25]. Another way is to use synthetic substrates as vesicles [26], oil-water emulsions [27], Langmuir monolayers [28], polymer dispersions [29], dendrimers [30], and self-assembled monolayers [31].

The last-mentioned model system was employed especially by Tremel et. al. as a model system. With this technique it is possible to vary the properties, such as the hydrophilicity or the complexation ability of the surface by using different head groups of the self-assembled α,ω-functionalized alkylthiol. These head groups have an immense impact on the crystallization products. It is also known, that crystals can follow the geometry of the underlying nucleating substrate [32].

The advantage of this method is the posibility to investigate the influence of the matrix surface on the mineral crystallization as well as the cooperative effect with soluble macromolecules in order to obtain model experiments that are close to biological systems. Till this day the main biomineral investigated with this technique is calcium carbonate both with sole matrix surface and with soluble macromolecules present. The crystallization of calcium phosphate on self-assembled monolayer was investigated less intensive whereas the main research interest was focussed on the crystallization in the absence of soluble additives [33]. Thus the aim of this work is to elucidate the influence of soluble proteins on the crystallization behaviour of calcium phosphate on self-assembled monolayers. Chapter 4 depicts the results of the influence of Perlucin and chapter 5, the influence of Nacrein.

References

1. Schmid, G; Decker, M.; Ernst H.; Fuchs, H.; Grünwald, W.; Grunwald, A.; Hofmann, H.; Mayor, M.; Rathgeber, W.; Simon, U.; Wyrwa, D.: *Small Dimenstions and Material Properties – A Definition of Nanotechnology*, Graue Reihe, Europäische Akademie, Bad Neuenahr, November **2003**.
2. J. de Jongh (edt.): *Physics and Chemistry of Metal Cluster Compounds*, Kluwer Academic Publishers, Dordrecht, **1994**.
3. R. Kubo, *J. Phys. Soc. Japan* **1962**, *17*, 975-986.
4. A. Bezryadin, C. Dekker, G. Schmid, *Appl. Phys. Lett.* **1997**, *71*, 1273-1275.
5. L. F. Chi, M. Hartig, T. Drechsler, Th. Schwaack, C. Seidel, H. Fuchs, G. Schmid, *Appl. Phys. A*, **1999**, *A66*, S187-S190.
6. a) G. Schön, U. Simon, *Colloid Polymer Sci.* ***1995***, *273*, 101-117. b) G. Schön, U. Simon, *Colloid Polymer Sci.* **1995**, *273*, 202-218.

7. a) C. N. Ramachandra Rao, G. U. Kulkarni, P. J. Thomas, P. P. Edwards, *Chem. Soc. Rev.* **2000**, *29*, 27–35. b) R Shenhar, T. B. Norston, V. M. Rotello, *Adv. Mater.* **2005**, *17*, 657-669. c) T. Teranishi, *C. R. Chimie*, **2003**, *6*, 979–987.
8. G. Schmid, R. Pugin, T. Sawitowski, U. Simon, B. Marler, *Chem. Commun.* **1999**, *1303-1304*.
9. V. Torma, O. Vidoni, U. Simon, G. Schmid, Eur. *J. Inorg. Chem.* **2003**, 1121-1127.
10. V. Torma, G. Schmid, U. Simon, *ChemPhysChem.* **2001**, *5*, 321-325.
11. G. Schmid, N. Beyer, *Eur. J. Inorg. Chem.* **2000**, 835-837.
12. G. Schmid, M. Bäumle, N. Beyer, *Angew. Chem.* **2000**, *112*, 187-189; *Angew. Chem. Int. Ed.* **2000**, *39*, 181-183.
13. S. Liu, R. Maoz, G. Schmid, J. Sagiv, *Nano Lett.* **2002**, *2*, 419-421.
14. a) G. Schmid, U. Simon, *Chem. Commun*. **2005**, 697-710. b) Z. Tang, N. A. Kotov, *Adv. Mater.* **2005**, *17*, 951-962. c) C. N. Ramachandra, G. U. Kulkarni, P. J. Thomas, *Chem. Soc. Rev.* **2000**, *29*, 27-35. d) N. I. Kovtyukhova, T. E. Mallouk, *Chem. Eur. J.* **2002**, *8*, 4354-4363. e) G. Schmid: *Metals*, in: K. J. Klabunde: *Nanoscale Materials in Chemistry*, Wiley-Interscience, New York, Chichester, Weinheim, 2001.
15. P. Karlson: *Biochemie*, Georg Thieme Verlag Stuttgart, New York **1985**.
16. S. V. Dorozhkin, M. Epple, *Angew. Chem.* **2002**, *114*, 3260-3277.
17. E. Baeuerlein, *Angew. Chem.* **2003**, *42*, 614-641.
18. A. Arakaki, J. Webb, T. Matsunaga, *J. Biol. Chem.* **2003**, *278*, 8745-8750.
19. U. Schubert, N. Hüsing: *Synthesis of Inorganic Materials*, Wiley-VCH, **2000**.
20. S. Mann: *Biomineralization*, Oxford University Press, Oxford **2001**.
21. K. J. Klabunde (edt.): *Nanoscale materials in chemistry*, Wiley-Interscience, New York, **2001.**
22. S. Weiner, L. Addady, *J. Mater. Chem.* **1997**, *7*, 689-702.
23. I. Weissbuch, M. Lahav, L. Leiserowitz, *Crystal Growth & Design*, **2003**, *3*, 125-150.
24. K. Naka, Y. Chujo, *Chem. Mater.* **2001**, *13*, 3245-3259.
25. a) S. Albeck, J. Aizenberg, L. Addadi, S. Weiner, *J. Am. Chem. Soc*. **1993**, *115*, 11691-11697. b) J. Aizenberg, J. Hanson, T. F. Koetzle, S. Weiner, L. Addadi, *J. Am.Chem. Soc.* **1997**, *119*, 881-886. c) B. A. Gotliv, L. Addadi, S. Weiner, ChemBioChem, 2003, 4, 522-529. d) A. M. Belcher, X. H. Wu, R. J. Christensen, P. K. Hansma, G. D. Stucky, D. E. Morse, *Nature*, **1996**, *381*, 56-58. e) A. Bermann, L. Addadi, S. Weiner, *Nature*, **1988**, *331*, 546-548.

26. S. Mann, J. P. Hannington, R. J. P. Williams, *Nature*, **1986**, *324*, 565-567.
27. E. G. Vrieling, T. P. M. Beelen, R. A. Van Santen, W. W. C. Gieskes, *J. Biotechnol.* **1999**, *70*, 39-51.
28. a) S. Mann, B. R. Heywood, S. Rajam, J. D. Birchal, *Proc. Roy. Soc. Lond. A*, **1989**, *423*, 457-460. b) D. Jacquemain, S. Grayer Wolf, F. Leveiller, M. Deutsch, K, Kjaer, J. Als-Nielsen, M. Lahav, L. Leiserowitz, *Angew. Chem.* **1992**, *104*, 134-158.
29. a) J. N. Cha, G. D. Stucky, D. E. Morse, T. J. Deming, *Nature*, **2000**, *403*, 289-292; b) H. Cölfen, L. Qi, *Chem. Eur. J.* **2001**, *7*, 106-116.
30. J. J. J. M. Donners, B. R. Heywood, E. W. Meijer, R. J. M. Nolte, N. A. J. M. Sommerdijk, *Chem. Eur. J.* **2002**, *8*, 2561-2567.
31. a) J. Küther, R. Seshadri, G. Nelles, H. J. Butt, W. Knoll, W. Tremel, *Adv. Mater.* **1998**, *10*, 401-404. b) J. Aizenberg, A. J. Black, G. M. Whitesides, *J. Am. Chem. Soc.* **1999**, *121*, 4500-4509.
32. a) J. Aizenberg, A. J. Black, G. M. Whitesides, *Nature*, **1999**, *398*, 495-498. b) J. Küther, R. Seshadri, W. Knoll, W. Tremel, *J. Mater. Chem.* **1998**, *8*, 641-650.
33. a) B. J. Tarasevich, C. C. Chusuei, D. L. Allara, *J. Phys. Chem. B* **2003**, *107*, 10367-10377. b) K. Onuma, A. Ayane, T. Kokubo, G. Trebkoux, N. Kanzaki, A. Ito, *J. Phys. Chem. B*, **2000**, *104*, 11950-11956. c) Q. Liu, J. Ding, F. K. Mante, S. L. Wunder, G. R. Baran, *Biomaterials*, **2002**, *23*, 3103-3111. d) S. P. Huang, K. C. Zhou, Y. Liu, B. Y. Huang, *Trans. Nonferrous Metals Soc. China*, **2003**, *13*, 595-599.

2. Templated Synthesis of Nanowires

2.1 Casting Au of Nanochains by Interlinking Gold Colloids Within Discrete Vanadiumpentoxid Nanotubes

2.1.1 Introduction

One-dimensional (1D) metallic nanowires have attracted much attention in recent years because of their novel physical properties [1] and potential applications as connecting elements in future generations of nanoscale electronics. A number of methods have been reported for preparing nanowires of controlled length and diameter. These preparation methods include the incorporation of nanoparticles inside mesoporous materials [2], electrochemical [3], photochemical [4], or chemical reduction [5] after solution impregnation with a metal salt inside carbon nanotubes [6], in and on titania nanotubes [7], on tubular polymer brushes [8] or using biological templates such DNA [9], viruses [10] or nanotubes formed of the Alzheimer β-amyloid diphenylalanine structural motif [11]. A very successful approach for the synthesis of nanowire arrays with well defined aspect ratio relies on the electrochemical deposition of metal in the cylindrical pores of nonconductive porous membranes [12]. In particular, the electrodeposition in porous alumina templates [13,14], as well as the electrochemical and electroless deposition inside the pores of inorganic [15] or polymeric template membranes [16] has been used for the fabrication of poly- and single crystalline [17,18] nanowires with diameters ranging from micrometers down to nanometers (≈ 70 nm). Although much effort has been devoted to the fabrication of crystalline nanowires, information on granular wires from metal colloids are scarce. This is surprising considering the fact that much research in current mesoscopic physics focuses on understanding properties of granular metals, where the interest is motivated by the fact that while their properties are generic for a wealth of correlated systems with disorder granular metals may be considered tunable systems where both the interaction strength and the degree of disorder can be controlled.

Au nanowires are of special interest because Au is widely used as a substrate for self-assembled monolayers (SAMs) [19-21], and a number of SAM-based molecular electronic devices have been described recently [22]. On the other hand, template and hydrothermal

synthetic routes made vanadium oxide nanotubes [23] with well defined dimensions and inner diameters of approximately 20 nm available as synthetic precursors for the chalcogenide nanotubes [24] and host materials for intercalation reactions [25]. Here we describe the synthesis of "granular" Au nanowires from Au nanoparticles with a large aspect ratio and of a uniform diameter by interlinking gold-nanoparticles with a dithiol inside the V_2O_5 nanotubes.

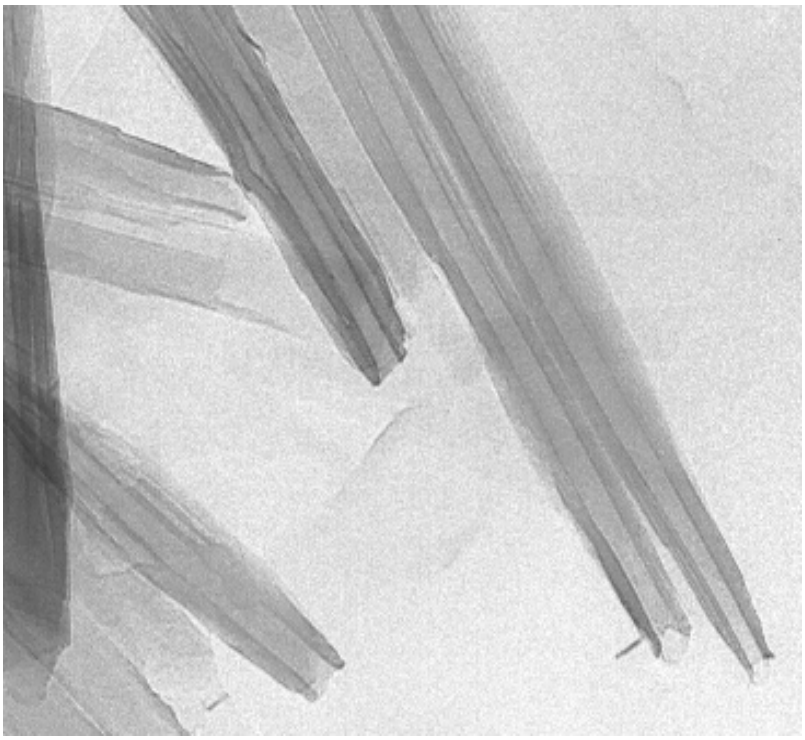

Figure 2.1.1: V_2O_5 nanotubes after hydrothermal synthesis (Nesper et. al.)[23]

2.1.2 Results and Discussion

Figure 2.1.1 shows a typical TEM image of VO_x nanotubes obtained by hydrothermal synthesis. The open ended tubes have a length of 1-3 μm and exhibit a number of defects at their outer walls. However, their inner portions are regular with inner diameters ranging from 25 to 30 nm.

After immersing the nanotubes in the colloid solution the colloids start to interpenetrate the tube by capillarity. The TEM image in Figure 2.1.2 shows, however, that only a part of the Au colloids are located inside the tubes, whereas a substantial portion of the gold nanoparticles remained outside, where aggregates are formed as concluded from the absence of a defined structure outside the tubes. The TEM image in Figure 2.1.2 reveals that the Au nanoparticles – although still separate but arranged in a linear fashion by the VO_x nanotube template – fill the interior of the tube completely. The nanoparticles are completely mobile because there are

only secondary interactions between the polar inner walls of the tube and the hydrophobic colloids, i.e. they can be removed completely from interior of the tube by a washing step.

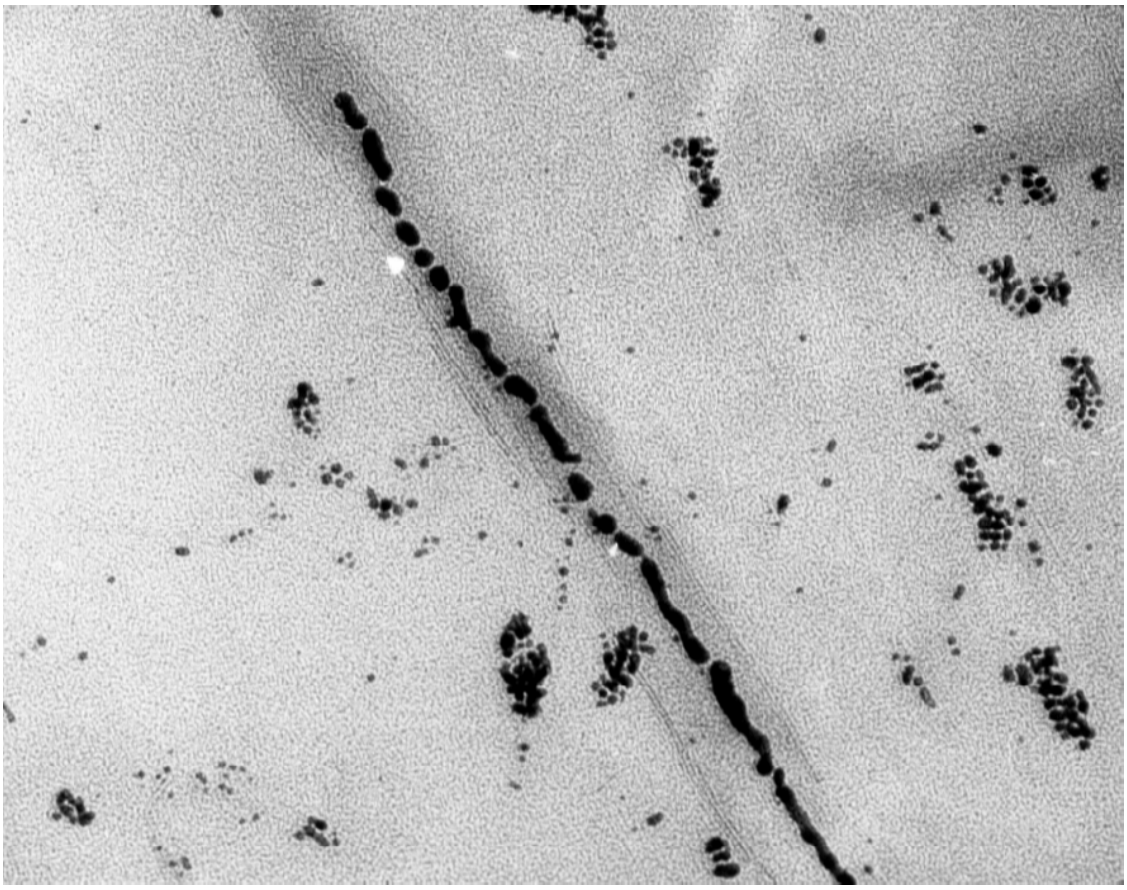

Figure 2.1.2: V_2O_5-nanotube filled with Au colloids without interlinking dithiol

Figure 2.1.3 shows the Au nanochains obtained by interlinking the individual Au colloids within the tubes with 1,12-dodecanedithiol. The synthetic protocol used to prepare the Au nanochains is illustrated in Scheme 1. In this step, the dithiol acts as bifunctional linker molecule which is attached to the surface colloids. Colloid particles residing inside the tube are linked in a linear fashion to nanochains, whereas colloids outside the tubes form aggregates with ill-defined nonlinear structures. In Figure 2.1.3a most of the Au nanochains are found inside the nanotubes, a few chains marked by a circle in Figure 2.1.3a

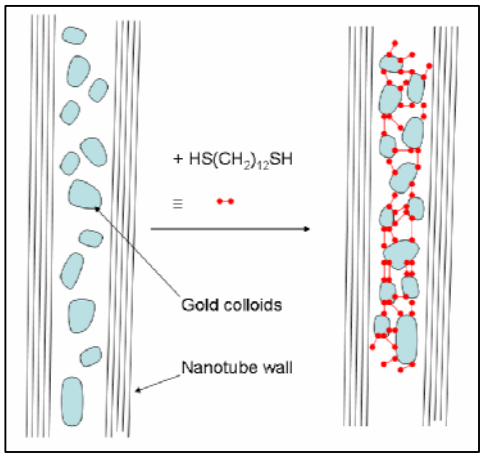

Scheme 1: Protocol for the preparation of the Au nanochains

have slipped out of the tubes, and few unstructured aggregates marked by dotted circles are found in the vicinity of the tubes. The Au nanochains can be released from the tubes by gently shaking a suspension if the tubes in an inert solvent such as toluene. Figure 2.1.3b shows a typical nanochain obtained in this manner as well as a number of shorter chains fragments.

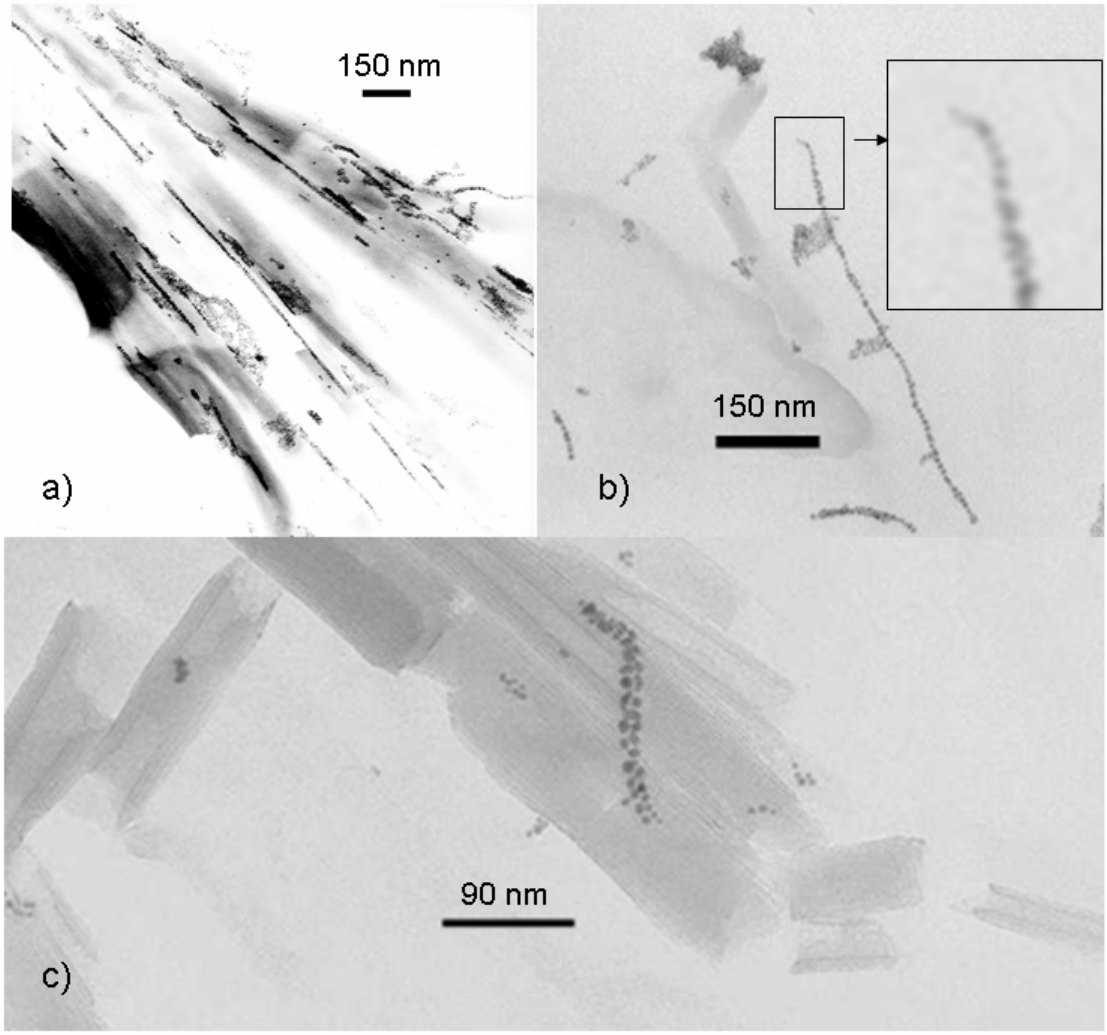

Figure 2.1.3: Au nanochains obtained by interlinking Au colloids with 1,12-dodecanedithiol inside and outside the templat V_2O_5 nanotubes

The longer nanochain and the shorter chain fragments are typical products obtained by the synthetic protocol. The diameter of the longer nanochain (whose end is show in higher magneification in the inset) is ≈ 20 nm (corresponding to the inner diameter of the VO_x template), while its length is approximately 1 μm. The image of a chain fragment in Figure 2.1.3c reveals the presence of interlinked quasi-independent particles within the chains.

Figure 2.1.4 shows a HRSEM image of a chain fragment. Although only small variations in the diameter of the nanochains are observed, their outer surface appears rough reflecting the individual Au component nanoparticles linked by α,ω-dithiol spacer. Furthermore, the non-rigid spacer ligand makes the nanochains highly flexible, as apparent from the curvature of the chain in Figure 2.1.4, a feature which makes the nanochains distinct from rigid nanowires or nanorods described in the literature.

2.1.3 Conclusion

We could demonstrate that granular gold nanochains consisting of individual Au colloid particles linked by a flexible α,ω-dithiol spacer can be synthesized from colloidal gold by making use of V_2O_5 nanotubes as templates. The diameter of the resulting nanochains reflects the inner diameter of the template nanotubes, while the chain lengths may vary from 200 nm to 1100 nm. These chains may be considered models of 1D-granular metals. The unique structural features could make them interesting objects for structuring and assembling in the nanoscale range.

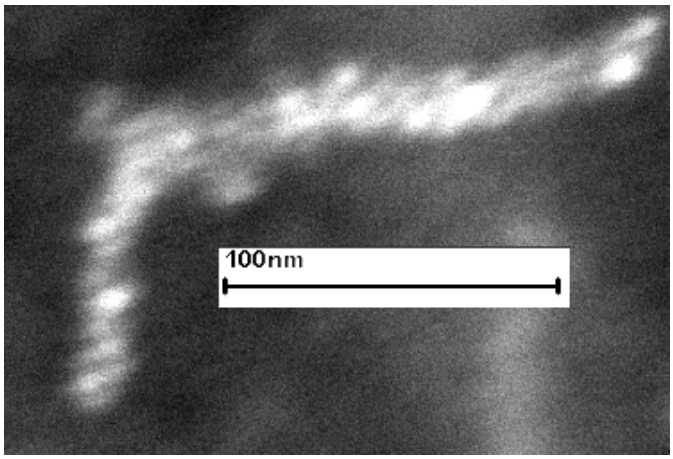

Figure 2.1.4: HRSEM image of a nanowire consisting of gold colloids interlinked with a α,ω-dithiol spacer.

2.1.4 Experimental Section

Synthesis of the VO_x nanotubes. In a typical synthesis procedure 0,912 g (0,0038mol) 1-hexadecylamine were dissolved under nitrogen in 8 ml of dry ethanol. Under stirring 5 g of vanadium(V)trisisopropoxide (Alfa) were added. After one hour 20 ml of water were added and the mixture was allowed to stand for 48 hours. Afterwards the suspension was transferred to a Teflon-coated reactor vessel and heated for three days at 180°C under hydrothermal

conditions. After cooling, the mixture was washed with ethanol and subsequently with cyclohexane at least ten times and finally vacuum-dried at a liquid-nitrogen-trap. The average yield was between 1,2 g and 1,4 g of VO_x nanotubes. For the structural analysis by Transmission Electron Microscopy (TEM) a small fraction of the black product was dispersed in a small volume of toluene and a drop of this suspension was transferred onto a carbon-coated TEM-grid. A TEM image of the nanotubes is presented in Figure 1.

Synthesis of the 1,12-dodecanedithiol [27]

1,12-dodecanedithiol was synthesized in a two-step reaction:

a) Synthesis of the Bunte salt: 11,6 g (35 mM) 1,12-dibromdodecane in 50 ml ethanol was mixed with 19,2 g (76 mM) sodium thiosulfate dissolved in 50 ml distilled water and heated for 4 hours under reflux to form the Bunte salt. After cooling the precipitated white product was filtered, washed with water and dried.

b) Synthesis of the 1,12-Dodecanedithiol: Without further purification 16 g of the Bunte salt was suspended in a degassed mixture of 100 ml distilled water and 5 ml ethanol and heated under reflux for 6 hours under inert atmosphere. After cooling to 4° C the product precipitated and was redissolved in dichloromethane. The organic phase was cleaned several times with a solution of 3 M sodium chloride and finally washed with water. Afterwards the solution was dried over calcium chloride and the dichloromethane was removed leading to a white product with an overall amount of 63 % (5,7 g, 22 mM).

Synthesis of the Au colloids. Gold colloids were prepared following the method of Brust [26] in two-phase toluene-water systems using tetraoctylammoniumbromide to transfer the chloroauric acid from water to toluene and then reducing the Au(III) to Au(0) at the water-toluene face boundary using aqueous $NaBH_4$ as a reductant. Typically, 2 g of $HAuCl_4$ in 100 ml of water were mixed in a separation funnel with toluene in a 1:10 ratio. After adding an appropriate amount of the solid phase transfer agent to the mixture, the gold complex was completely transferred into the toluene phase, where it was reduced by addition of $NaBH_4$. The colour of the toluene phase turned ruby indicating the formation of the gold colloids. After the reaction was complete the two phases were separated. The toluene phase was dried over Na_2SO_4 and centrifugated at 4000 rpm resulting in a ruby solution of colloids in toluene. Analysis of the products by TEM indicated the presence of Au colloids withs diameter of 8±2 nm..

Synthesis of the Au nanowires. About 1 mg of the VO_x nanotubes were placed in a 1,5 ml PP Plastibrand reaction tube and covered with 200 µl of the Au colloid solution. Afterwards the mixture was allowed to stand for 20 minutes so that the colloids could interpenetrate the nanotubes by capillary forces. A fivefold amount (5 mg) of synthesized solid 1,12-dodecanedithiol was added and a black precipitate appeared indicating the interlinking of the colloids. After another 20 minutes the reaction was complete.

Samples for TEM analysis were prepared by placing a drop of the mixture on a carbon coated Cu grid. Then the grid was carefully washed with toluene, dried at room temperature and analyzed in a Zeiss EM 900 transmission electron microscope at 80 kV extraction voltage. The images were recorded on a Kodak EM film Type 4489 and subsequently scanned with a resolution of 600 dpi. HRSEM iamges were obtained using a LEO 1550 scanning electron microscope with 3 kV extraction voltage.

2.1.5 References

1. D.Y. Li, Y. Wu, R. Fan, P. D. Yang, A. Majumdar, *Appl. Phys. Lett.* **2003**, *83*, 3186-3188.
2. L. M. Worboys, P. P. Edwards, P. A. Anderson, *Chem. Commun*. **2002**, 2894-2895.
3. Y. Y. Yu, S. S. Chang, C. L. Lee, C. R. C. Wang, *J. Phys. Chem. B* **1997**, *101*, 6661-6664.
4. (a) K. Franklin, S. Jae Hee, Y. Peidong, *J. Am. Chem. Soc*. **2002,** *124*, 14316-14317. (b) K. Esumi, K. Matsuhisa, K. Torigoe, *Langmuir* **1995**, *11*, 3285-3287. (c) F. Kim, J. H. Song, P. Yang, *J. Am. Chem. Soc*. **2002**, *124*, 14316- 14317.
5. M. H. Huang, A. Choudry, P. Yang, *Chem. Commun.* **2000**, 1063-1064 .
6. (a) J. Sloan, D.M. Wright, H.-G. Woo, S. Bailey, G. Brown, A. P. E. York,. K. S. Coleman, J. L. Hutchison, M. L. H. Green, *Chem. Commun*, **1999**, 699-700. (b) G. Che, B. B. Laxmi, C. R. Martin, E. R. Fischer, R.S. Ruoff, *Chem. Mater*. **1998**, *10*, 260-267.
7. R. Ma, T. Sasaki, Y. Bando, *J. Am. Chem. Soc*. **2004**, *126*, 10382-10388.
8. R. Djalali, Y.-F. Chen, H. Matsui, *J. Am. Chem. Soc*. **2003**, *125*, 5873-5879.
9. C.F. Monson, A.T. Wolley, *Nano Lett.* **2003**, *3*, 359-363.
10. M. Knez, A. M. Bittner, F. Boes, C. Wege, H. Jeske, E. Maiß, K. Kern, *Nano Lett*. **2003**, *3*, 1079-1082.
11. M. Reches, E. Gazit, *Science* **2003**, *300*, 625-627.
12. M. Zhang, S. Lehnhart, M. Wang, L. Chi, N. Lu, H. Fuchs, N. Ming, *Adv. Mater*. **2004**, *16*, 409-413.

13. (a) Y. Jong-Sung, K. Jeong Yeon, L. Seungho, J. K. N Mbindyo, B. R. Martin, T. E. Mallouk, *Chem. Commun*. **2000**, 2445-2446. (b) N. I. Kovtyukhova, T. E. Mallouk, T. S. Mayer, *Adv. Mater*. **2003**, *15*, 780-785.
14. J. K. N. Mbindyo, T. E. Mallouk, J. B. Mattzela, I. Kratochvilova, B. Razavi, T. N. Jackson, T. S. Mayer, *J. Am. Chem. Soc*. **2002**, *124*, 4020-4026.
15. Z. Zhang; S. Dai; D.A. Blom, J. Shen, *Chem. Mater*. **2002**, *14*, 965-968.
16. K. Jong-Uk, C. Sang-Ho, S. Kyusoon, J. Jae Young, L. Jong-Chan, *Adv. Mater*. **2004**, *16* 459-464.
17. H. Zeng, M. Zheng, R. Skomsky, D.J. Sellmyer, Y. Liu, L. Menon, S. Bandyopadhyay, *J. Appl. Phys*. **2000**, *87*, 4718-4720.
18. D. Dobrev, J.Vetter, N. Angert, R. Neumann, *Appl. Phys. A* **1999** *69* 233-237.
19. J. Chen, M. A. Reed, A. M. Rawlett, J.M.; Tour, *Science* **1999**, *286*, 1550-1552.
20. M. A. Read, J. Chen, A. M. Rawlett, D. W. Price, J. M. Tour, *Appl. Phys. Lett*. **2001**, *78* 3735-3737.
21. J. Küther, R. Seshadri, G. Nelles, H.-J. Butt, W. Assenmacher, W. Mader, W. Tremel, *Chem. Mater*. **1999**, *11*, 1317-1325.
22. C. Joachim, J. K. Kimzewski, A. Aviram, *Nature* **2000**, *408*, 541-548.
23. F. Krumeich, H.-J. Muhr, M. Niederberger, F. Bieri, B. Schnyder, R. Nesper, *J. Am. Chem. Soc.* **1999,** 121, 8324-8331.
24. H. A. Therese, F. Rocker, A. Reiber, J.X. Li, M. Stepputat, G. Glasser, U. Kolb, W. Tremel, *Angew. Chem. Int. Ed. Engl.* **2005**, 44, 262-265.
25. R. Nesper, *Chimia* **2001**, *55*, 787-790.
26. M. Brust, D. Bethell, D. J. Schiffrin, C. J. Kiely, *Adv. Mater*. **1995**, *7*, 795-797.
27. M. Jaschke, H. Schönherr, H, Wolf, H.-J. Butt, E. Bamberg, M. K. Besocke, H. Ringsdorf, *J. Phys. Chem*. **1996**, *100*, 2290-2301.

2.2 Nanowires obtained by metallization of Type I Collagen fibres

2.2.1 Introduction

In recent years miniaturization of structured electronic devices has attracted the attention of researchers from a various fields. New approaches for structuring have had to be developed, due to the demands recognized for structuring at the nanometer size range, from ~ 1 to 100 nm, which is not easily accessible by classical chemical, physical or engineering techniques. One principal field of miniaturization has been the synthesis of one-dimensional structures as nanowires or nanotubes composed of conductive or semi-conductive material [1].

One approach is directed to the metallization of biochemical molecules such as proteins and DNA due to their appropriate size, their programmable structural features and their ability to complex metal ions at the surface where they afterwards are reduced to elemental metal forming the nanowire. Thus, it is possible to create DNA supported wires of copper [2], platinum [3], palladium [4], silver [5] and gold [6], often attached to a silica-surface. Also, conductivity measurements of those nanowires were realized [7]. Also other biomaterials, like sequenced histidine-rich peptide [8], nanotubes formed by the Alzheimer diphenylalanine-β-amyloid structural motif [9], glycolipid nanotube hollow cylinders [10], microtubules [11], which are components of the cytoskeletons of eukaryotic cells, and other templates such as the tobacco mosaic virus [12] were used for metallization leading to one-dimensional nanostructures.

A second alternative approach is the selective deposition of metallic nanoparticles on biological templates to obtain nanostructured hybrids [13]. Thus nanowire-like structures were formed by hierarchical assembly of gold nanoparticles on living templates, such as filamentous fungus Aspergillus Niger [14], or on cellulose fibres covered with TiO_2 [15], on self-assembled amyloid fibres [16], on DNA strands [17] and on a polylysine [18] protein.

Another type of biomolecule which shows one dimensional structure (amongst others) is collagen. To-date 25 [19] different types of human collagen are known whose complete constitution and function are not yet completely understood. Collagen can be classified as fibril forming (I, II, III, V, XI, XIV), network building (IV, VII) and associated fibre building (IX, XII, XIV, XVI, XIX - XXI) types. Only a few studies are known concerning the use of natural collagen for nanoscience and nanotechnology [20] and the functionalizing of collagen

to expand its structural and topological variations for nanotechnological purposes is in the early stage [21].

The most common type is the type I-collagen which represents the organic part of bones and teeth forming a composite with calcium phosphate and is also an essential component of tendon, ligaments and skin. The collagen peptide chain has about 1030 amino acids, contains characteristic features consisting of a repeated sequence motif with Glycine-Proline-Hydroxyproline and the formation of an atypically left-handed helix. Due to its helical structure and side-chain amino acids that introduce charged groups along the helix, this macromolecule is chiral and polar. The electrostatic attraction between the helices is the driving force for the alignment of three helices by longitudinal alignment resulting in a right-handed triple helix. These triple helices can self-assemble into fibres that are up to hundreds of micrometers long, which have a repeating charge distribution on the fibre surface. Here we use this surface charge of the fibres to adsorb gold colloids which can be easily enhanced in size resulting in a complete covering of the collagen fibres thus forming nanowires with diameters of 100-120 nm and a length of various µm.

2.2.2 Results and discussion

Figure 2.2.1 shows the typical horizontal strips of collagen I, wherein the micrograph a) shows a with uranyl acetate stained collagen strand and b) a collagen fibre as it is obtained after preparation without any staining agent. The fibre show horizontal stripes due to the staggered alignment of the repeating triple helices [25]. The metallization of the collagen fibres starts with the binding of gold colloids to the peptide surface. Because of the polarity of the collagen fibres and the fact, that many metallic nanoparticles such as Au, Ag and Pt, are charged, the adsorption of the nanoparticles lead to a non-specific binding to the surface of biomolecules by electrostatic interactions [26]. For this reaction we used gold colloids prepared by reduction of gold tetrachloride acid with THCP in water at alkaline pH described by Duff and co-workers [24b] and commercially available gold colloids (2 and 5 nm) from British Biocell International.

TEM images of the adsorbed gold colloids on collagen fibres are shown in Figure 2.2.2. The collagen images show a regular pattern of the colloids on the fibre surface which underlines the regular assembly of collagen molecules within the fibre. As smaller the particles are as

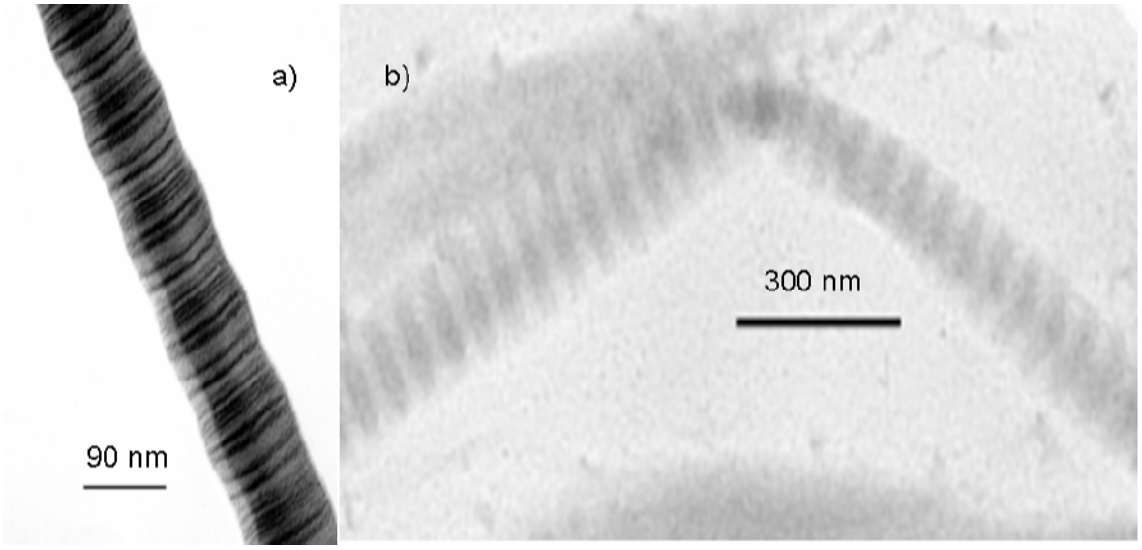

Figure 2.2.1: Collagen fibre as synthesized a) negatively stained with 2% w/v uranyl acetate, and b) unstained. The banded structure is formed due to the staggered alignment of collagen triple helices

better the mapping of the collagen structure as seen in Figure 2.2.2 a) and especially in b) with the lab-synthesized colloids, which have a variable diameter. Remarkably, in Figure 2.2.2 c) the spacing between the 5-nm-colloids and the less dense packing of the colloids on the surface of the collagen fibre is apparent. This can be explained by the covering and protecting the available binding sites on the collagen fibre by the larger colloids thus sterically hindering the binding of more particles to the surface. Due to the inhomogeneous distribution at the surface, the collagen sample with the 5-nm-colloids was excluded from the following growth enhancement step.

To achieve complete coverage of the fibres, a mild size enhancement procedure of the gold

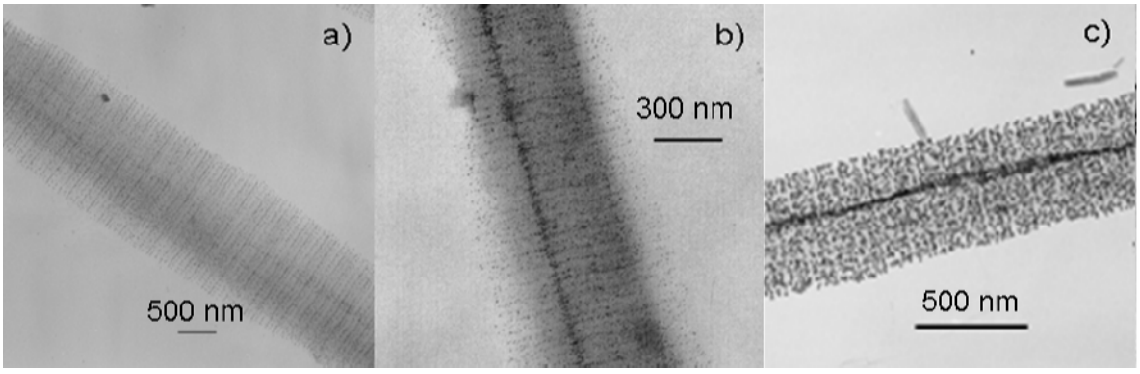

Figure 2.2.2: Collagen fibres with adsorbed gold colloids of different sizes. a) 2 nm colloid (BBI, London) b) synthesized colloid (about 1 to 2 nm); c) and 5 nm colloid (BBI, London).

particles was used which is described elsewhere [27]. Figure 2.2.3 shows the obtained metallized collagen-gold fibres after 11 and 20 cycles of enhancement. The gold pattern of the fibres is still observable. From the TEM data it seems that the fibres do not have a complete covering, but the analysis with a high resolution scanning electron microscope (LEO 1550) shows a different image, as shown in Figure 2.2.4, with 16 and 30 cycles of enhancement.

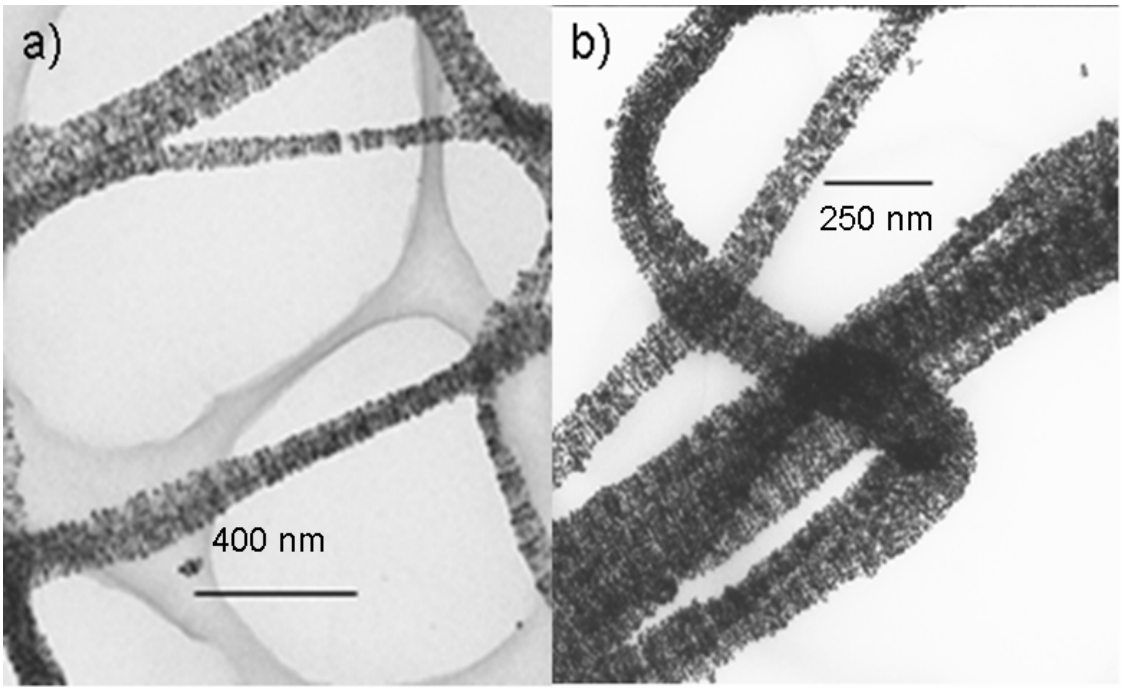

Figure 2.2.3: TEM-Pictures of collagen-fibres with synthesized colloids after a) 11 and b) 20 enhancement cycles

The collagen fibres are completely covered after 16 enhancement cycles. The colloids have grown up to about 30 to 50 nm diameter and form a polycrystalline layer along the fibres. The increase of cycles did not affect the quality of covering, but increase the thickness of the gold layer and leads to aggregation of the fibres, resulting in a clumped material which shows no discrete wires. These experiments were done with the BioCell 2-nm-gold colloids and with the synthesized gold colloids, with a variable size between 1 and 2 nm and there was no different perceivable between the final obtained collagen-gold wires.

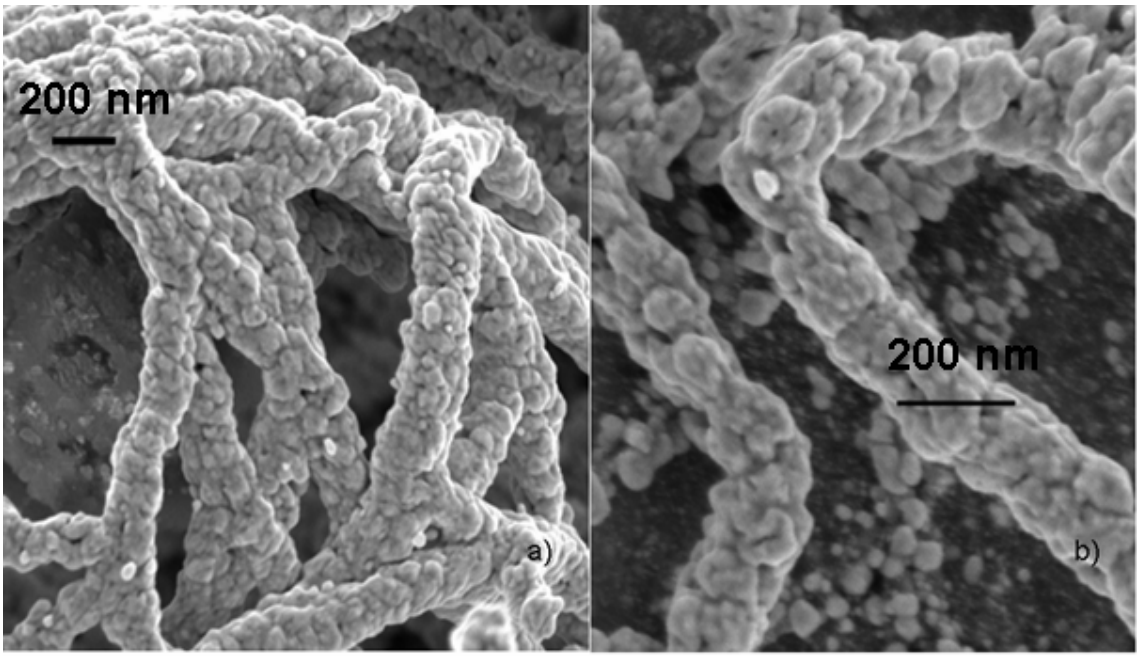

Figure 2.2.4: HRSEM-Pictures of the collagen-fibres with synthesized gold nanoparticles after a) 16 and after 30) enhancement cycles (scales: 200 nm) (unsputtered, 3 kV, working distance 3 mm)

2.2.3 Conclusions

We could show that collagen fibres can act as template for the synthesis of nanometer-sized gold wires with high aspect ratio. The spontaneous immobilization of gold colloids onto the collagen fibres permitted controlled reduction of gold tetrachloride acid from solution to form a defined mantle of gold on the collagen fibre surface. Even though reduction conditions have to be carefully observed in order to avoid aggregation of the discrete wires, we have used a new valid method for the synthesis of gold nanowires.

2.2.4 Experimental section

Synthesis of collagen fibres. Collagen fibres were produced by an established procedure [22]. At first the Collagen R solution (2 mg/mL in 0.1% acetic solution) supplied by SERVA (Heidelberg, Germany) was dialysed against 10 mM acetic acid over night at 4°C. The

received solution was then diluted with a fourfold amount of 10 mM acetic acid and allowed to stand for several hours at 4°C. Then equal volumes of collagen solution and double strength phosphate buffer (124 mM Na_2HPO_4; 29,2 mM KH_2PO_4) were warmed up to 34°C for about 10 minutes and mixed. The final solution has a pH ~ 7,4. Fibril reconstitution started and the mixture was incubated at 34°C for several hours until a cloudy gel was formed. The collage fibres were analyzed by transmission electron microscopy (Figure 2.2.1). Typically they have a diameter of ~ 30 to 90 nm. The fibre solution was stored at 4°C until use. For adsorption of Au colloids, the fibre solution was dialysed against water over several hours to remove the high salt concentration. A faster way to remove the salt was centrifugation of the solution at 1000 rpm, with removal of the overlaying solution, followed by washing the residue with water and centrifugation again. After two water-washings, the final volume of the collagen suspension was 0.3 ml.

Synthesis of the gold colloids. Stock solutions were prepared of gold tetrachloride acid trihydrate (Merck, 0,2 g/100 ml) and NaOH (Acros (p.a.), 3 M). Tetrakishydroxymethylphosphonium chloride (THPC) was purchased from Aldrich as an 80 % solution in water. For use 1,2 ml of this solution was diluted with water up to 100 ml. Gold colloids were prepared by mixing consecutively 4,7 ml water (Barnstead Easypure UV, ρ > 18,3 MΩ cm-1), 188 µl NaOH solution, 125 µl THPC solution and 1230 µlgold tetrachloride acid solution under stirring [23]. The obtained gold sol has a red-brown colour.
Gold colloids in aqueous solution (2 and 5 nm) also were purchased from British Biocell International (London, GB)

Adsorbtion of gold colloids to collagen fibres. The gold colloid sol was added drop wise to the desalted collagen solution. After a few minutes the solution turns colourless and the collagen fibres turn red due to the adsorption of the colloids. For analysis by transmission electron microscopy (TEM), a small part of the product was transferred on a carbon coated TEM-grid. Then the grid was carefully washed with water, dried at room temperature and analysed with a Zeiss EM 900 transmission electron microscope at 80 kV. Electron micrographs were recorded on Kodak EM-Film Type 4489 and scanned with a SNAPSCAN 1236-scanner from AGFA with 600 dpi.

Enhancement step of the colloids. 8.6 ml of the gold tetrachloride acid stock solution was diluted up to 25 ml and mixed with 100 mg of solid potassium carbonate. After aging over night the solution turned colourless due to the formation of gold hydroxide [24]. Because of the small volume of the reactant only one drop of the $HAuCl_4/K_2CO_3$-solution was added to the solution with collagen which has adsorbed the colloidal gold. Then two drops of a freshly prepared hydroxylamine hydrochloride solution (130 mg/l) was added to initiate the growth of the existing gold colloids. This cycle of growth enhancement was repeated several times.

2.2.5 References

1. a) Y. Xia, Y. Sun, B. Mayers, B. Gates, Y. Yin, P. Yang, Y. Wu, F. Kim, H. Yan, *Adv. Mater.* **2003**, *15*, 353-389. b) H. Jiangtao, W. O. Teri, C. M. Lieber, *Acc. Chem. Res.* **1999**, *32*, 435-445. c) S. Banerjee, D. Dan, D. J. Chakravorty, *Mater. Sci.* **2002**, *37*, 4261-4271. d) V. V. Pokropivnyi, *Powder Metal. Metal Ceram.* **2001**, *40*, 485-496; *Powder Metal. Metal Ceram.* **2001**, *40*, 582-594; *Powder Metal. Metal Ceram.* **2002**, *41*, 123-135.
2. C. F. Monson, A. T. Woolley, *Nano Letters* **2003**, *3*, 359-363.
3. a) M. Mertig, L. C. Ciacchi, R. Seidel, W. Pompe, A. De Vita, *Nano Letters* **2002**, *2*, 841-844; b) D. Zhaoxiang, M. Chengde, *Nano Letters* **2003**, *3*, 1545-1548.
4. J. Richter, R. Seidel, R. Kirsch, M. Mertig, W. Pompe, J. Plaschke, H. K. Schackert, *Adv. Mater.* **2000**, *12*, 507-510.
5. K. Keren, R. S. Berman, E. Braun, *Nano Letters* **2004**, *4*, 323-326.
6. F. Patolsky, Y. Weizmann, O. Lioubashevski, I. Willner, *Angew. Chem.* **2002**, *114*, 2429-2433.
7. a) E. Braun, Y. Eichen, U. Sivan, G. Ben-Yoseph, *Nature* **1998**, *391*, 775-778. b) J. Richter, M. Mertig, W. Pompe, I. Mönch, H. K. Schackert, *Appl. Phys. Let.* **2001**, *78*, 536-538. c) J. Richter, M. Mertig, W. Pompe, H. Vinzelberg, *Appl. Phys. A* **2002**, *74*, 725-728. c) F. Griffin, A. Ongaro, D. Fitzmaurice, *Analyst*, **2004**, *129*, 1171-1175.
8. a) R. Djalali, C. Yung-fou, H. Matsui, *J. Am. Chem. Soc. 2002, 124*, 13660-13661. b) R. Djalali, Y. Chen, H. Matsui, *J. Am. Chem. Soc.* **2003**, *125*, 5873 – 5879; c) L. Yu, I. A. Banerjee, H. Matsui, *J. Am. Chem. Soc.* **2003**, *125*, 14837 – 14840.
9. M. Reches, E. Gazit, *Science* **2003**, *300*, 625-627.
10. B. Yang, S. Kamiya, K. Yoshida, T. Shimizu, *Chem. Commun.* **2004**, 500 – 501.

11. a) M. Mertig, R. Kirsch, W. Pompe, R. Wahl, K. J. Böhm, E. Unger, G. Sadowski, *Thin Solid Films*, **1997**, *305*, 248-253. b) M. Mertig, R. Kirsch, W. Pompe, *Appl. Phys. A* **1998**, *66*, S723-S727. c) W. Fritzsche, K. J. Böhm, E. Unger, J. M. Köhler, *Appl. Phys. Lett.* **1999**, *75*, 2854-2856. d) S. Behrens, K. Rahn, W. Habicht, K. J. Böhm, H. Rösner, E. Dinjus, E. Unger, *Adv. Mater.* **2002**, *14*, 1621 – 1625.
12. a) M. Knez, A. M. Bittner, F. Boes, C. Wege, H. Jeske, E. Maiß, K. Kern, *Nano Letters*, **2003**, *3*, 1079-1082. b) M. Knez, M. Sumser, A. M. Bittner, C. Wege, H. Jeske, S. Kooi, M. Burghard, K. Kern, *J. Electroanal. Chem.* **2002**, *522*, 70. c) E. Dujardin, C. Peet, G. Stubbs, J. N. Culver, S. Mann, *Nano Letters* **2003**, *3*, 413-417.
13. a) C. M. Niemeyer, *Angew. Chem.* **2001**, *113*, 4254-4287. b) E. Katz, I. Willner, *Angew. Chem.* **2004**, *116*, 6166-6235.
14. L. Zhi, C. Sung-Wook, N. Jwa-Min, D. S. Ginger, C. A. Mirkin, *Angew. Chem.* **2003**, *115*, 2408-2411.
15. J. Huang, T. Kunitake, S.-Y. Onoue, *Chem. Commun.* **2004**, 1008-1009.
16. T. Scheibel, R. Parthasarathy, G. Sawicki, L. Xiao-Min, H. Jaeger, S. L. Lindquist, *PNAS*, **100**, 4527-4532.
17. a) O. Harnack, W. E. Ford, A. Yasuda, J. M. Wessels, *Nano Letters*, **2002**, *2*, 919-923. b) A. Kumar, M. Pattarkine, M. Bhadbhade, A. B. Mandale, K. N. Ganesh, S. S. Datar, C. V. Dharmadhikari, M. Sastry, *Adv. Mater.* **2001**, *13*, 341-344. c) T. Yonezawa, Shin-ya Onoue, N. Kimizuka, *Chem. Lett.* **2002**, 1172-1173. d) Y. Maeda, H. Tabata, T. Kawai, *Appl. Phys. Lett.* **2001**, *79*, 1181-1183. e) W. E. Ford, O. Harnack, A. Yasuda, J. M. Wessels, *Adv. Mater.* **2001**, *13*, 1793 – 1797.
18. F. Patolsky, Y. Weizmann, O. Lioubashevski, I. Willner, *Angew. Chem.* **2002**, *114*, 2429-2433.
19. Z. Deyl, I. Miksik, A. Eckhardt, *J. Chromatography B*, **2003**, *790*, 245-275.
20. a) C. C. Dupont-Gillain, E. Pamula, F. A. Denis, P. G. Rouxhet, *Progr. Colloid Polym. Sci.* **2004**, **128**, 98-104. b) N. Gadegaard, S. Mosler, N. B. Larsen, *Macromol. Mater. Eng.* **2003**, *288*, 76-83. c) D. Koruga, A. Tomic, Z. Ratkaj, L. Matija, *Mater. Sci. Forum* **2004**, 453-454 and 529-536. d) Y. Imanishi, N. Kawazoe, K. Ichizawa, *J. Polym. Sci. Part A: Polym. Chem.* **2003**, *41*, 3632–3639.
21. a) M. Goodman, J. Kwak, *Proc. Indian Acad. Sci. - Chem. Sci.* **1999**, *111*, 35-49. b) L. Verestiuc, M. D. Bucevschi, M. Popa, J. C. Alupe, *Europ. Polymer J.* **2003**, *39*, 1501-1508. c) B. M. Syed, T. Gustafsson, J. Kihlberg, *Tetrahedron*, **2004**, *60*, 5571-5575.

22. D. F. Holms, K. E. Kadler, in: J. R. Harris (Edt.): Current protocols in cell biology protocol; in preparation
23. D. G. Duff, A. Baiker, P. P. Edwards, *Langmuir*, **1993**, *9*, 2301-2309.
24. a) H. B. Weiser, The Colloidal Elements; Wiley: New York, **1933**. b) D. G. Duff, A. Baiker, I. Gameson, P.P. Edwards, *Langmuir*, **1993**, *9*, 2310-2317.
25. D.J. Prockop, K. I. Kivirikko, L. Tuderman, and N. A. Guzman *New Engl. J. Med.* **1979**, *301*, 13-23.
26. M. A. Hayat, Colloid Gold: Principles, Methods, and Applications; Academic Press: New York, **1989**; Vol. 1, p 3.
27. C. Graf, A. van Blaaderen, *Langmuir*, **2002**, *18*, 524-534.

3. Controlled Crystallization of Calcium Phosphate and Mineralization Studies with Additives on Functionalized Self-assembled Monolayers

3.1 Cooperative Effect of Self-assembled Monolayer and Perlucin on the Crystallization of Hydroxyapatite

3.1.1 Introduction

Living organisms are able to control the crystallization process of inorganic minerals like silica, calcium carbonate, calcium tartrate or calcium phosphate leading to inorganic-organic composite materials with specific polymorphic structure, size, morphology and function [1]. One of the most important biomineral, in addition to calcium carbonate, is calcium phosphate. It is a constituent in bone, tooth, and other mammalian hard tissue often as hydroxy- or fluoro apatite, sometimes accompanied with carbonate. The calcium phosphate formation in vivo takes place under controlled nucleation and growth [2]. It also plays a role in medical application when undesired nucleation and growth onto biomaterial implant surfaces [3] or arteriosclerotic vessel walls [4] occur, which cause a major problem by resulting in implant failure.

The apatite formation in vivo is a very complex process. The mineral nucleates directly onto collagen fibrils [5], onto noncollagenous proteins associated with the collagen surface [6], or within matrix phosphoprotein vesicles which are transported to the collagenous matrix within woven bone and cartilage [7]. Noncollageneous glycoproteins which were isolated from mineralized tissue include bone sialoprotein [8], osteonectin [9], osteopontin [10], bone acidic glycoprotein-75 [11] and others [12].

Extensive studies on the mechanisms of calcium phosphate crystallization have been accomplished over the last two decades [13] even though it is not yet completely understood so far. It was shown, that biomacromolecules like proteins and carbohydrates play a central role in this process and that the formation of biominerals occurs at an organic-inorganic interface [1, 14, 15]. The most important reason for understanding the calcium phosphate

crystallization mechanism, amongst others, is the compatibility improvement of medicinal implants. Hence, it is not surprising that there have been numerous previous studies of calcium phosphate growth concerning the modelling in in-vitro-systems. Some of these works can be summarized as growth of calcium phosphate thin films [16] from high supersaturated solutions like physiological solutions onto planar substrates like oxides, metals or glass [17], on collagen [18] and studies concerning the constant composition methods [19] which study the nucleation and growth kinetic onto suspended particles and macromolecules. Nucleation has been related to titania surfaces [20], amino acid-capped gold nanoparticles [21], porous calcium phosphate ceramics [22], negatively charged surfaces such as silica [23], polymers [24], and charged macromolecules [25]. Other substrates for crystallization are liposomes [26], giant ABA triblock copolymer vesicles [27], a water-in-water mesophase [28] and polyelectrolyte multilayer films [29]. A model system which could reveal the fluoroapatite formation in teeth is the double diffusion technique [30]. Other works relating to solution based precipitation of calcium phosphate were done in presence of dendrimers [31] or other organic additives [32] and foreign cations [33]. Also the crystallization behaviour on langmuir monolayer was studied [34].

The macromolecules which promote the mineralization in living organisms can be divided in two classes namely in hydrophilic proteins or carbohydrates which have a high solubility and an insoluble matrix like collagen or chitin which support the crystallization process.

Our research group is focussed on the investigation of the crystallization behaviour of calcium carbonate on self-assembled monolayers [35] (SAM) and the cooperative effect by soluble additives [36]. Studies of calcium phosphate crystallization on self-assembled monolayers is less common [37] and the cooperative effect of soluble additives was not object so far with the exception of at least two studies, where calcium phosphate was crystallized on different substrates in the present of additives [38].

To bridge this gap we want to present in this work the influence of the cooperative effect of Perlucin, a soluble protein isolated from abalone shells which promote the calcium carbonate precipitation, and self-assembled monolayers as substrate on calcium phosphate formation. We used the gas diffusion technique to initiate by a pH switch the precipitation of calcium phosphate onto self-assembled monolayer tethered to gold slides from an acidic phosphate buffer solution in the presence and absence of Perlucin at room temperature and 34 °C. After the reaction is finished the dried gold slides were analyzed by high resolution scanning electron microscopy (HRSEM) and the formed crystals composition identified by micro

Raman spectroscopy (μ-RS). Further quartz crystal microbalance – dissipation (QCM-D) and plasmon spectroscopy were used to monitor the adsorption of Perlucin onto the SAMs as the latter method was used for following the crystallisation kinetic onto SAMs. At least it was tried to demonstrate the adsorption of Perlucin onto two different phospholipids monolayers and the kinetic of calcium phosphate crystallization.

3.1.2 Results and Discussion

Crystallization Experiments in the absence of Perlucin. Previous crystallisation studies onto SAMs were carried out exclusively under pseudo physiological conditions at a pH of 7.4 and a high ionic strength from supersaturated aqueous solutions. Most of the studies propose a crystallization mechanism by a heterogenic induction of crystal formation by the SAMs [37c,d]. However Tarasevich and co-workers could show that the nucleation mechanism involves solution-formed nuclei which are adsorbed or transported to growth sites onto the SAMs [37a]. This hypothesis of precipitation mechanism is in agreement with observations made in living systems during natural biomineralization of calcium phosphate. Nuclei may be preformed in separated compartments in vivo where nucleation takes place under fine controlled conditions and afterwards carried to the bone growth sites. Colloidal calcium phosphate was found within matrix vesicles aligned with the mineralization front of bone and cartilage [6]. But ruptured vesicles were also found at bone growth sites indicating that the vesicle-derived calcium phosphate is involved in bone growth [39].

Tarasevich [37a] could reveal the formation of colloidal calcium phosphate by atomic force microscopy which is adsorbed onto SAMs with a diameter of ~185 Å or less. It was tried to remove the colloids by ultrafiltration before the start of the reaction but did not succeed and thus they were still existent. The Posner cluster, $Ca_9(PO_4)_6$, is another particle in discussion to be formed in solution prior to adsorption [40]. The cluster is supposed to be formed under alkaline and neutral and probably under acidic conditions in aqueous solution but the clusters have a diameter of 8-10 Å whereas the observed particles were larger.

This work, where we use a gas diffusion method to initiate the calcium phosphate precipitation onto SAMs by a pH switch, is also based on the adsorption of primarily formed colloidal particles. Afterwards these particles are adsorbed to the surfaces. After one week

crystal growth is supposed to be finished due to the final alkaline pH of ~8-9 resulting in a very low concentration of reactants in solution.

For crystallization experiments were used self assembled monolayers with hydrophilic head groups like the polar and acidic surface (COOH), the polar but alkaline surface (NH_2), the polar and neutral surface (OH), and a hydrophobic end group (CH_3) were used. Figure 3.1.1 shows high-resolution scanning electron micrographs of the different terminated surfaces after crystallization. At a pH of 5.3 all reactants are dissolved completely in water because the solubility product of all modifications of calcium phosphate is not reached. The crystallization was initialized by a pH sweep from 5.3 up to ~8-9 caused by a slow diffusion of ammonia into the reaction solution which increases the hydrogenphosphate concentration. At a pH of 5.8, calcium phosphate begins to precipitate. As mentioned above, under these conditions of relatively high concentrations of the reactants, colloidal particles of calcium phosphate which adsorb onto the surface are produced.

On all surfaces needle like crystals are grown that at first view are apatite needles. The size of the needles is nearly equal independent from the surface modification that ranges in a length of ~200-300 nm and a width of ~50 nm. However the number of crystals differs from one surface to another indicating a variation of seed crystal density depending on the surface. NH_2 terminated monolayers show a dense carpet of interleaved needles, and the OH terminated surface also displays a carpet of needles but less dense with an incomplete covering of the monolayer. On the other hand the COOH and the CH_3 terminated surfaces show island like bundles of needles whereas the COOH surface has a denser distribution than that of the CH_3 terminated surface. Though it can be given a ranking of the surfaces regarding the induction of the seed formation:

$$NH_2 >> OH > CH_3 > COOH$$

The NH_2 terminated surface has the highest seed induction potency can be explained by the protonation of the terminal functional group at the precipitating pH forming a positive charged $–NH_3^+$ group. The calcium phosphate particles are formed in solution and stabilized by electrostatic interaction as they have a negatively charged surface at an acidic pH stabilized by hydroxoniumions which form a small layer on the particles. Thus they can be adsorbed onto the surface by removing the protecting layer and afterwards the typical needles of hydroxo apatite are formed. The OH and COOH terminated surfaces are polar but not deprotonated at a pH of 5.8 whereas the OH group is showing a stronger interaction with the apatite colloids forming a more dense covering of needles over the surface. The hydrophobic

surface interacts only slightly with the charged colloids thus the surface shows a low allocation of crystals. The absence of a continuous plane layer of calcium phosphate on all surfaces is an evidence for the adsorption of previously formed calcium phosphate colloids. Also the round needle bundles point out a growth of a particulate seed crystal.

The seed crystal density distribution on SAMs with different polarities described in literature is varying especially in respect to the ranking of NH_2 and COOH terminated monolayers [37 a,d]. The crystal density distribution is contrary to that found in this work. This can be explained by the different pHs which are used in experiment. The studies described in literature are using pseudo physiological solutions with a pH of 7.4. For this reason the NH_2 surface is not protonated. On the other hand the COOH surface is deprotonated at pH values higher than 5.8.

The composition of the crystals was revealed by Raman micro-spectroscopy. On all surfaces hydroxyapatite was found. A typical and representative Raman spectrum measured from crystals grown on the CH_3 SAM is shown in Figure 3.1.4c along with a reference spectrum of hydroxyapatite in 4a. The spectrums are showing the typical peak with a very strong intensity of all hydroxyapatites at a wavenumber of 965 cm^{-1} [41]. All peaks in the spectrums of the crystals grown on the CH_3 SAM are showing a peak broadening. This can be explained by a low crystallinity of the crystals due to a disorder in the crystal structure by fast growth. A chemical disorder by incorporating foreign ions into the apatite structure can be excluded due to the defined composition of the reaction mixture.

Crystallization experiments in presence of Perlucin. When Perlucin, a protein extracted from Abalone shells, is added to the reaction mixture before the pH switch is initiated, the seed formation is different. Figure 3.1.2 shows characteristic scanning electron micrographs of calcium phosphate crystals grown on the different terminated monolayer surfaces. The NH_2 and COOH modified surfaces still display hydroxyapatite needles wherein the NH_2 surface shows a compacter and denser covering. On the OH terminated surface only isolated needle conglomerates and mainly the bare monolayer surface is found. The hydrophobic surface is very different compared to the other surfaces and to the hydrophobic surface, when used in absence of Perlucin. The monolayer is covered completely with a sponge like structure. Measurement with Raman micro-spectroscopy reveals that the sponge is composed of hydroxyapatite (Figure 3.1.4b). It is not possible to distinguish individual needles as the needles are orientated along distorted axes and associated with each other. This represents a

surprising and unexpected result that can not be explained easily, but should be influenced by the Perlucin. By taking into account that the concentration of the Perlucin is extremely low, the influence of the protein is impressive. Repeated experiments resulted in the same observation. The ranking of the crystal density distribution on the surface is completely different:

$$CH_3 >> NH_2 > COOH > OH$$

The ranking for NH_2 and COOH SAMs can be explained as above. The presence of Perlucin seems to have no effect on the seed crystal density or at most a small influence. For the appearance of the OH surface we do not have an explanation.

The influence of temperature on the crystallization behaviour in the presence of Perlucin was investigated by carrying out the same experiment at a higher temperature, at 34 °C. The result of the SEM analysis of the surface is shown in figure 3.1.3. On all surfaces hydroxyapatite needles are organized mainly in the form of islands. The covering on the NH_2 surface is now comparable to the CH_3 surface. On these two surfaces a high number of bundles of needles in the form of round island. On the other two surfaces are mainly grown small bundles of needle along with large ones with diameters of ~6-8 µm. The small needle bundles seem to have short time of growth. On the NH_2 surface the bundles seems to grow together. The density distribution of the crystals on the SAMs is:

$$NH_2 \approx CH_3 > OH > COOH$$

For the NH_2 terminated SAMs, the surface charge is determined by the amount of precipitated material on the surface as explained above. The high amount of material on the CH_3 surface can be ascribed to the presence of the Perlucin. Further investigation was focussed on the interaction of Perlucion with the SAMs. QCM-D measurements and surface plasmon resonance spectroscopy were used for the kinetic study of the adsorption of Perlucin onto the SAMs.

QCM-D measurements. The influence of Perlucin on the crystallization of calcium phosphate by precipitation out of solution was analysed by measuring the adsorption of Perlucion as a soluble component onto the self-assembled monolayers as substrate. The measurements were done at a constant pH of 5.3. The oscillation of the quartz crystal was followed until equilibration was reached. The Perlucin solution was then diluted in solvent mixture, injected into the reaction chamber; the frequency shift and the dissipation shift were observed. The experiments were carried out isothermally at 25 °C. The results are shown in

figure 3.1.5. The frequency shift varies depending on the surface. COOH shows the mayor shift of ~21 Hz, OH and NH_2 show a less shift of ~11 and ~10 Hz resp. and whereas CH_3 shows the slightest shift of around 8 Hz. The following washing steps reveal that ~75 percent of the Perlucin is permanently attached to the surfaces. As the dissipation is low in all measurements, which means that there is an adsorption of rigid or flat laying proteins on the surface and the Sauerbrey equation [42] can be used for determining the amount of adsorbed Perlucin (Table 3.1.1). The COOH terminated monolayer adsorb 372 ng/cm^2 which is in line with one molecule of Perlucin (18128.8 g/mol) occupies 8 nm^2. On a CH_3 terminated SAM, one molecule of Perlucin occupies about 21 nm^2, which means that one molecule disposes off a surface area of 2.6 over that of COOH surface. This means, on one hand, the Perlucin molecule on the COOH surface seems to be packed densely on the CH_3 surface or on the other hand, the Perlucin molecule on the CH_3 SAM is perhaps altered by the surface and is lying as a flat molecule on the surface compared to the molecule on the COOH surface, thus forming a dense packing. For the other two surfaces values in-between can be found. In order to decide these situations kinetic studies of adsorption of perlucin were carried out with SPR.

	COOH	OH	NH_2	CH_3
Δ f [Hz]	21	11	10	8
m [ng/cm^2]	372	195	177	142
surface area occupied by one molecule of Perlucin [nm^2/Perlucin molecule]	8	15	17	21

Table 3.1.1: Frequency shift of quartz crystals of the adsorption of Perlucin onto self-assembled monolayers with different polarities determined from QCM-D measurements and the calculated occupation of the surface areas using the Sauerbrey relation for rigid molecules: $\Delta m = -\frac{C \cdot \Delta f}{n}$, where C = 17.7 ng Hz^{-1} cm^{-2} for a 5 MHz quartz crystal and n = 1,3,5,7 is the overtone number. (Molecular mass of Perlucin: 18128.8 g/mol)

Kinetic studies with surface plasmon resonance spectroscopy. The surface plasmon resonance spectroscopy is a versatile and sensitive tool for kinetic measurements of adsorption of material onto gold surfaces. Here it is used to measure the adsorption of Perlucin onto the different surfaces by modified self-assembled monolayers of different ω-terminated thiols. Figure 3.1.6 shows the time dependent measurements for the adsorption of Perlucin onto the COOH, OH, CH_3 and NH_2 SAMs using SPR. As the picture shows the thickness of layers varies depending on the layer composition. On CH_3 ($\Delta\theta$ = 0.16°) the smallest amount of Perlucin is adsorbed. On the OH ($\Delta\theta$ = 0.54°) terminated monolayer more

Perlucin is adsorbed while on the COOH ($\Delta\theta$ = 0.60°) and NH_2 ($\Delta\theta$ = 0.66°) terminated surfaces the strongest adsorption can be observed. Perlucin is adsorbed on each surface even on the CH_3 terminated SAM which represents a remarkable result. This indicates that Perlucin must have a broad variability due to his composition and spatial structure which permits an interaction with these different surfaces of such different properties. The curve of the adsorption of Perlucin onto the OH, COOH and CH_3 SAMs indicate a step-like increase. This means that in a real short time of ~5-10 minutes these surfaces reach a thermodynamic equilibrium. The interaction between these surfaces must differ. Perlucin has a theoretical isoelectrical point (pI) of ~7.15, which results in a positive charge of the protein at a pH of 5.3. The interaction between OH and COOH SAMs (COOH: should be nearly completely protonated), and the Perlucion should be based on ionic-polar forces, while the interaction between CH_3 and Perlucin should consist of hydrophobic-hydrophobic forces. The curve progression of the Perlucin adsorption shows a different picture. At first a sharp step is observed, which seem to level up to a certain coupling angle, but is not stable for a long time and starts to increase after a while and reaches the final value after ~3 days. The NH_2 surface should be partially protonated and thus positively charged in parts. The sharp step can be explained by an interaction between the surface and protein defined by polar-polar or polar-ionic forces, but when the curve slowly increases an interaction between two positively charged reactants must take place. A rearrangement of the Perlucin molecules can be the reason for the long equilibrium time which clearly demonstrates the flexibility and multifunctionality of the protein.

The increase of the coupling angle by the COOH, OH and NH_2 SAMs is nearly the same (0.6°, 0.54° resp. 0.66°) which means that the thickness of the layers formed by the protein is more or less the same for all surfaces. The QCM-D measurements of the adsorption of Perlucin onto the above mentioned surfaces above show a decreasing amount of surface area of the protein in the same order. Thus, in conclusion it can be stated that having the same layer thickness, the protein molecules are relatively more dense packed on the COOH-SAM, while the packing density decreases over the OH- to the NH_2-SAM whereas the volume i. e. the form of the protein molecules does not change during the adsorption process not even on the NH_2 modified surface. CH_3 terminated SAM shows the thinnest layer and smallest amount of Perlucin. If the Perlucin molecules were unaltered like on the other surfaces, the CH_3 SAM would also show the same layer thickness, because the SPR cannot distinguish single protein molecules. Thus, we can conclude that the Perlucin molecules are altered at the CH_3

terminated SAMs, maybe by the hydrophobic surface alone or together with some influence from the dissolved species.

SPR as a tool for tracking kinetics of calcium phosphate crystallization

Measurements in the absence of Perlucin during nucleation and crystal growth: Figure 3.1.7 shows the time dependence of the surface plasmon reflectivity for the growth of calcium phosphate onto SAMs with a mixture of the calcium chloride and phosphate buffer (both 0.01 M; pH 5.3) in the measuring cell. Crystallization was induced by a slow diffusion of ammonia gas into the solution causing a pH switch. As it can be seen the thickness of the formed calcium phosphate layer varies from one surface to another. The thickest layer is formed on the NH_2 terminated surface with a coupling angle shift of ~0.75°. The OH-SAM follows with ~0.73°, followed by the CH_3 terminated surface with an angle shift of ~0.29°. The least increment shows the COOH surface with ~0.19°. The thickness relation can be compared to the crystallization experiments described above and it is in accordance with them. The different final thicknesses of the layers can also be explained by different densities of the mineral. The experiments were accomplished always with the same concentrations of reactants, thus it cannot precipitate more product on one as on another surface. This means that the COOH surface builds a very dense calcium phosphate while CH_3 surface forms a lighter and the NH_2 and OH surfaces lead to the lightest product. But the micrographs in Figure 3.1.1 show only needles of hydroxyapatite, thus the differences in density can be explained only by the arrangement of the needles. If the density is low but the layer thick, a stack of needles is observed building a dense overlayer as shown in Figure 3.1.1 for the NH_2 or the OH SAMs. If the density is high but the layer thin as in the case of CH_3 or COOH terminated surfaces the needles are packed in island like bundles, like hay stacks.

In addition the curve progression is different. The curve obtained by the CH_3 surface shows a simple progression. Once the crystallization started the angle shift reaches a maximum in a short time which keeps constant. All the other curves show a local maximum during progression which is arrived also in a very short time comparable to that of the CH_3 SAM. These local maximums remain constant for a while. Depending on the modified surface a further increase up to a final maximum begins earlier regarding the NH_2 surface, after ~3500 minutes, followed by the OH surface at ~4500 minutes and latest on the COOH SAM after ~8500 minutes of crystallization. These steps cannot be explained easily. We assume that in the beginning the adsorption speed and amount of colloidal calcium phosphate which is

formed in solution, is independent of the NH_2, OH and CH_3 SAMs. Afterwards the calcium phosphate layers formed on the NH_2 and OH surface start to grow again. In an acidic solution this surfaces seem to be favoured for the adsorption process while the protonated COOH SAM seems to inhibit or at least reduce the amount of adsorbed material. The second maximum observed on the NH_2, OH and on the COOH surface can be attributed to an induced rearrangement of the calcium phosphate crystals caused by the surface functionality i. e. a redissolution and reprecipitating of the material forming larger crystals which are thermodynamically more stable and thus increase the coupling angle. This rearrangement should be a short range process due to the final alkaline pH which means that the concentrations of the calcium and phosphate ions are very low which do not permit a large scale and long distance material transport. This slow mobility explains the long time to reach the second maximum. The time shift until the second step takes place varies from the NH_2, OH to the COOH SAM. On the COOH surface the layer growth needs 8500 minutes, nearly a week, for initialization while on the NH_2 surface the increase begins after around 3500 minutes. This can be explained by a stronger force between the COOH surface and the adsorbed colloidal calcium phosphate which prevents the redissolution of the calcium phosphate and thus prolonging the time needed for rearrangement and crystal growth. On the other hand the NH_2 surface seems to promote a rearrangement due to a weaker interaction between surface and colloidal calcium phosphate as on the OH or COOH surfaces.

Measurements in the presence of Perlucin during precipitation. Figure 3.1.8 shows the time dependence of the surface plasmon reflectivity for the growth of calcium phosphate onto SAMs in presence of Perlucin. The adsorption of Perlucin is not shown in this figure. The curve progression is nearly the same for all functionalized surfaces. The crystallization begins quickly after initialization and reaches a constant maximum during a short time of equilibration, between ten and twenty minutes. The remarkable feature in this graph is the induction of the formation of the thickest calcium phosphate layer by the CH_3 terminated surface. Onto the other three surfaces nearly the same thickness was found. These properties of the graphs can be explained only by the presence of Perlucin. Perlucin is adsorbed on each surface as shown above even though the adsorbed amount is different. The CH_3 SAM forms the thickest layer which is in agreement with the crystallisation experiments which show a complete covering of the substrate with a spongy calcium phosphate (Figure 3.1.2). The presence of Perlucin results in nearly the same thickness of the calcium phosphate layer

regarding the COOH, OH and NH_2 modified surfaces. That means that the density of the formed calcium phosphate is the same for these three surfaces but less dense as a sponge in the case of the crystallisation on the CH_3 modified surface. In each experiment the same amount of reactants is used.

The final maximum is reached on each surface maybe due to the catalytic properties of Perlucin onto the crystallization, leading to the densest packing of the thermodynamically stable phase of calcium phosphate.

SPR as an experimental tool for kinetic measurement of the calcium phosphate crystallization onto phospholipid monolayers. Here we demonstrate the use of phospholipid monolayers to simulate cell wall like structures to study the influence of adsorbed Perlucin onto the calcium phosphate crystallization and growth. Even if the Perlucin is not classified as a membrane protein the interaction of the membrane and adsorbed Perlucin can be considered as an important factor on the crystallization process. Figure 3.1.9 shows the time dependence of the surface plasmon reflectivity for the growth of calcium phosphate onto a phospholipid monolayer. For all three measurements it can be observed that the phospholipid monolayers are formed quite good over night. Both phospholipids used in this study are able to adsorb Perlucin, but from the PLP1 monolayer it is washed away after two cleaning steps while on the PLP2 monolayer the Perlucin remains even after washing with solvent. This can be explained by the permanent zwitterionic property of the PLP1 monolayer (For structure formula see Table 3.1.2). This feature seems to be responsible for the inhibition of a permanent adsorption of the Perlucin. Taking into account the slow adsorption of Perlucin onto NH_2 SAM accompanied by a long period to

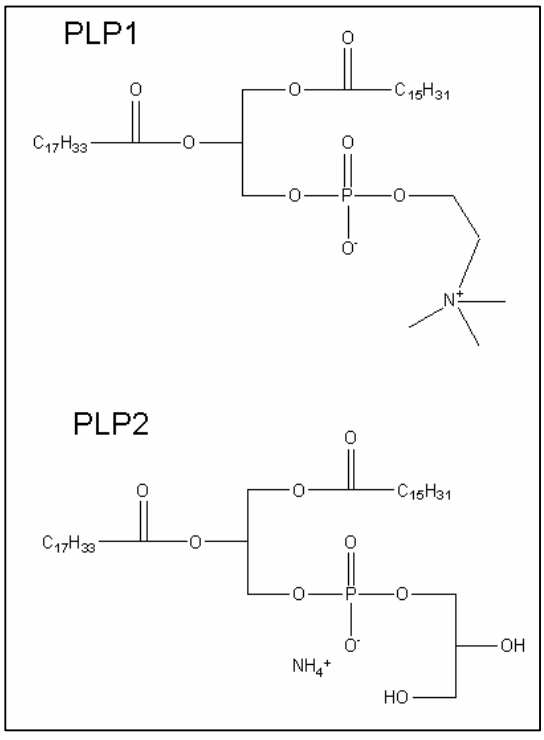

Table 3.1.2: Formulas of phospholipids used for kinetic measurements of Perlucion adsorption and crystallization experiments: 2-Oleoyl-1-palmitoyl-sn-glycero-3-phosphocholine (PLP1) and 1-Palmitoyl-2-oleoyl-sn-glysero-3-phospho-rac-(1-glycerol) ammonium salt (PLP2)

reach a thermodynamic equilibrium shown in figure 3.1.6 can be concluded that also a possible rearrangement of the SAM surface by charge displacement can have an influence on the amount of adsorbed Perlucin. The zwitterionic PLP1 is not able to relocate his charges thus, also if a structural rearrangement of the Perlucin molecule is probable, the interaction force between Perlucin and PLP1 monolayer is not strong enough and though the adsorption is reversible.

The kinetic measurements of the crystallization onto PLP2 in the presence and in the absence of Perlucin are depicted in figure 3.1.6. The curve progression of the calcium phosphate crystallization reveals that, in the case of Perlucin presence, a very fast increase of layer thickness occurs. The exact thickness could not be measured but the thickness´ increase is impressive. This can be explained by the formation of a very low dense calcium phosphate material. On the other hand the plain PLP show a calcium phosphate thickness increase comparable to the mineral layer formed on OH and NH_2 SAMs in absence of Perlucin. This behaviour can be ascribed to a glycerol rest (OH functionalities) that works as end group of the PLP2.

From this experiments can be concluded, that Perlucin can adsorb onto phospholipid monolayers and induce and promote the crystallization of calcium phosphate. At the same time it was demonstrated that it is possible to study the kinetic behaviour of the crystallization process on phospholipids monolayers by SPR spectroscopy which is a powerful tool for future investigations around the biomineralization.

Final discussion. Perlucin has a wide influence of the crystallization and growth of calcium phosphate on CH_3 terminated monolayers as could be demonstrated in this work. A comparable influence of Perlucin adsorbed on a hydrophobic surface on the crystallization of calcium carbonate was shown previously [39]. This influence can be ascribe to the structure of the Perlucin molecule. For that reason it is interesting to take a deeper insight into the molecular properties of Perlucin. Perlucin belongs to the group of “C-type lectines”. This means, that the molecule can bind a sugar molecule like D-mannose/D-glucose and D-galactose [43]. The conditions for the extraction and cleaning procedure are extreme and it is not sure if this treatment negatively affects the molecule leading to a loss of structure. However the purified Perlucin still shows biological activity and this can be ascribed to two reasons: either the Perlucin renaturates quickly or it has a rest of activity that resisted the cleaning operations. Also the computed instability index [44] of the amino acid sequence of

Perlucin is ~56.5 which classifies the protein as instable (Calculated by [49]). Taking into account this probable instability of the Perlucin molecule it can be assumed that the molecule can unfold at least partly effected by the hydrophobic CH_3 surface. Perlucin consists of 155 amino acids. From these, ~30 % are hydrophobic and ~70 % hydrophilic amino acids. The aliphatic index of the molecule is 59, which means that the percentage of the relative volume occupied by aliphatic side chains which in comparison to a low amount of hydrophobic amino acids is interesting. The polarity of the amino acid sequence of Perlucin was analyzed by the method described by Bull and Breese. The diagram is depicted in Figure 3.1.10 [49]. The diagram reveals that there are a couple of short hydrophobic sequence pieces which appear alternately with hydrophilic pieces along the sequence. The protein seems to be instable and perhaps tends to unfold partly. Thus we can assume that the protein can be tethered onto the surface by hydrophobic interactions without hindering the active side which promotes the mineral crystallization. This hydrophilic part of the protein should be turned upside. This theory is supported by the observation, that Perlucin molecules, bonded to the CH_3 surface, occupy more surface area than on the other SAMs and at the same time form a thinner layer which can be accomplished only by an unfolding of the protein. Moreover, the lowest amount of Perlucin is adsorbed onto CH_3 terminated substrates. The exact hydrophilic part of the protein responsible for the crystal growth cannot be determined by the methods used in this study and should be investigated in a further study.

In addition it is interesting that Perlucin has nearly no influence on the crystal growth on another more hydrophilic support. Taking into account the flexibility which is shown by the Perlucin on the hydrophobic surface one could expect that the protein has to be activated in vivo by the cell double membrane which mainly consists of lipids. But to reveal the influence it is necessary to do more experiments.

3.1.3 Conclusion

In this study we could demonstrate that there is existent a cooperative effect between a hydrophobic self-assembled monolayer and Perlucin, a soluble protein, which acts as a promoter for the biomineralization. This work suggests that Perlucin molecule is a very flexible molecule when it is adsorbed onto CH_3 modified surface. Here it is able to accelerate the crystal formation by unfolding the active side of the protein. This kind of behaviour was

also found on a phospholipid monolayer. However this activation is not observed on other modified and more hydrophilic self-assembled monolayers. Thus it can be speculated if the protein must be activated in vivo by the cell double membrane which mainly consists of lipid molecules. Future work is necessary to understand the crystallization size of the Perlucin molecule.

3.1.4 Experimental Section

Chemicals. 4-Aminothiophenol (abbreviated **NH_2**) (96%) was purchased from Acros and hexadecanethiol (abbreviated: **CH_3**) (synthesis grade) from Merck. $CaCl_2 \cdot 4\ H_2O$ (Suprapur, Merck), H_3PO_4 (98 %, Merck) NaOH (p.a., Acros), H_2O_2 (35%, Acros), water (Barnstead Easypure UV, $\rho > 18{,}3\ M\Omega\ cm^{-1}$), ethanol (p.a., Riedel de Haen), ammonia (25 %, Riedel de Haen). Stock solutions with a concentration of 0,1 mol/l were prepared of calcium chloride by dissolution of the solid compound and of phosphate buffer by dilution of concentrated phosphoric acid adjusting the pH with 0,1 M NaOH to 5,3.

Synthesis of 1,11-mercaptoundecanoic acid (abreviated: COOH). a) Bunte salt: 17.6 g of sodiumthiosulfate pentahydrate was dissolved in 50 ml water and added to a hot solution of 15 g (57 mmol) 1,11-Bromundecanoic acid (Acros) in 80 ml ethanol. Afterwards the mixture was heated under reflux for four hours. After cooling the white product was filtered, cleaned with ethanol and dried.

b) 1,11-mercaptoundecanoic acid: 14.3 g of the Bunte salt was dispersed in a degassed mixture of 80 ml distilled water and 5 ml ethanol and 16 ml concentrated hydrochloric acid was added. The suspension was heated under reflux in nitrogen atmosphere for six hours and then it was cooled down to 4° C. The white product was filtered and dissolved in 30 ml dichloromethane, and the resulting solution was washed with 3 M sodium chloride solution and with distilled water. After desiccation over calcium chloride the organic solvent was removed and a white product obtained.

Yield: 5.9 g (24.4 mmol, 46.3%)

Synthesis of 11-mercapto-1-undecanol (abreviated: OH). a) Bunte salt: 20.1 g (80 mmol) 11-brom-1-undekanol (Acros) was dissolved in 60 ml ethanol and mixed with a solution of

24.8 g sodium thiosulfate pentahydrate in 60 ml distilled water. The mixture was heated under reflux for four hours. The product precipitated during cooling to room temperature. The white solid was filtered, recrystallized from ethanol and dried.

b) 11-mercapto-1-undecanol: The Bunte salt (20.5 g) was hydrolysed in a mixture of ethanol/water (50:5 ml) by addition of 10 ml concentrated hydrochloride acid and heating under reflux for 6 h. After cooling to 4° C the precipitated product was filtered and extracted with petrolether. The organic solution was washed with water and the solvent evaporated. The residue was redissolved in dichloromethane and washed with 3 M sodium chloride solution, dried over calcium chloride and afterwards the solvent was removed. After drying in vacuum the white product was recrystallized twice from ethanol.

Yield: 9.7 g (48.5 mmol, 54 %)

Isolation and purification of Perlucin [45]. Shells of the species Haliotis laevigata were purchased from the Australien Abalone Exports Pty. (Victoria, Australia). The shells consist of a calcite and an aragonite fraction. To remove the calcite outer-layer fraction of the shells, they were sand blasted. The aragonite inner-layer fraction, which is called nacre (mother of pearl), was rinsed with 25 mM Tris buffer, pH 7.4, cracked in small parts, placed into a dialysis tubing (Visking Typ 8/32 Roth, cut-off 15 kDa, Karlsruhe, Germany) and this filled with the same buffer. The open ended dialysis tubing was connected to a tube for collection of the overflow. The following steps were carried out at 4 °C. By addition of 10 % acetic acid, the solution began to develop foam resulting from the release of carbon dioxide. The overflow of the foaming solution was collected until foaming stopped. By replacing the dialysis buffer against fresh 10 % acetic acid, the foaming started again and the overflow was collected in a second tube. Afterwards this procedure was repeated for four times resulting in totally six fractions of 4-40 ml of foam raw extract during one week of treatment. All fractions and the remaining suspension were centrifuged at 5445 g for 50 min at 4 °C. The supernatant solution were dialysed against three changes of 30 volumes of 25 mM Tris, pH 7.4, 0.002 % NaN_3, sterilized by filtration through a 0.22-mikrom filter and stored at 4 °C. For purification, ion exchange chromatography was performed using a Pharmacia CM-Sepharose Fast Flow HiTrap column with a linear gradient of 0-1 M NaCl in 25 mM citrate buffer, pH 5.0, for 20 min at a flow rate of 1 $mLmin^{-1}$. The obtained protein fractions were concentrated in a speed vac concentrator and analyzed by SDS-PAGE sing a 10-20 % gradient Bio-Rad Ready-Gel system. N-terminal amino acid sequence analysis was performed using a PE-Applied

Biosystems Procise sequencer model 473A after desalting of the sample with the ProSorb device (PE-Applied Biosystems) or after reversed phase HPLC.

Preparation of gold substrates and SAMs. Glass slides (B 270/38 X 26 X 1 mm) were cleaned by heating at 80 °C in a mixture of water-ammonia-H_2O_2 (5:1:1, v/v/v) during 10 minutes followed by rinsing with water and ethanol and then blowing dry with a nitrogen gas. The glass slides were transferred to a Balzer BAE 250 vacuum coating system and coated at a pressure lower than 5 x 10^{-6} hPa coated first with 2 nm Cr to improve adhesion, and then with 50 nm Au (rate 0.1 nm s^{-1}). After cooling the gold slides were used as soon as possible but not more than two hours after preparing. They were added to solutions of **COOH** in toluene, **OH** in ethanol, **CH_3** in toluene and **NH_2** in a mixture of toluene/ethanol (5:1; v,v) at concentrations of ~1 x 10^{-3} M. After 24 h of adsorption and equilibrating the slides were removed, rinsed vigorously with solvent to remove unbound thiols and blown dry with nitrogen gas. The SAMs were used for crystallization experiments and for kinetic measurements with plasmon resonance spectroscopy.

Crystallization Experiments. Growth experiments were performed with the gas diffusion technique. The crystallization was accomplished in a Glass Coplin Staining Jar, containing 30 ml of a mixture of the calcium chloride and phosphate buffer (both 0.01 M; pH 5.3). 0.1 ml of Perlucin solution (0.05 mg/ml citrate buffer (20 mM)) was added. The final concentration of Perlucion was 1.7 x 10^{-4} mg/ml (9.6 x 10^{-9} M). The gold slides with SAMs and a glass slide were placed vertically into the solution that they were submerged completely. Then the reaction vessel was placed into a desiccator. For thermal equilibration the whole crystallization batch was reposed for two hours at room temperature or in a digitally controlled oven (Heraeus Instruments) at 34 °C. The crystallization was started by placing a snap-cap-vial with 60 µl half concentrated ammonia into the desiccator. The crystallization took place by the slow diffusion of NH_3 gas into the solution causing a switch of pH up to a value of 8-9 over a 7 day period. Afterwards the substrates were removed, dried at room temperature and prepared for microscopy analysis.

Scanning electron microscopy studies. For microscopic studies the slides used for crystallization were cut into small pieces and fixed with conducting glue or tabs on alumina sample holders and analyzed with a Zeiss Digital Scanning Microscope 962 at acceleration

potentials of 5-15 kV or with a LEO 1550 high resolution Scanning electron microscope at acceleration potentials of 1-3 kV.
Samples for the Zeiss Microscope were sputtered with gold before analyzing while the samples for the LEO Microscope were used without sputtering.

Quartz Crystal Microbalance – Dissipation (QCM-D). QCM-D measurements were carried out on a Q-sense D 300 system (Q-sense, Sweden). AT-cut quartz crystals coated with gold films are cleaned prior to use by a treatment with H_2O_2/NH_3/Millipore-water (1:1:5, v/v/v), 10 min. 80°C) and afterwards rinsed consecutively with Millipore-water and iso-propanol. After drying with a N_2-flow, crystals were exposed for at least 24 hours to a diluted thiol-solution, subsequently rinsed with solvent and dried with N_2. After installing the quartz crystals, the measuring cell was set to 25 °C and equilibrated. Then the cell was filled with a mixture of calcium chloride and phosphate buffer (both final concentrations: 0.01 M; buffer: pH 5.3). By exchanging the solvent consecutively with a corresponding solution containing Perlucin (100 µl Perlucion solution/2 ml solvent), the adsorption of the protein onto the thiol-terminated gold surface was monitored by a decrease of the frequency. Furthermore the energy dissipation D was measured simultaneously. The measurements were performed in a static solution (batch mode).

Raman micro-spectroscopy[46]. Raman micro-spectroscopy was performed with a LabRAM HR800 (Horiba Jobin Yvon). This confocal Raman system is based on a dispersive spectrometer with notch-filter and focal length of 800 mm. It was equipped with Olympus BX41 optical microscope and Peltier-cooled hCCD (charge-coupled device) detector. The spectra were excited with the 514,5 nm emission of an Argon-ion-laser. The lateral resolution was better than 1.5 µm and the volume resolution was ca. 5 μm^3. The wavenumber accuracy was 0.5 cm^{-1} and the spectral resolution was about 1.0 cm^{-1}.

Surface plasmon resonance spectroscopy (SPR). SPR was used in the Kretschmann configuration[47] to evaluate the adsorption of Perlucion onto self-assembled monolayers and for following the kinetics of crystal building and growth. Sample slides were placed in a liquid filled Teflon cuvette filled with 2 ml of a mixture of calcium chloride and phosphate buffer (both 0.01 M; pH 5.3). A few experiments were performed under the addition of 100 µl Perlucin and measured until equilibrium was reached. To measure the kinetic of

crystallization a reservoir with half-concentrated ammonia was connected by capillary tubing with the Teflon cuvette and the crystallization was initiated by opening the stop cock. The backside of the slides was coupled optically via an optical matching fluid (n=1.7000) to an LASFN9 prism (n=1.85 at λ= 632.8 nm). The optical source was a He-Ne laser (λ = 632.8 nm, 5 mV power). The kinetic experiments were performed in the coupled angle mode by following the minimum over a period of several days.

Kinetic measurement of Perlucin binding and calcium phosphate crystallization onto phospholipid (PLP) monolayer by SPR

25 mg 2-Oleoyl-1-palmitoyl-sn-glycero-3-phosphocholine (99%) (**PLP1**) and 25 mg 1-Palmitoyl-2-oleoyl-sn-glycero-3-phospho-rac-(1-glycerol) ammonium salt (99%) (**PLP2**) (For formula see Table 3.1.2) both purchased from Sigma were dissolved at a time in 20 ml Dichloromethane. 0,5 ml of the PLP solution was dried in a nitrogen flow, 5 ml of a mixture of calcium chloride and phosphate buffer (both 0.01 M; pH 5.3) was added, and hold for 15 minutes in a ultrasonic bath. With the final dispersion the measuring cell, which had a CH_3 SAM installed, was washed and awaited for equilibration indicating the end of the PLP monolayer formation onto the CH_3 terminated SAM. After cell washing with a mixture of calcium chloride and phosphate buffer (both 0.01 M; pH 5.3), as much Perlucin solution (100-150 µl) was added to reach stable signal. The cell was washed again with solvent, connected with the ammonia reservoir and the crystallization initialized.

3.1.5 Figure Part

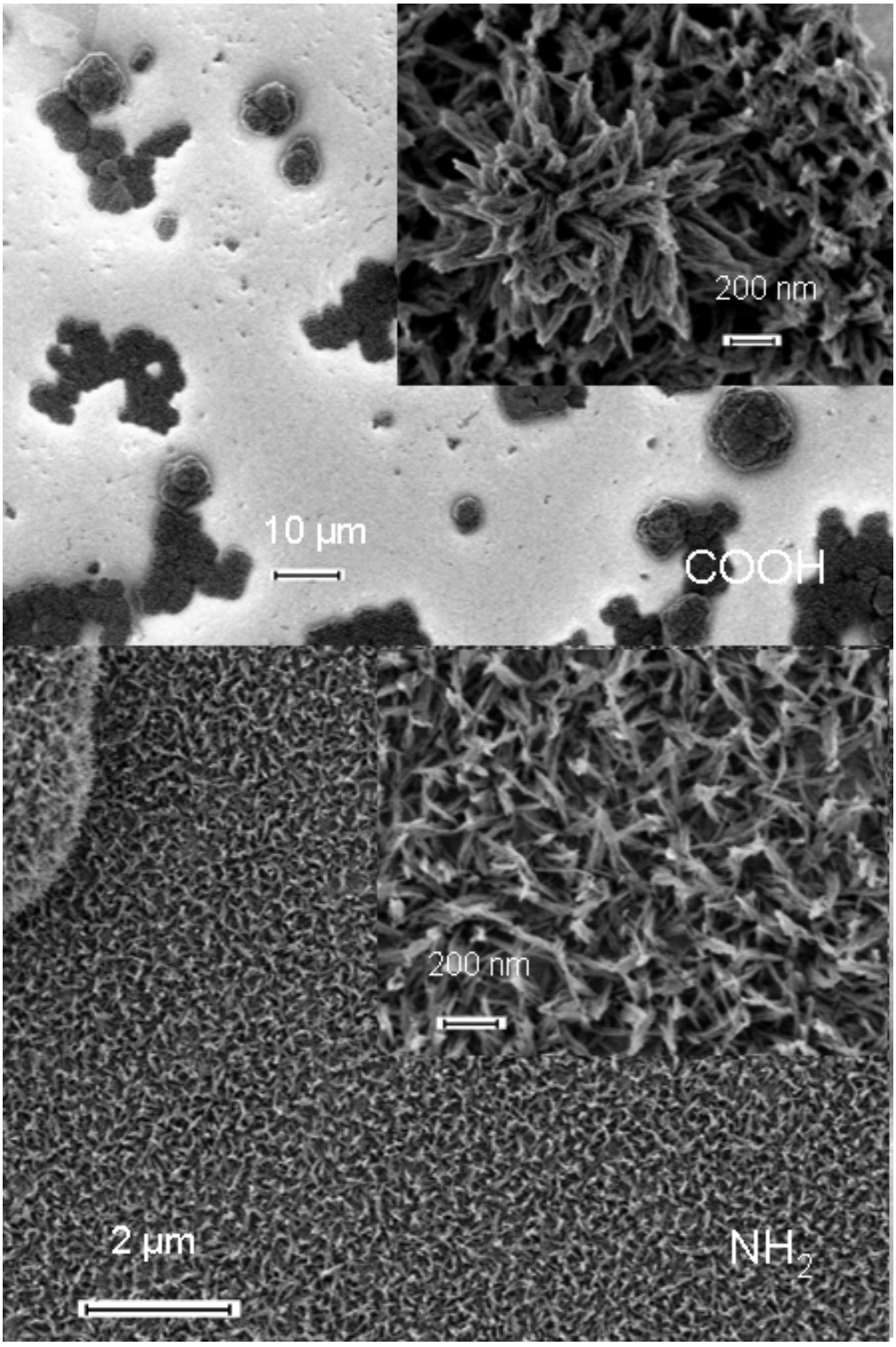

Figure 3.1.1 (a): Scanning electron micrographs of calcium phosphate precipitated without any additive on self-assembled monolayer with different polarities, pH switch 5.3-9 at room temperature after a reaction time of 7 days. All samples are

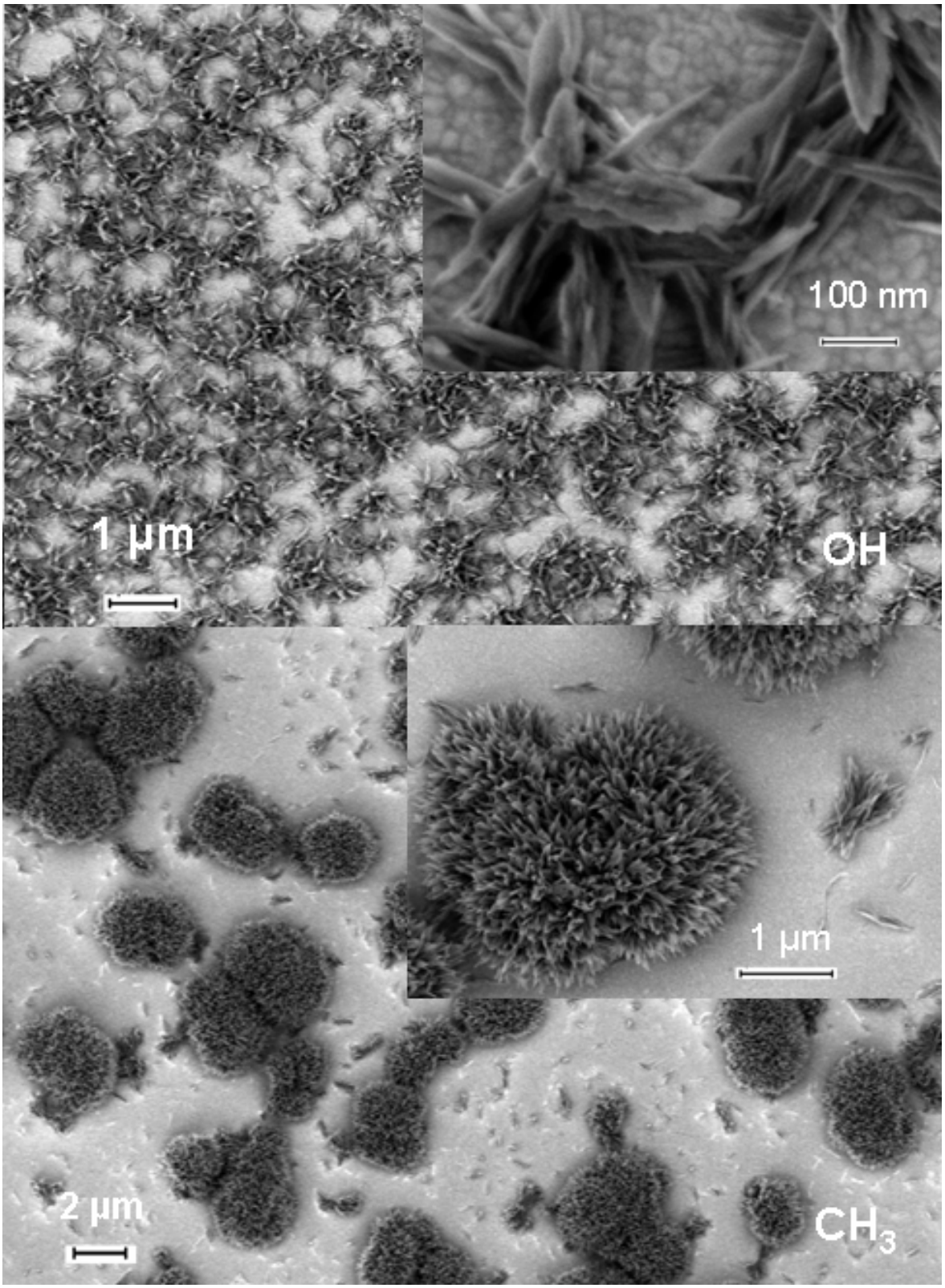

Figure 3.1.1 (b): Scanning electron micrographs of calcium phosphate precipitated without any additive on self-assembled monolayer with different polarities, pH switch 5.3-9 at room temperature after a reaction time of 7 days. All samples are unsputtered.

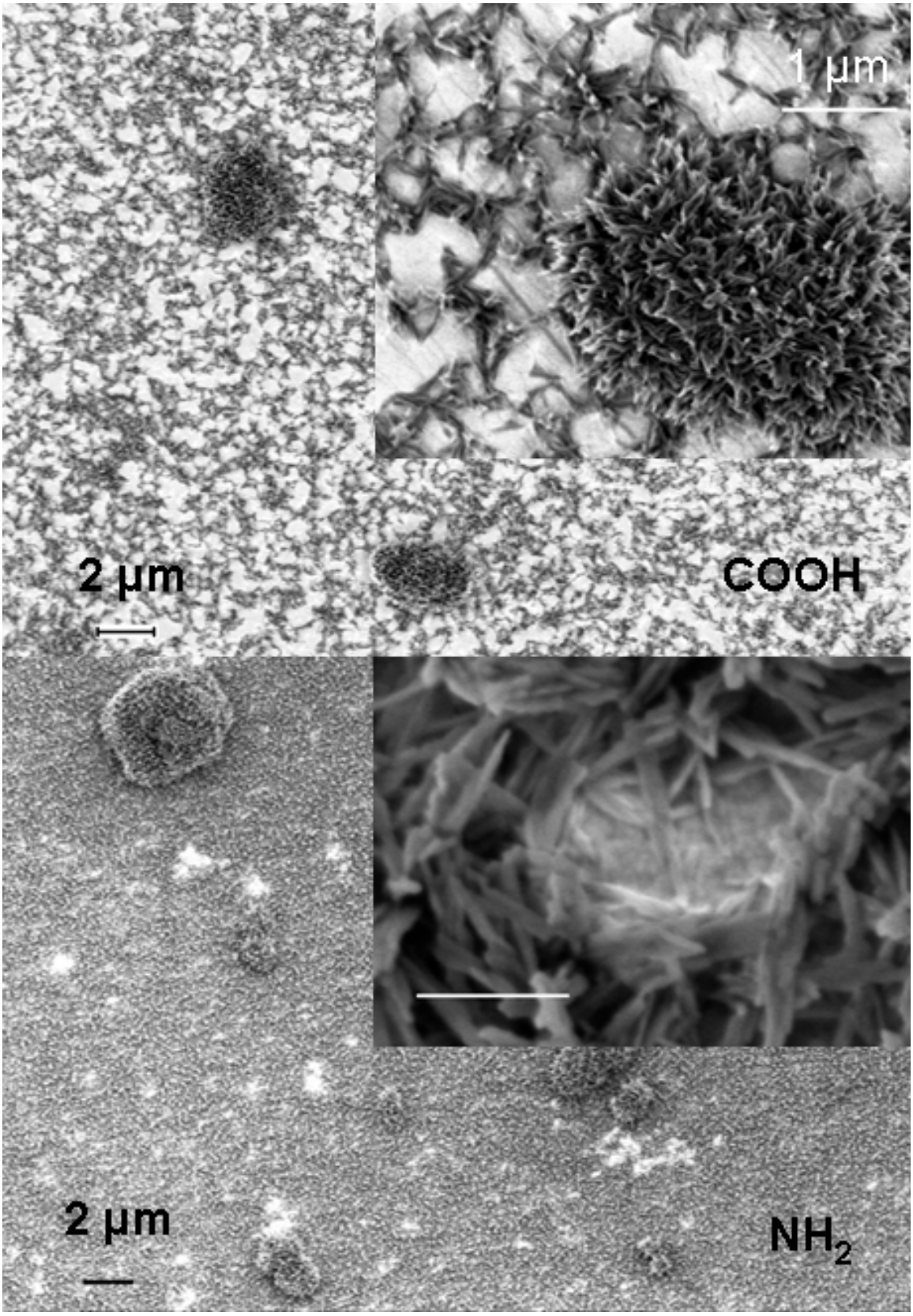

Figure 3.1.2 (a): Scanning electron micrographs of calcium phospate precipitated in the presence of Perlucin on self-assembled monolayers with different polarity, pH switch 5.3-9 and room temperature after 7 days reaction time. All samples are unsputtered.

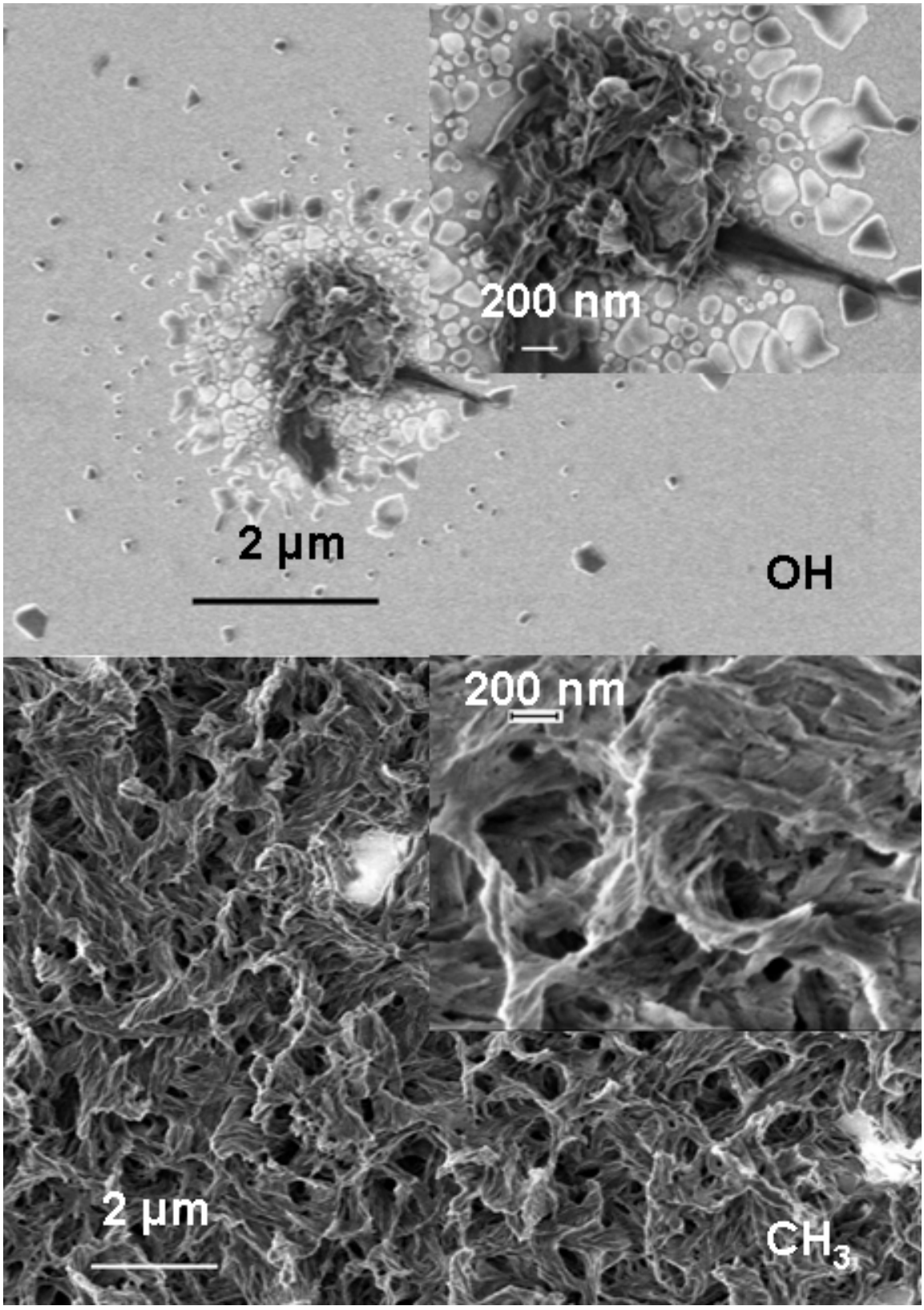

Figure 3.1.2 (b): Scanning electron micrographs of calcium phospate precipitated in the presence of Perlucin on self-assembled monolayers with different polarity, pH switch 5.3-9 and room temperature after 7 days reaction time. All samples are unsputtered.

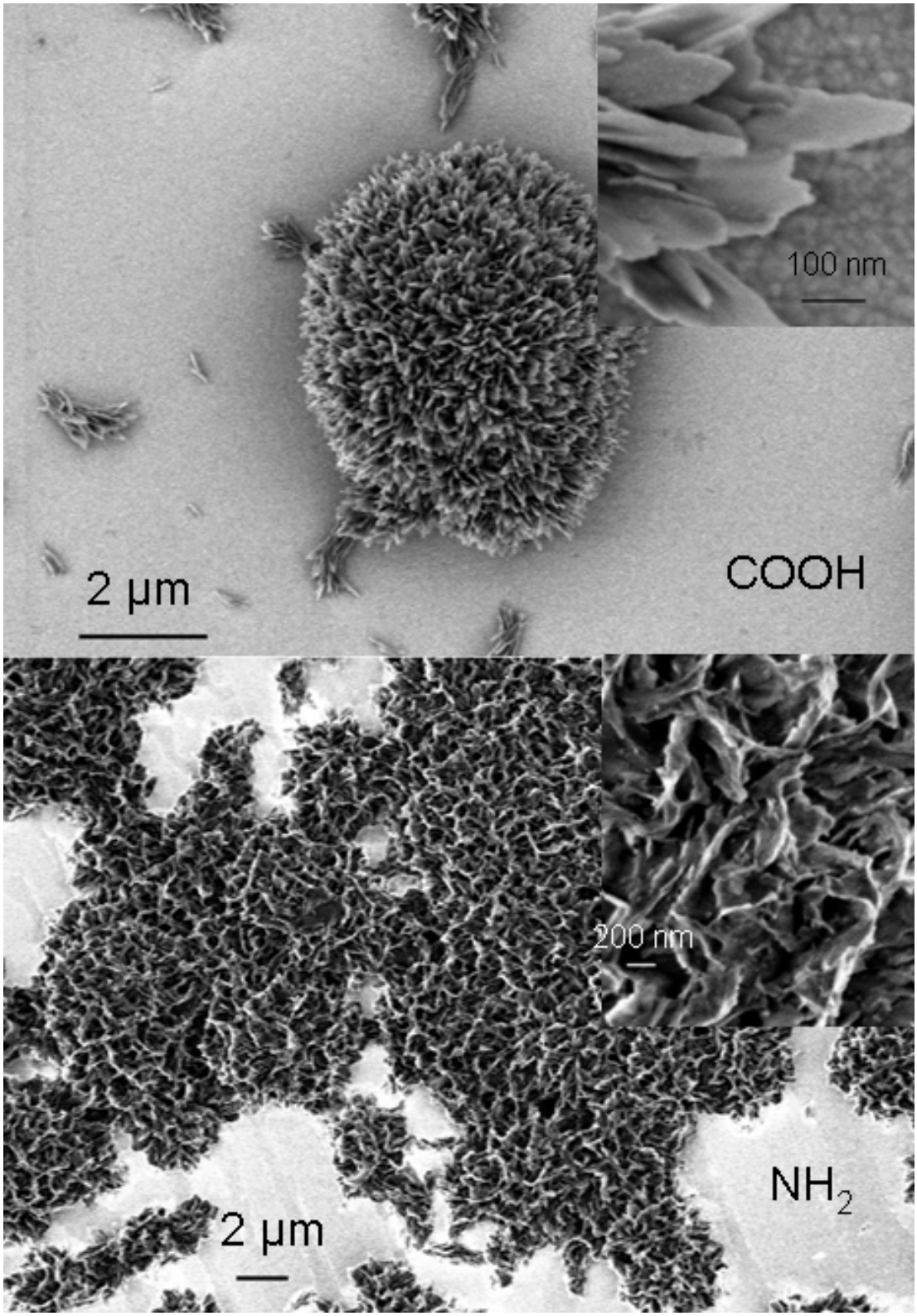

Figure 3.1.3 (a): Scanning electron micrographs of calcium phospate precipitated in the presence of Perlucin on self-assembled monolayers with different polarities, pH switch 5.3-9 and at 34 °C after 7 days reaction time. All samples are unsputtered.

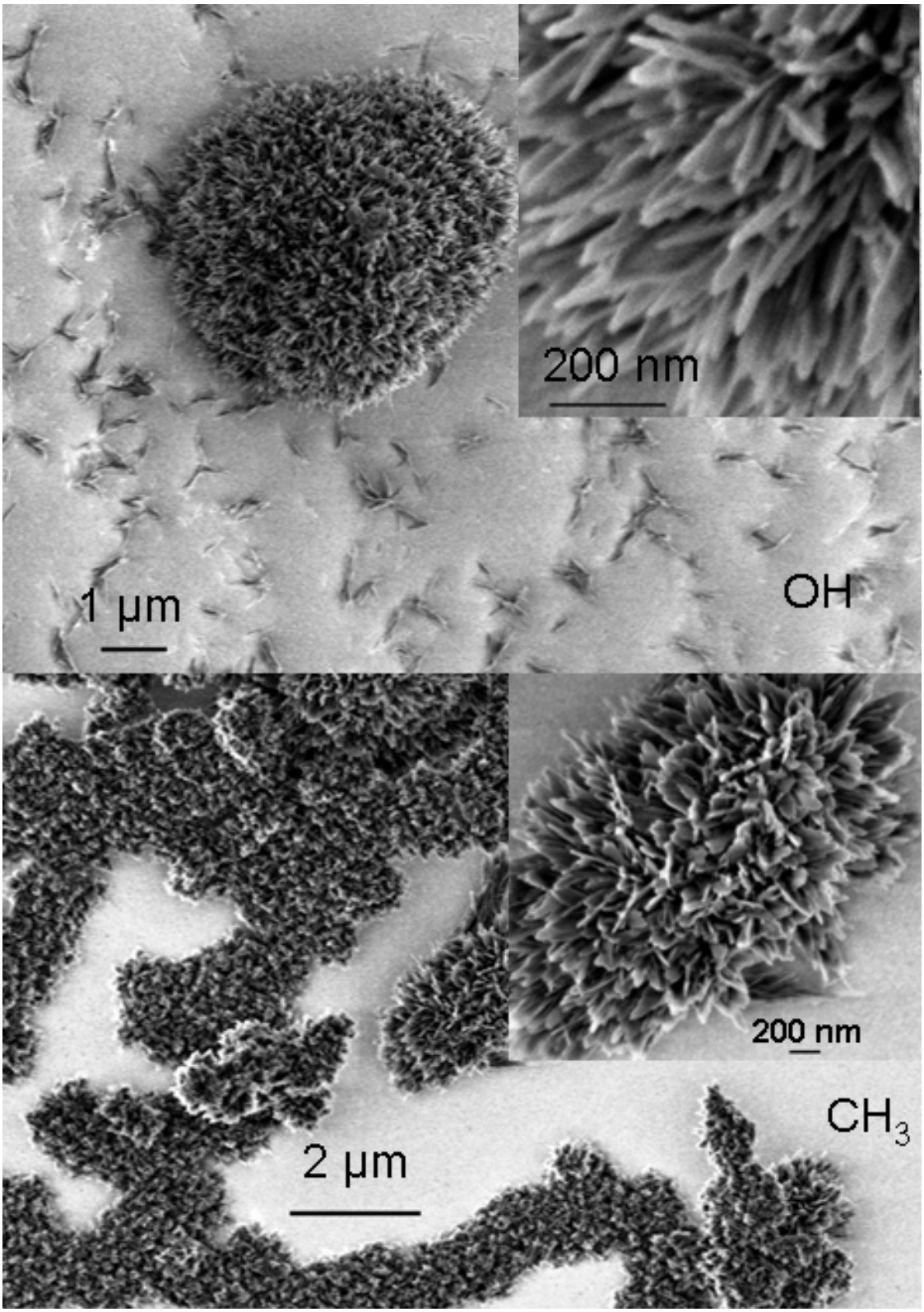

Figure 3.1.3 (b): Scanning electron micrographs of calcium phospate precipitated in the presence of Perlucin on self-assembled monolayers with different polarities, pH switch 5.3-9 and at 34 °C after 7 days reaction time. All samples are unsputtered.

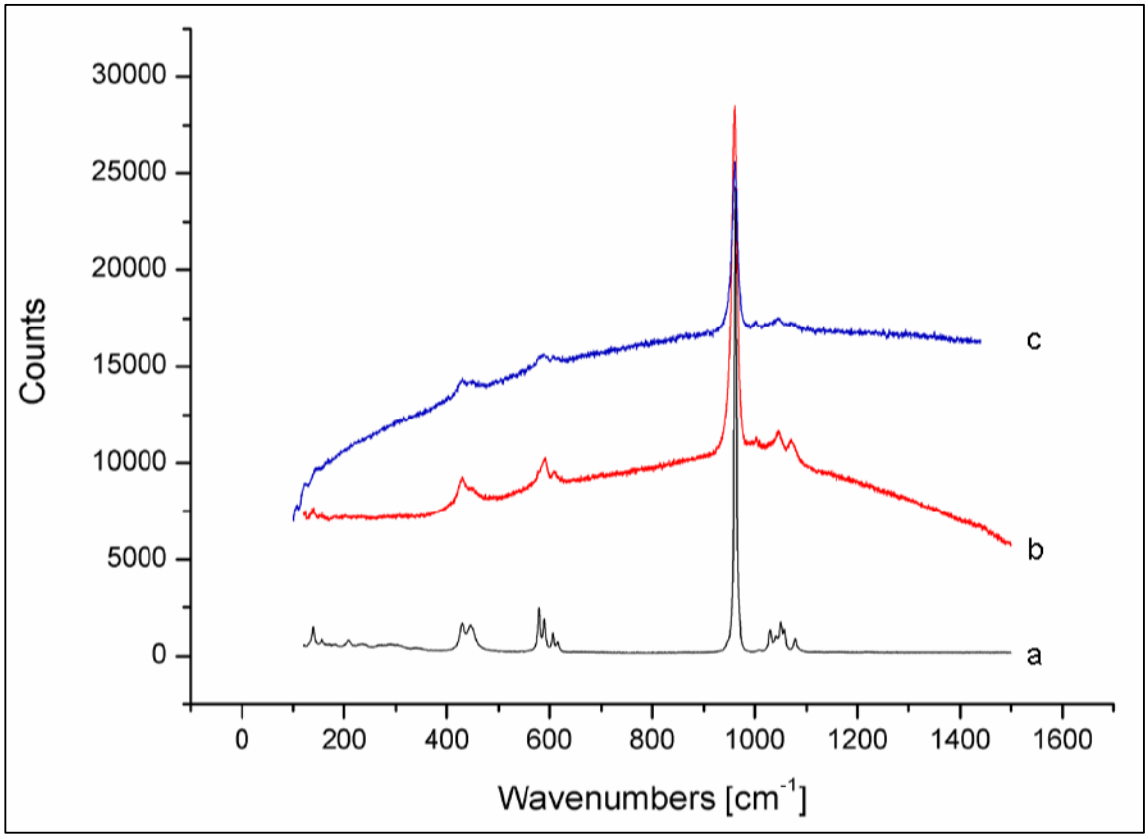

Figure 3.1.4: Raman spectra of calcium phosphate crystallized on self-assembled monolayer with or without Perlucin: a) Reference spectrum apatite, b) spectrum of apatite crystallized on CH_3-monolayer in presence of Perlucin at room temperature, c) apatite formed in the absence of Perlucin on CH_3-monolayer at room temperature

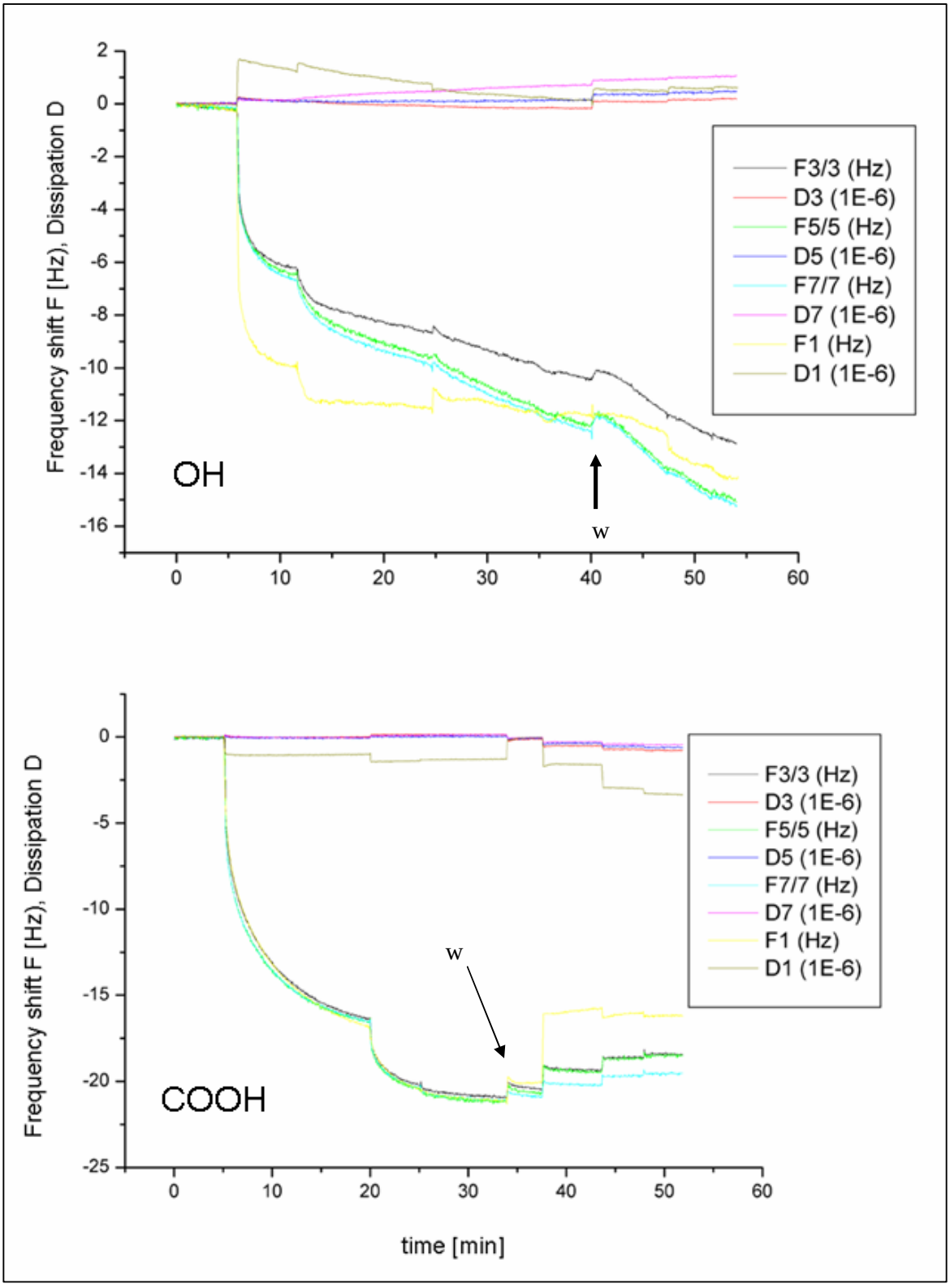

Figure 3.1.5 (a): Perlucin adsorption to self-assembled monolayer with different polarities revealed by isothermal QCM-D measurements from crystallization solution at a pH of 5.3 at 25 °C. (w = cell washed with solvent)

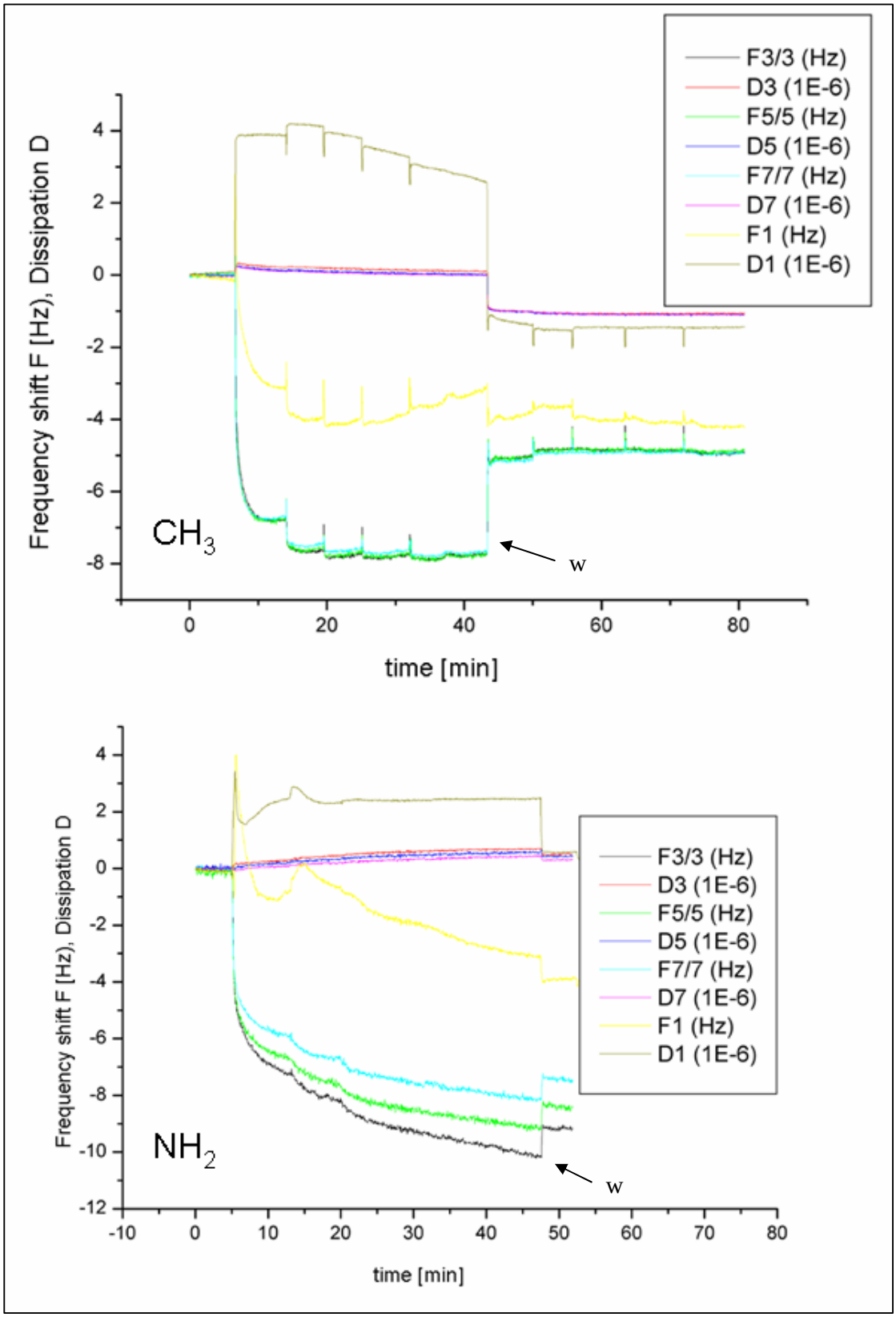

Figure 3.1.5 (b): Perlucin adsorption to self-assembled monolayer with different polarities revealed by isothermal QCM-D measurements from crystallization solution at a pH of 5.3 at 25 °C. (w = cell washed with solvent)

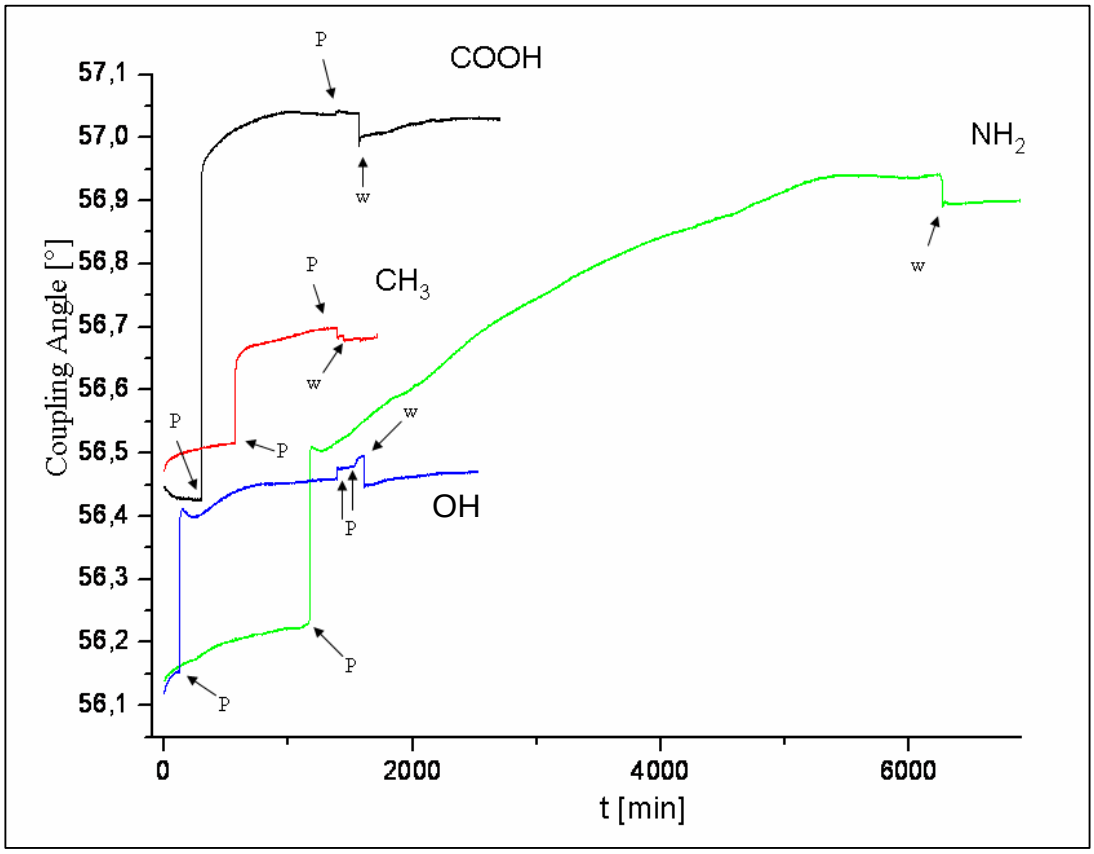

Figure 3.1.6: Time dependence of the surface plasmon reflectivity for the adsorption of Perlucin onto self-assembled monolayer in a mixture of calcium chloride and phosphate buffer at pH 5,3. (p: addition of Perlucin solution; w: washing with solvent)

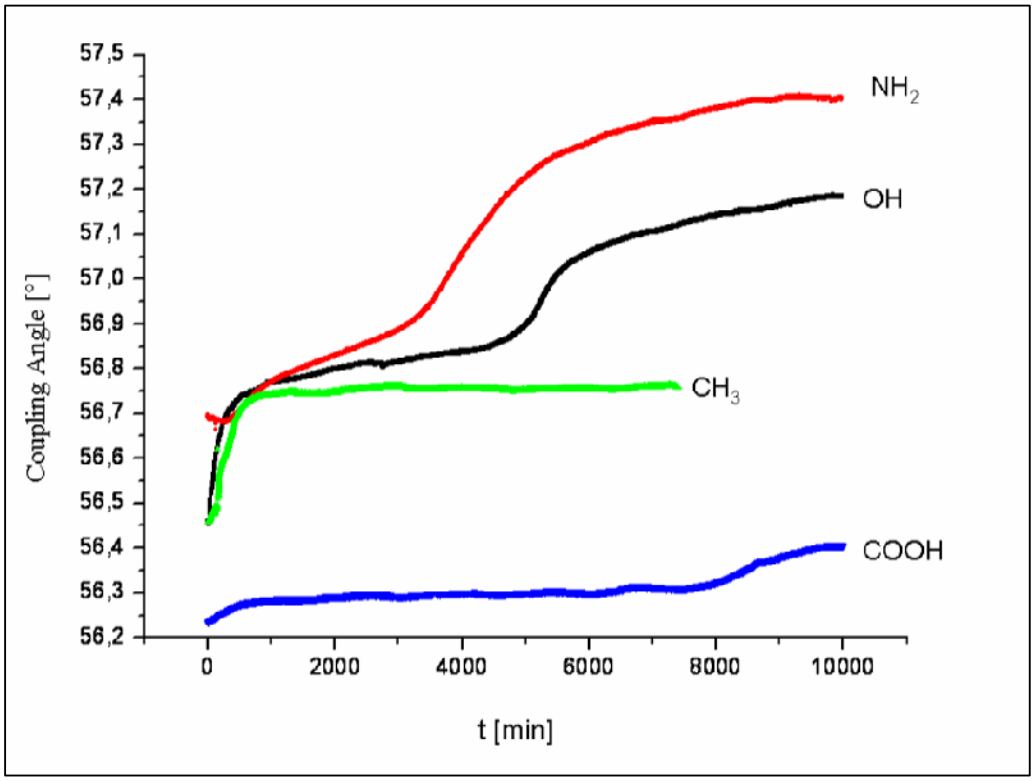

Figure 3.1.7: Kinetic measurement of the crystallization of calcium phosphate on self-assembled monolayers in the absence of additives.

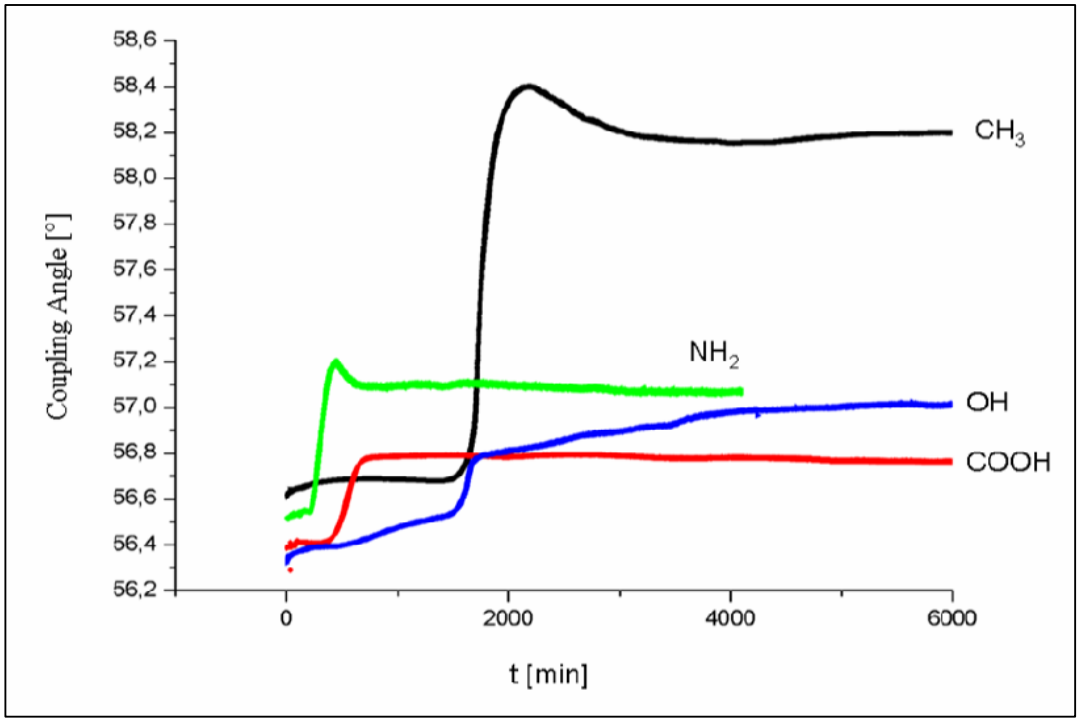

Figure 3.1.8: Kinetic measurement of the crystallization of calciumphosphate on self-assembled monolayers in the presence of Perlucin (adsorption from Perlucin is not shown)

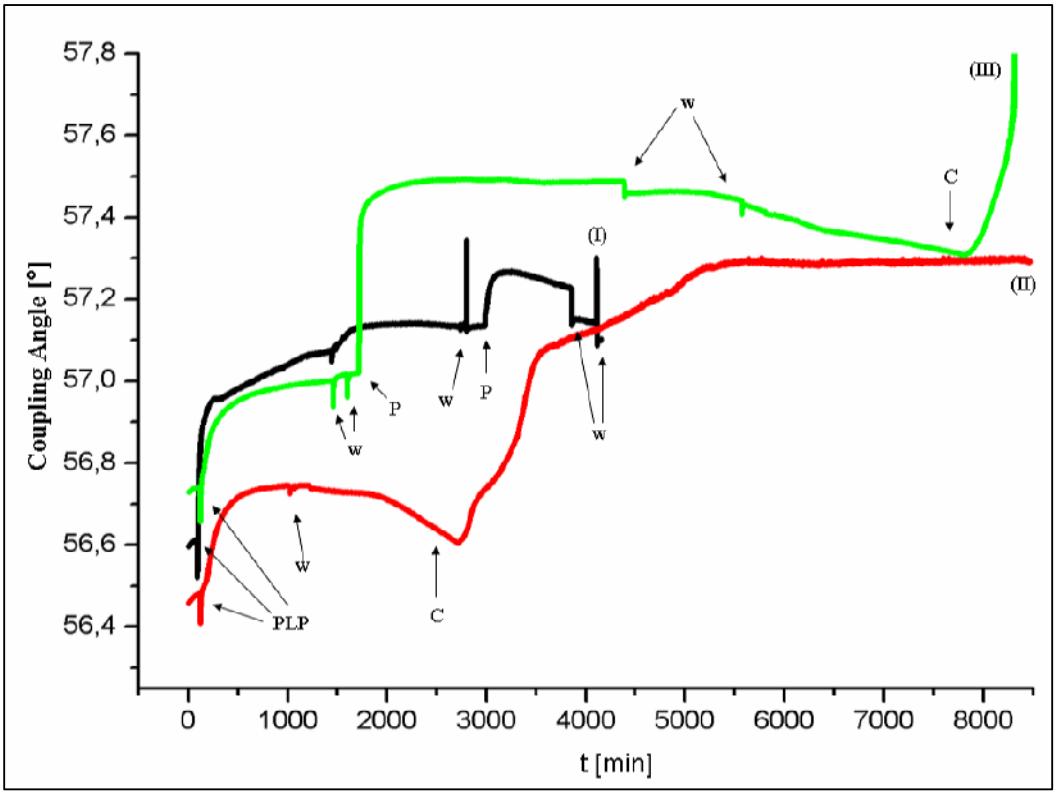

Figure 3.1.9: Time dependence of the surface plasmon reflectivity for the adsorption of Perlucin onto CH_3 surface with two different phospholipid monolayers and afterwards the crystallisation of calcium phosphate from a mixture of calcium chloride and phosphate buffer at pH 5,3. (I, black line): PLP1 monolayer with the adsorption of Perlucin, but Perlucin is washed away after two washing cycles ; (II, red line): formation of a monolayer of PLP2 without adsorption of Perlucin on it and afterwards the crystallization of calcium phosphate; (III, green line): Formation of a monolayer of PLP2 with the adsorption of Perlucin an afterwards the crystallization of calcium phosphate (PLP: washing with the corresponding phospholipid dispersion; P: addition of Perlucin solution; w: washing with solvent)

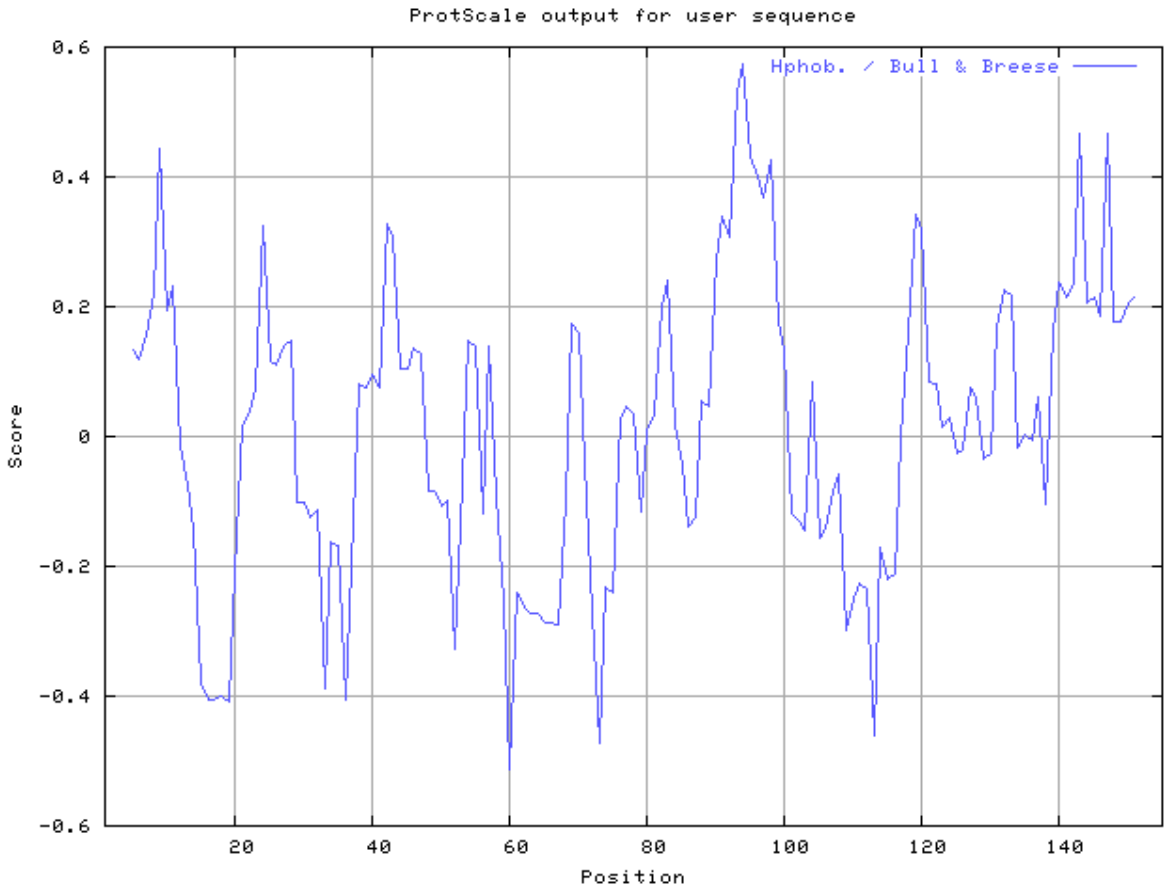

Figure 3.1.10: Polarity of the amino acid sequence of Perlucin analyzed using the hydrophobic scale of amino acid residues by H. B. Bull and K. Breese[1]. (Negative values mean more hydrophobic, positive values mean more hydrophilic amino acid). Calculated online by the ExPASy Proteomic Server [49]

3.1.6 References

1) (a) E. Baeuerlein, (Edt.): *Biomineralization - Progress in Biology, Molecular Biology and Application*, 2nd ed,. Wiley-VCH, Weinheim, **2004.** b) S. Mann: *Biomineralization - Principles and Concepts in Bioinorganic Materials Chemistry*, Oxford University Press, New York, **2002**. c) Lowenstam, S. Weiner (Eds.), *On Biomineralisation*, Oxford University Press, New York, **1989**. d) S. Mann, J. Webb, R.J.P. Williams, *Biomineralization: Chemical and Biochemical Perspectives*, VCH Publishers, New York, **1989**.
2) H. A. Lowenstam, S. Weiner: *On Biomineralization*, Oxford University Press: New York, **1989**.
3) a) R. J. Levy, J. Wolfrum, F. J. Schoen, M. A. Hawley, S. A. Lund, R. Langer, *Science*, **1985**, *228*, 190-192 b) F. J. Schoen, J. W. Tsao, R. J. Levy, *Am. J. Pathol.* **1986**, *123*, 134-144. c) F. J. H. Schoen, H. K. H. Kim, H. C. Anderson, R. J. Levy, *Biomed. Mater. Res. Appl. Biomater.* **1988**, *22*, 11-36.
4) a) M. Epple, P. Lanzer, *Z. Kardiol.* **2001**, *90 Suppl. 3*, 2-5. b) P. Peters, M. Epple, *Z. Kardiol.* **2001**, *90 Suppl. 3*, 81-85. c) T. Kokubo, H.-M. Kim, M. Kawashita, T. Nakamura, *Z. Kardiol.* **2001**, *90 Suppl. 3*, 86-91. d) R. Z. LeGeros, *Z. Kardiol.* **2001**, *90 Suppl. 3*, 116-124. e) I. B. Rosanova, B. P. Mischenko, V. V. Zaitsev, S. L. Vasin, V. I. Sevastianov, *J. Biomed. Mater. Res.* **1991**, *25*, 277-280.
5) M. J. Glimcher in: *Handbook of Physiology-Endocrinology*; E. B. Astwook (Ed.), Williams & Wilkins, Baltimore, **1976**.
6) a) G. K. Hunter in: B. K. Hall (Ed.): *Bone Metabolism and Mineralization*, CRC Press: Boca Raton, Fl, **1992**, pp 225-247. b) H. I. Roach, *Cell Biol. Int.* **1994**, *18*, 617-628.
7) H. C. Anderson: *Bone and Mineral Research, Excerpta Medica*, Amsterdam, **1985**, Vol. 109.
8) a) L. W. Fisher, S. W. Whitson, L. V. Avioli, J. D. Termine, *J. Biol. Chem.* **1983**, *248*, 12723-12727. b) H. S. Shapiro, J. Chen, J. L. Wrana, Q. Zhang, M. Blum, J. Sodek, *Matrix* **1993**, *13*, 431-441.
9) J. D. Termine, H. K. Kleinman, S. W. Whitson, K. M. Conn, M. L. McGarvey, G. R. Martin, *Cell* **1981**, *26*, 99-105.
10) A. Franzen, D. Heinegard, *Biochem. J.* **1985**, *232*, 715-724.

11) J. P. Gorski, K. Simizu, *J. Biol. Chem.* **1988**, *263*, 15938-15945.

12) A. L. Boskey, *J. Cellular Biochem. Suppl.* **1998**, *30/31*, 83-91.

13) E. Dalas, J. K. Kallitsis, P. G. Koutsoukos, *Langmuir*, **1991**, *7*, 1822-1826. b) B. C. Bunker, P. C. Rieke, B. J. Tarasevich, A. A. Camell, G. E. Fryxell, G. L. Graff, L. Song, J. Liu, J. W. Vifden, G. L. McVay, *Science*, **1994**, *264*, 48-55.

14) a) L. Addadi, S. Weiner, *Angew. Chem.* **1992**, *104*, 159-176; *Angew.Chem. Int. Ed. Engl.* **1992**, *31*, 153-170. (b) S. Mann, D.D. Archibald, J.M. Didymus, T. Doughlas, B.R. Heywood, F. Meldrum, N.J. Reeves, *Science* **1993**, *261*, 1286-1292.

15) L. Addadi, S. Weiner, *Proc. Natl. Acad. Sci. U.S.A.* **1985**, *82*, 4110-4114.

16) A. L. Oliveira, J. F. Mano, R. L. Reis, *Curr. Opinion Solid State Mater. Sci.* **2003**, *7*, 309-318.

17) a) T. Kokubo, S. Ito, Z. T. Huang, T. Hayashi, S. Sakka, *J. Biomed. Mater. Res.* **1990**, *24*, 331-343. b) M. Tanashi, T. Kokubo, T. Matsuda, *J. Biomed. Mater. Res.* **1996**, *31*, 243-249. c) O. N. Tretinnikov, K. Kato, Y. Ikada, *J. Biomed. Mater. Res.* **1994**, *28*, 1365-1373. d) M. M. Pereria, A. E. Clark, L. L. Hench, *J. Biomed. Mater. Res.* **1994**, *28*, 693-698. e) R. L. Reis, A. M. Cunha, M. H. Fernandes, R. N. Correia, *J. Mater. Sci.: Mater. Med.* **1997**, *8*, 897-905. f) T. Kokubo, *Acta Mater.* **1998**, *46*, 2519-2527. g) H. M. Kim, Y. Kim, S. J. Park, C. Rey, H. M. Lee, M. J. Glimcher, J. S. Ko, *Biomaterials* **2000**, *21*, 1129-1134. h) M. G. Nooney, A. Campbell, T. S. Murrell, X.-F. Lin, L. R. Hossner, C. C. Chusuei, D. W. Goodman, *Langmuir*, **1998**, *14*, 2750-2755.

18) a) J. Chen, C. Burger, S. C. Krishnan, B. Chu, B. S. Hsiao. M. J. Glimcher, *Macromol. Chem. Phys.* **2005**, *206*, 43-51. b) E. L. Mertz, S. Leikin, *Biochemistry*, **2004**, *43*, 14901-14912. c) L. J. Zhang, X. S. Feng, H. G. Liu, D.J. Qian, L. Zhang, X. L. Yu, F. Z. Cui, *Mater. Let.* **2004**, *58*, 719-722. d) J.-H. Bradt, M. Mertig, A. Teresiak, W. Pompe, *Chem. Mater.* **1999**, *11*, 2694-2701.

19) a) W. Wu, G. H. Nancollas, *Langmuir* **1997**, *13*, 861-865. b) P. G. Koutsoukos, G. H. Nancollas, *Colloids Surf.* **1987**, *28*, 95-108. c) E. Dalas, J. K. Kallitsis, P. G. Koutsoukos, *Langmuir*, **1991**, *7*, 1822-1826. d) N. Spanos, P. G. Koutsoukos, *J. Mater. Sci.* **2001**, *36*, 573-578. e) S. Koutsopoulos, P. C. Paschlakis, E. Dalas, *Langmuir* **1994**, *10*, 2423-2428.

20) W. Wu, G. H. Nancollas, *J. Colloid Interface Sci.* **1998**, *199*, 206-211.

21) D. Rautaray, S. Mandal, M. Sastry, *Langmuir* **2005**, *21*, 5185-5191.

22) a) M. M. Pereria, A. E. Clark, L. L. Hench, *J. Biomed. Mater. Res.* **1994**, *28*, 693-698. b) A. Sáenz, M. L. Montero, G. Mondragón, V. Rodríguez-Lugo, V. M. Castagno, *Mat. Res. Innovat.* **2003**, *7*, 68-73.

23) a) M. M. Pereria, A. E. Clark, L. L. Hench, *J. Biomed. Mater. Res.* **1994**, *28*, 693-698. b) A. Sáenz, M. L. Montero, G. Mondragón, V. Rodríguez-Lugo, V. M. Castagno, *Mat. Res. Innovat.* **2003**, *7*, 68-73.

24) a) E. Dalas, *J. Mater. Chem.* **1991**, *1*, 473-474. b) O. N. Tretinnikov, K. Kato, Y. Ikada, *J. Biomed. Mater. Res.* **1994**, *28*, 1365-1373. c) E. Dalas, *J. Mater. Sci. Lett.* **1992**, *11*, 1408-1410. d) T. Miyazaki, C. Ohtsuki, Y. Akioka, M. Tanihara, J. Nakao, Y. Sakaguchi, S. Konagaya, *J. Mater. Sci.: Mater. Medicine*, **2003**, *12*, 569-574. e) I. B. Leonor, R. L. Reis, *J. Mater. Sci.: Mater. Medicine* **2003**, *14*, 435-441.

25) E. Dalas, J. K. Kallitsis, P. G. Koutsoukos, *Langmuir* **1991**, *7*, 1822-1826.

26) a) B. Derfus, S. Kranendonk, N. Camacho, N. Mande, V. Kushnaryov, K. Lynch, L. Ryan, *Calcif. Tissue Int.* **1998**, *63*, 258-262 b) W. L. Murphy, P. B. Messersmith, *Polyhedron*, **2000**, *19*, 357-363. c) P. B. Messersmith, S. Starke, *Chem. Mater.* **1998**, *10*, 117-124. d) P. B. Messersmith, S. Vallabhaneni, V. Nguyen, *Chem. Mater.* **1998**, *10*, 109-116. e) M. Michel, M. Winterhalter, L. Darbois, J. Hemmerle, J. C. Voegel, P. Schaaf, V. Ball, *Langmuir*, **2004**, *20*, 6127-6133. f) H. T. Schmidt, A. E. Ostafin, *Adv. Mater.* **2004**, *14*, 532-535.

27) M. Sauer, T. Haefele, A. Graff, C. Nardin, W. Meier, *Chem. Commun.* **2001**, 2452-2453.

28) A. Taubert, E. Furrer, W. Meier, *Chem. Commun.* **2004**, 2170-2171.

29) P. A. Ngankam, P. Lavalle, J. C. Voegel, L. Szyk, G. Decher, P. Schaaft, F. J. G. Cuisinier, *J. Am. Chem. Soc.* **2000**, *122*, 8998-9005.

30) a) K. Schwarz, M. Epple, *Chem. Eur. J.* **1998**, *4*, 1898-1903. b) R. Kniep, S. Busch, *Angew. Chem.* **1996**, *108*, 2788-2791. c) S. Busch, U. Schwarz, R. Kniep, *Chem. Mater.* **2001**, *13*, 3260-3271. d) S. Busch, U. Schwarz, R. Kniep, *Adv. Funct. Mater.* **2003**, *13*, 189-198.

31) J. J. J. M. Donnersl, R. J. M. Nolte, N. A. J. M. Sommerdijk, *Adv. Mater.* **2003**, *15*, 313-316.

32) a) Y. Li, W. Wenig, K. Cheng, P. Du, G. Shen, J. Wang, G. Han, *J. Mater. Sci. Lett.* **2003**, *22*, 1015-1016. b) A. Peytcheva, H. Cölfen, H. Schnablegger, M. Antonietti, *Colloid Polym. Sci.* **2002**, *280*, 218-227. c) A. Zieba, G. Sethuraman, F. Perez, G. H.

Nancollas, D. Cameron, *Langmuir*, **1996**, *12*, 2853-2858. d) K. Flade, C. Lau, M. Mertig, W. Pompe, *Chem. Mater.* **2001**, *13*, 3596-3602. e) M. Iijima, Y. Moriwaki, T. Takagi, J. Moradian-Oldak, *J. Cryst. Growth*, **2001**, *222*, 615-626. e) H. Furedi-Milhofer, P. B. Y. Ofir, M. Sikiric, N. Garti, *Bioceramics*, **2004**, *VOL 16 Key Engin. Mater. 254-2*, 11-14. f) S. Eiden-Assmann, M. Viertelhaus, A. Heiss, K. A. Hoetzer, J. Felsche, *J. Inorg. Biochem.* **2002**, *91*, 481-486.

33) a) R. I. Martin, P. W. Brown, *Calcif. Tissue Int.* **1997**, *60*, 538-546. b) H. E. Lundager Madsen, F. Abbona, E. Barrese, *Cryst. Res. Technol.* **2004**, *39*, 235-239.

34) L. J. Zhang, H. G. Liu, R. J. Zhang , L. Zhang, D. J. Qian, Y. D. Mu, X. L. Yu, X. S. Feng, *Colloids Surf. A – Physiochem. Engin. Aspects* **2005**, *257-58*, 307-312. b) Y. J. Zhang, P. He, X. D. Xu, J. H. Li, *Thin Solid Films*, **2004**, *468*, 273-279. c) F. A. Muller, L. Jonasova, P. Cromme, C. Zollfrank, P. Greil, *Bioceramics*, **2004**, *16 Key Engin. Mater. 254-2*, 1111-1114. d) N. Costa, P. M. Maquis, *Medical Engin. & Phys.* **1998**, *20*, 602-606.

35) a) J. Küther, W. Tremel, *Chem. Commun.* **1997**, 2029-2030. b) J. Küther, G. Nelles, R. Seshadri, M. Schaub, H.-J. Butt, W. Tremel, *Chem. Eur. J.* **1998**, *4*, 1834-1842. c) J. Küther, R. Seshadri, W. Knoll, W. Tremel, *J. Mater. Chem.* **1998**, **8**, 641-650.

36) a) M. Balz, E. Barriau, H. Frey, W. Tremel, *Langmuir*, **2005**, *21*, 3987-3991. b) M. Balz, H. A. Therese, M. Kappl, L. Nasdala, W. Hofmeister, H. J. Butt, W. Tremel, *Langmuir*, **2005**, *21*, 3981-3986. c) M. Balz, H. A. Therese, J. X. Li, J. S. Gutmann, M. Kappl, L. Nasdala, W. Hofmeister, H. J. Butt, W. Tremel, *Adv. Funct. Mater.* **2005**, *15*, 683-688.

37) a) B. J. Tarasevich, C. C. Chusuei, D. L. Allara, *J. Phys. Chem. B* **2003**, *107*, 10367-10377. b) P. Zhu, Y. Masuda, T. Yonezawa, K. Koumoto, *J. Am. Ceram. Soc.* **2003**, *86*, 782-790. c) K. Onuma, A. Oyane, T. Kokubo, G. Treboux, N. Kanzaki, A. Ito, *J. Phys. Chem. B* **2000**, *104*, 11950-11956. d) M. Tanahashi, T. Matsuda, *J. Biomed. Mater. Res.* **1997**, *34*, 305-315. e) S.-P. Huang, K.-C. Zhou, Y. Liu, B.-Y. Huang, *Trans. Nonferrous Metals Soc. China*, **2003**, *13*, 595-599.

38) a) E. K. Girija, Y. Yokogawa, F. Nagata, *J. Mater. Sci.: Mater. Med.*, **2004**, *15*, 593-599. b) K. Onuma, *J. Phys. Chem. B* **2005**, *109*, 8257-8262.

39) B. D. Boyan, Z. Schwartz, L. D. Swain, L. F. Bonewald, A. Khare, *Connect. Tissue Res.* **1989**, *22*, 3-6.

40) a) A. S. Posner, F. Betts, Acc. Chem. Res. 1975, 8, 273. b) K. Onuma, A. Ito, Chem. Mater. 1998, 10, 3346-3351.

41) L. Nasdala, *Neues Jahrbuch* Miner. Abh. **1992**, *164*, 211-227.

42) a) M. Rodahl, F. Höök, A. Krozer, P. Brzezinski, B. Kasemoa, *Rev. Sci. Instrum.* **1995**, *66*, 3924-3939. b) M. Rodahl, F. Höök, B. Kasemo, *Anal. Chem.* **1996,** *68*, 2219-2227.

43) K. Mann, I. M. Weiss, S. Andre, H.-J Gabius, M. Fritz, *Eur. J. Biochem.* **2000**, *276*, 5257-5264.

44) K. Guruprasad, B.V.B. Reddy, M.W. Pandit *Protein Eng.* **1990**, *4*, 155-161.

45) I. M. Weiss, S. Kaufmann, K. Mann, M. Fritz, *Biochem. Biophys. Res. Commun.* **2000**, *267*, 17-21.

46) L. Nasdala, A. Banerjee, T. Häger, W. Hofmeister, *Microscopy and Analysis, Eur. Ed.* **2001**, *70*, 7-9.

47) a) E. Kretschmann, *Z. Physik*, **1971**, *241*, 313-324. b) W. Knoll, *MRS Bulletin*, **1991**, *16*, 29-39.

48) H. B. Bull, K. Breese, *Arch. Biochem. Biophys.* **1974**, *161*, 665-670.

49) http://www.expasy.ch/tools/protscale.html

3.2 Templated Crystallization of Hydroxyapatite on Self-Assembled Monolayer Substrates in Presence of Nacrein as Soluble Component

3.2.1 Introduction

Crystallization of inorganic solids in living organisms is an outstanding complex process and combines the mineral strength together with organic toughness in so called biocomposites. There are found several minerals like silica, calcium carbonate and calcium phosphate amongst others. The control on the crystallization process is assigned mainly to soluble proteins or carbohydrates together with a substrate like the cell wall which control the nucleation and growth [1, 2]. A variety of certain polymorphic structures, sizes and morphologies maintain specific function. One of the most important biomineral, in addition to calcium carbonate, is calcium phosphate. It is found in mammalian hard tissue like bone or tooth as hydroxy- or fluoro apatite sometimes accompanied with carbonate replacing hydrogen phosphate or heavy metal ions in place of calcium ions in their crystal structure. In medical applications, uncontrolled nucleation and growth of calcium phosphate onto implant surfaces [3] or arteriosclerotic vessel walls [4] cause major problems leading to an implant failure.

Calcium phosphate is supposed to nucleates directly onto collagen fibrils [5], onto noncollagenous proteins affiliated with the collagen surface [6], or inside of matrix phophoprotein vesicles which are transported to the collagenous matrix within the porous bone structure and cartilage [7]. Noncollageneous glycoproteins which were isolated from mineralized tissue include bone sialoprotein [8], osteonectin [9], osteopontin [10], bone acidic glycoprotein-75 [11] and others [12].

Several studies on the crystallization mechanisms of calcium phosphate have been accomplished over the last two decades [13]. To date the mechanism is not yet completely understood but it was proved that biomacromolecules like proteins and carbohydrates play a central role in this process. The formation and growth of biominerals takes place at an organic-inorganic interface [1, 14, 15]. The comprehension of the calcium phosphate crystallization mechanism plays a major role by the improvement of compatibility of medicinal implants. Hence, it is not surprising that there have been numerous previous studies of calcium phosphate growth concerning the modelling in in-vitro-systems. Some of these works can be summarized as growth of calcium phosphate thin films [16] from high

supersaturated solutions like physiological solutions onto planar substrates like oxides, metals, glass [17], collagen [18] and the studies concerning the constant composition methods [19] which study the nucleation and growth kinetic onto suspended particles and macromolecules. Nucleation has been related to titania surface [20], amino acid-capped gold nanoparticles [21], porous calcium phosphate ceramic [22], negatively charged surfaces such as silica [23], polymers [24], and charged macromolecules [25]. Other substrates for crystallization are liposomes [26], giant ABA triblock copolymer vesicles [27], a water-in-water mesophase [28] and polyelectrolyte multilayer films [29]. A model system which could reveal the fluoro apatite formation in teeth is the double diffusion technique [30]. Other works relating to solution based precipitation of calcium phosphate were done in presence of dendrimers [31] or other organic additives [32] and foreign cations [33]. Also the crystallization behaviour on Langmuir monolayer had been studied [34].

Our working group has main interest in investigation of the crystallization behaviour of calcium carbonate on self-assembled monolayers [35] and the cooperative effect by soluble additives [36]. The crystallization behaviour of calcium phosphate on SAMs is less common [37], while the cooperative effect of soluble additives has not been used till day with the exception of at least two works, where calcium phosphate was crystallized on different substrates in the presence of additives [38].

In the preliminary work, we have investigated the cooperative effect of Perlucin [39] and a hydrophobic self-assembled monolayer on the crystallization behaviour of calcium phosphate [40]. Thus we were encouraged to use another protein which is involved in the biomineralization process of calcium carbonate like Perlucin as well. In this work we have extended our findings about the effect of Nacrein [41], (a soluble mainly acidic organic matrix protein from the nacreous layer of oyster pearls,) on the crystal morphology of calcium phosphate grown on self-assembled monolayers.

3.2.2 Results and discussion

Crystallization experiments were done in the same manner as described elsewhere [40]. The nucleation and growth was initialized by a pH switch caused by a diffusion of ammonia into the reaction solution. Various authors [37 b,c] have discussed a heterogenic nucleation of the calcium phosphate on the self-assembled monolayers (SAM) but Tarasevich and co-workers [37 a] have revealed that in a physiological solution at a constant pH 7.4 colloidal particles

are formed at first and afterwards adsorbed onto the (SAM). Also so called Posner clusters $Ca_9(PO_4)_6$ were in discussion by Tarasevich but they seem to be very small to fit the particle size observed by authors. Thus it can be assumed, that also by gas diffusion used in this study which causes a solvent based precipitation of calcium phosphate, colloidal particles play a crucial role in the nucleation.

Crystallization experiments were accomplished at room termperature and at increased temperature (34 °C). The crystallization time used was 1 day, 3 days, 7 to 28 days in the presence and absence of Nacrein. The morphology of crystals in the presence of nacrein was almost independent of surface, as exclusively crystals were like rose blossoms as showing Figure 3.2.1a,b,c,e. Only two exceptions were observed where the crystals were grown on OH and NH_2 SAMs at 34 °C. These crystals show a structure like a single of very thin petals of roses as shown in Figure 3.2.1d whereas on the CH_3 SAM these two general forms of crystals are present (Figure 3.2.1e). Differences can be found in the fine structures of the crystals. Calcium phosphate precipitated at room temperature onto the COOH terminated SAM, shows frayed petals while the end of the petals grown at 34 °C is plain and has a layer like structure (Figure 3.2.1a,c). The calcium phosphate found on the other surfaces and grown at room temperature has the same morphology but the petals are not smooth anymore and seem to peel off or to restructure. Parts of the petal surface are still flat which means that the rose like structure was formed before the restructuring process began. These morphologies are in contrast to the needle like hydroxyapatitic crystals which are formed in the absence of Nacrein (Figure 3.2.2).

Further studies of the different morphologies by raman micro-spectroscopy reveal a distinct crystal structure. Typical and representative spectra are depicted in figure 3.2.3. Crystals grown on the OH, NH_2 and CH_3 terminated SAMs at room temperature consist of hydroxyapatite showing the typical intensive peak at ~965 cm^{-1} in the raman spectra. In contrast the spectra of the other crystals show two peaks at the same position. Compared with literature data [42] the crystal composition can be identified as octacalcium phosphate. All peaks in the spectra are broader than the peaks in the reference spectra. This can be explained by a low crystallinity of the crystals due to a disorder in the crystal structure by fast growth. A chemical disorder by incorporating foreign ions into the apatite structure can be excluded due to the defined composition of the reaction mixture.

The formation of two different modification of calcium phosphate grown on different SAM at room temperature with a very similar morphology was a surprise. This can be ascribed to the

presence of the same initial morphology on all SAM, a rose blossom structure with the octacalcium phosphate modification. Afterwards the octacalcium phosphate is transformed to hydroxyapatite whereas the octacalcium phosphate grown on the COOH terminated SAM is protected at the petal surface by the Nacrein, which seems to form a thin layer or adsorbate on the crystals which stabilizes the thermodynamically more instable modification.

Moreover, it seems that exist a cooperative effect between the Nacrein and at least the COOH terminated SAM because only on this surface the octacalcium phosphate phase can resist the transformation to hydroxyapatite. As we suppose the solution based formation of colloidal calcium phosphate before adsorption onto the surface, it is possible that the presence of Nacrein has a significant influence on the colloid stabilization but cannot be evidenced with our experiments in this study. QCM-D studies of the adsorption of Nacrein onto the COOH SAM revealed that a small amount of the protein is adsorbed at a pH 5.3 and washed away easily by each washing step. Nevertheless it was found that a slight reversible adsorption occurs which can have an influence on the colloid adsorption or on the crystal growth process (Figure 3.2.4). A good and permanent adsorption of Nacrein to the COOH terminated SAM (5753 ng/cm^2; calculated with the Sauerbrey relation [43]) can be observed only at a higher pH. This can be explained by the very acidic properties of Nacrein [41] and due to the capacity of calcium ions to bind onto the surface of the protein by complexation.

At the crystallization temperature of 34 °C only octacalcium phosphate crystals are formed even though in different morphologies which means that a cooperative effect between the SAMs and Nacrein must exist. If there were no cooperation effect, one would expect the same sort of crystals on all surfaces.

Taking into account these observations the octacalcium phosphate crystals seem to be protected and stabilized by Nacrein. If the Nacrein looses the protective characteristics as observed on the CH_3, OH and NH_2 SAMs at room temperature observed the transformation to hydroxyapatite takes place. AFM was used to investigate the influence of nacrein on calcium phosphate. For this purpose we chose the final conditions reached by the crystallization experiment (pH 8) to reveal the reaction between natural hydroxyapatite and Nacrein. An alkaline solution is necessary to prevent the dissolution of the crystals due to the solubility in acidic solution. Octacalcium phosphate and hydroxyapatite are structurally related to each other and due to the lack of big octacalcium phosphate crystals for AFM studies a hydroxoapatite mineral was used. Figure 3.2.5 shows high resolution scanning electron micrographs of the mineral surfaces without any treatment, one and seven days after the

exposure to the crystallization solution in the presence of Nacrein, and one day after exposure to the crystallization solution in the absence of Nacrein. If Nacrein is not present in the solution a very quick and vigorous reaction takes place (Figure 3.2.5d). The crystal surface is covered/blotched with a lot of typical bunches of hydroxyapatite. On the other hand, in the presence of Nacrein after one day no apparent difference can be observed in comparison to the untreated mineral surface (Figure 3.2.5a,b) . If the solution acts on the crystal for seven days, the typical hydroxyapatite crystals can be observed as well as on crystals after one day of exposure to the crystallization solution without Nacrein, but there is still less material formed (Figure 3.2.5c). To gain a deeper insight into the process AFM studies were done. AFM micrographs are shown in figure 3.2.6 of the untreated apatite mineral surface and after one and seven days of exposure to the crystallization solution containing Nacrein. Figure 3.2.6a shows the natural mineral surface. The height images show small particles laying on the generally smooth surface which has scratches. The scratches are recognized very well in the phase image. After one day of reaction the scratches seem to disappear and the amount of small particles seems to increase (Figure 3.2.6b). By comparison of the images of the untreated surface this can also be explained by the formation spots like concavities which are growing out of the surface. Figure 3.2.6c shows the images from the mineral surface after seven days of treatment and now it is very well recognizable that the prior spots has grown to bigger particles. The phase image is showing a dark net like structure which is definitely another phase. We assume that a thin organic layer by Nacrein enfolding the mineral surface is formed. After one day exposed to solution, the thin layer is pressed slightly outwards by growing and rearranging calcium phosphate beneath the layer forming the spots at the surface. After one week of reaction the thin organic rips open showing the big calcium phosphate crystals and the organic layer convoluted to a net structure. In conclusion it can be stated that Nacrein has the ability to form a protecting covering on a hydroxyapatite surface. As the hydroxyapatite crystals do not have a determined fractured surface which can be assigned to a definite lattice plane, the exact specification of the interaction between the mineral surface and the protein is not possible to analyze by the experiments described in this work.

3.2.3 Conclusion

In conclusion it can be stated that Nacrein is capable of covering hydroxoapatite crystals and probably also crystals of octacalcium phosphate due to its structural relationship. If Nacrein is present as additive in the crystallization solution it is interacting with the surface of the at first primarily formed octacalcium phosphate stabilizing the crystals for a long period in contact at a temperature of 34 °C on each SAM used in experiment, however only on the COOH terminated surface at room temperature. This can be ascribed to a cooperative effect between substrate and soluble component. On the other surfaces it is not able to inhibit the transformation to the thermodynamically more stable hydroxyapatite which suggests that a less intensive cooperative effect is existent.

3.2.4 Experimental Section

Chemicals. The following chemicals were purchased: 4-Aminothiophenol (abbreviated NH_2) (96%, Acros), Hexadecanthiol (abbreviated: CH_3) (synthesis grade, Merck), NaOH (p.a., Acros), H_2O_2 (35%, Acros), water (Barnstead Easypure UV, $\rho > 18{,}3$ MΩ cm-1), ethanol (p.a., Riedel de Haen), ammonia (25 %, Riedel de Haen). Concentrated phosphoric acid (98 %, Merck) was diluted to 0,1 M and adjusted to a pH of 5.3 using 0,1 M NaOH solution. A stock solution (0.1 M) of calcium chloride was prepared by dissolving 18,3 g (0,1 mol) $CaCl_2 \cdot 4\ H_2O$ (Suprapur, Merck) in one litre of water. Natural green hydroxyapatite crystals from Madagascar were made available by Prof. Dr. W. Hofmeister, Institute of Geological Science, Mainz.

Synthesis of 1,11-mercaptoundecanoic acid (abreviated: COOH). 1,11-mercaptoundecanoic acid was prepared in a two step reaction. First 15 g (57 mmol) of 1,11-Bromundecanoic acid (Acros) was dissolved in 80 ml ethanol and transformed to the Bunte salt by mixing with 17,6 g of sodiumthiosulfate pentahydrate, dissolved in 50 ml water, by heating under reflux for four hours. The white product precipitated after cooling, was collected, washed with ethanol and dried. The obtained Bunte salt (14,2 g) was dispersed in a degassed mixture of 80 ml distilled water and 5 ml ethanol. Afterwards 16 ml of concentrated hydrochloric acid was added and the suspension was heated under reflux in nitrogen

atmosphere for six hours. Cooling the reaction mixture down to 4° C, the white product was filtered of, dissolved in 30 ml dichloromethane, and was washed with 3 M sodium chloride solution and distilled water. After drying over calcium chloride the organic layer was separated and product (white powder) was concentrated under vacuum.
Yield: 5,9 g (24,4 mmol, 46,3%)

Synthesis of 11-mercapto-1-undecanol (abreviated: OH). 11-mercapto-1-undecanol was prepared in the same way as mentioned above for the synthesis of 1,11-mercaptoundecanoic acid: 20.1 g (80 mmol) 11-brom-1-undekanol (Acros) was dissolved in 60 ml ethanol, mixed with a solution of 24.8 g sodium thiosulfate pentahydrate in 60 ml distilled water and heated under reflux for four hours. The Bunte salt was precipitated over night at room temperature and was filtered and recrystallized from ethanol and dried under vacuum. 20.5 g of the Bunte salt was hydrolysed in a mixture of ethanol/water (50:5 ml) by addition of 10 ml of concentrated hydrochloride acid and heating under reflux for 6 h. After cooling to 4° C, the crude 11-mercapto-1-undecanol precipitated and was filtered and subsequently extracted with petrolether. The organic layer was washed with water and the solvent was evaporated using rotary evaporation. The residue was redissolved in dichloromethane; the solution was washed with 3 M sodium chloride solution and dried over calcium chloride. After removing of the solvent the product was dried in vacuum and recrystallized twice from ethanol.
Yield: 9,7 g (48,5 mmol, 54 %)

Synthesis of Nacrein. Nacrein was expressed in Top10 E. coli strain (Invitrogen) with final concentration of L-arabinose 0.2 %. The culture incubated overnight at 37° C with vigorous shacking. The bacterial pallet was lysated by BugBuster (Novagen) in presence of proteinase inhibitors cocktail (Roche). Insoluble fraction was purified under denaturing condition on Ni-NTA columns (Qiagen) according instruction.The molecular weight of recombinant protein is ~ 35 KDa.

Preparation of gold substrates and SAMs. Glass slides (B 270/38 X 26 X 1 mm) were cleaned by heating at 80 °C in a mixture of water-ammonia-H_2O_2 (5:1:1, v/v/v) for 10 minutes, rinsed with water and ethanol and dried with a nitrogen gas. In a Balzer BAE 250 the glass slides were coated first with 2 nm Cr to improve adhesion followed by a cover of 50 nm Au (rate 0.1 nm s^{-1}) under vacuum below 10^{-6} mbar. The gold slides were transferred to

solutions of **COOH** in toluene, **OH** in ethanol, **CH_3** in toluene and **NH_2** in a mixture of toluene/ethanol (5:1; v,v) at concentrations of ~1 x 10^{-3} M. After 24 h of adsorption and equilibrating the slides were ready for use. After intensive rinsing with solvent to remove unbound thiols the slides were dried under streaming N_2. The obtained SAMs were used immediately for crystallization experiments.

Crystallization Experiments. Growth experiments were performed with the gas diffusion technique. The crystallization experiments were carried out in a Glass Coplin Staining Jar, containing 30 ml of a mixture of the calcium chloride and phosphate buffer (both 0.01 M; pH 5.3). 25 µl of Nacrein solution (0.2 mg/ml; in 8 M urea, and 250 mM Imidazol) was added. The final concentration of Nacrein was 1.7 x 10^{-4} mg/ml. The gold slides were placed vertically into the solution to be finally covered completely. The jar was kept into a desiccator for thermal equilibration. The reaction was initialized by placing a snap-cap-vial with 60 µl half concentrated ammonia into the desiccator. The slow diffusion of NH_3 gas into the solution caused a pH-switch value of 8-9 during different reaction times. Afterwards the substrates were removed, dried at room temperature and prepared for microscopy analysis.

Scanning electron microscopy studies. After crystallization the slides were cut into small pieces and fixed with conducting tabs on alumina sample holders for microscopic studies. A LEO 1550 high resolution scanning electron microscope at acceleration potentials of 1-3 kV were used for miscroscopic studies.

Atomic Force Microscopy (AFM). For AFM studies, calcium phosphate was crystallized as described above at pH 8. Precipitated calcium phosphate was removed by centrifugation. Afterwards Nacrein was added (25 µl solution of Nacrein/30 ml solution) and crystals of natural hydroxyapatite from Madagascar were dipped into the solution and left in this solution for one and seven days. Afterwards they were analyzed by AFM. A blank sample in the absence of Nacrein after a period of 24 hours and the untreated apatite crystal was also studied by AFM. Atomic force microscopy studies were carried out in the tapping mode on a Nanoscope III Multimode (Digital Instruments and alternatively on a Dimension 3000 (Digital Instruments) using Olympus Tapping mode Cantilever Typ OMCL-AC160TN-W2.

Raman micro-spectroscopy [44]. Raman micro-spectroscopy was performed with a LabRAM HR800 (Horiba Jobin Yvon). This confocal Raman system is based on a dispersive

spectrometer with notch-filter and focal length of 800 mm and equipped with Olympus BX41 optical microscope and Peltier-cooled hCCD (charge-coupled device) detector. The spectra were excited with the 514,5 nm emission of an Argon-ion-laser. The lateral resolution was better than 1.5 µm and the volume resolution was ca. 5 μm^3. The wavenumber accuracy was 0.5 cm^{-1} and the spectral resolution was about 1.0 cm^{-1}.

Quartz Crystal Microbalance – Dissipation (QCM-D). QCM-D measurements were carried out on a Q-sense D 300 system (Q-sense, Sweden). AT-cut quartz crystals coated with gold films are cleaned prior to use by a treatment with H_2O_2/NH_3/Millipore-water (1:1:5, v/v/v), 10 min. 80°C) and afterwards rinsed with Millipore-water and iso-propanol. After drying with a nitrogen, crystals were exposed to a diluted COOH-solution for at least 24 hours, subsequently rinsed with solvent and dried with N_2. After installing the quartz crystals, the measuring cell was set to 25 °C and equilibrated. Then the cell was filled with a) a mixture of calcium chloride and phosphate buffer (both final concentrations: 0.01 M; buffer: pH 5.3), or b) a calcium chloride solution (0.01 M) with NaOH (0,1 M) set to a pH 10). By exchanging the solvent consecutively with a corresponding solution containing Nacrein (100 µl Nacrein solution/2 ml solvent), the adsorption of the protein onto the COOH terminated gold surface was monitored by a decrease of the frequency. Furthermore the energy dissipation D was measured simultaneously. The measurements were performed in a static solution (batch mode).

3.2.5 Figure Part

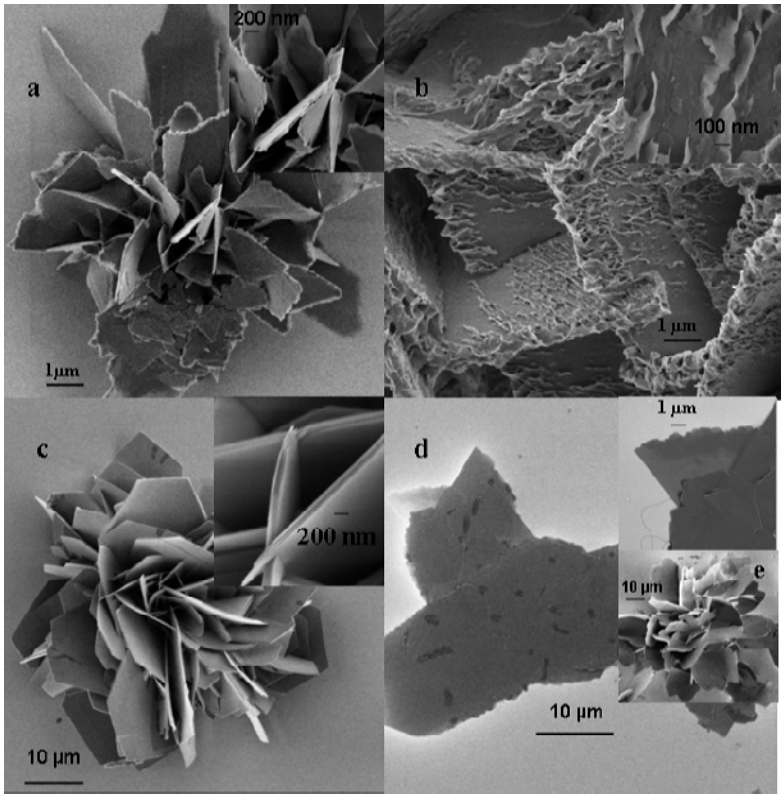

Figure 3.2.1: High resolution scanning electron migrographs of precipitated calcium phosphates onto self-assembled monolayers in the presence of Nacrein. a) COOH SAM, and b) OH, NH_2, CH_3 SAMs at room temperature, c) COOH SAM, d) OH and NH_2 SAMs, and e) CH_3 at 34 ℃ after a period of crystallization of 28 days.

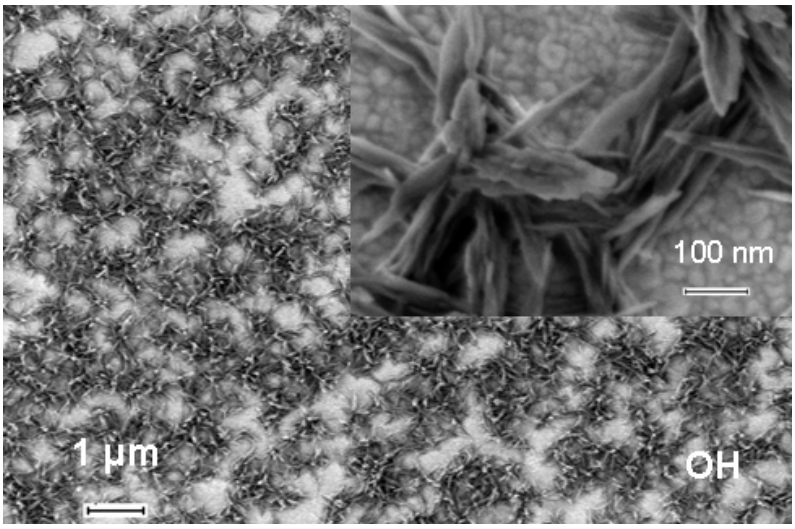

Figure 3.2.2: High resolution scanning electron migrographs of precipitated calcium phosphate onto OH SAM at room temperature, after a period of crystallization of 7 days.

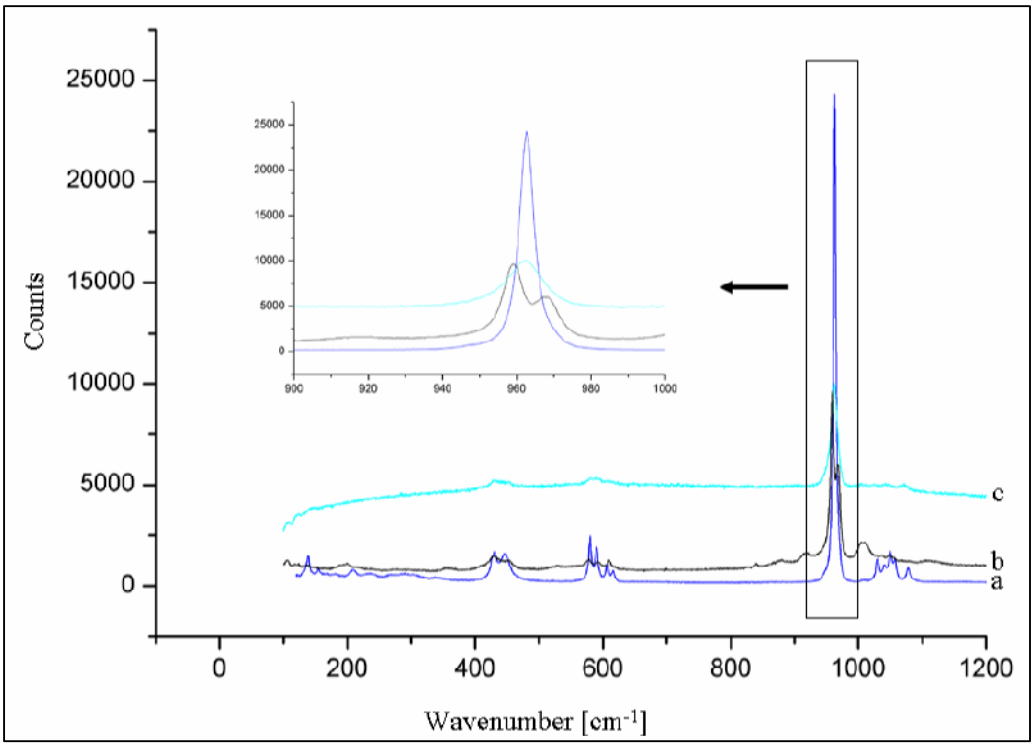

Figure 3.2.3: Raman spectra of calcium phosphate crystallized on self-assembled monolayer in the presence of Nacrein: a) Reference spectrum apatite, b) spectrum of octacalcium phosphate crystallized on COOH-terminated SAM in presence of Nacrein at 34 °C (Referenz spectra: [42], c) apatite formed in the presence of Nacrein on OH terminated SAM at room temperature

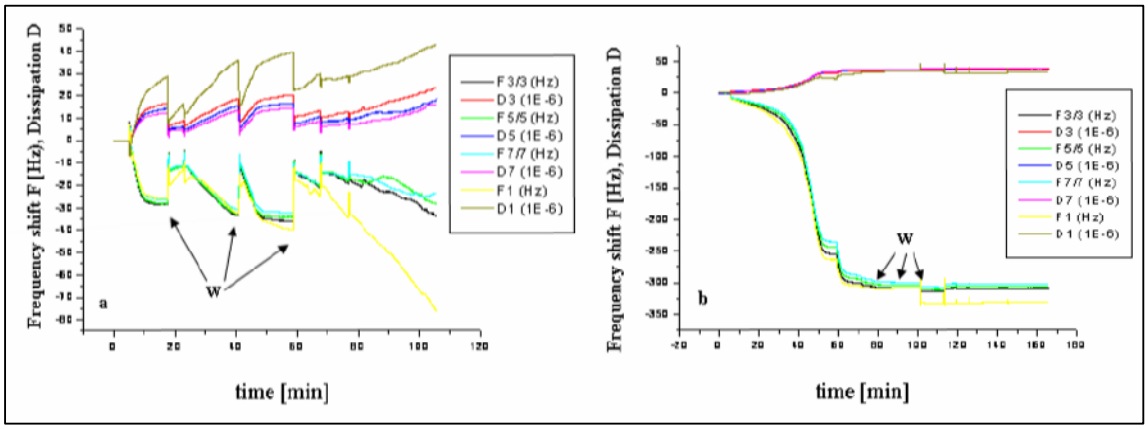

Figure 3.2.4: Nacrein adsorption to a COOH terminated self-assembled monolayer revealed by isothermal QCM-D measurements from a) a mixture of the calcium chloride and phosphate buffer (both 0.01 M; pH 5.3) and b) a calcium chloride solution (0.01 M) with NaOH (0,1 M) set to a pH 10 at 25 °C. (w = cell washed with solvent)

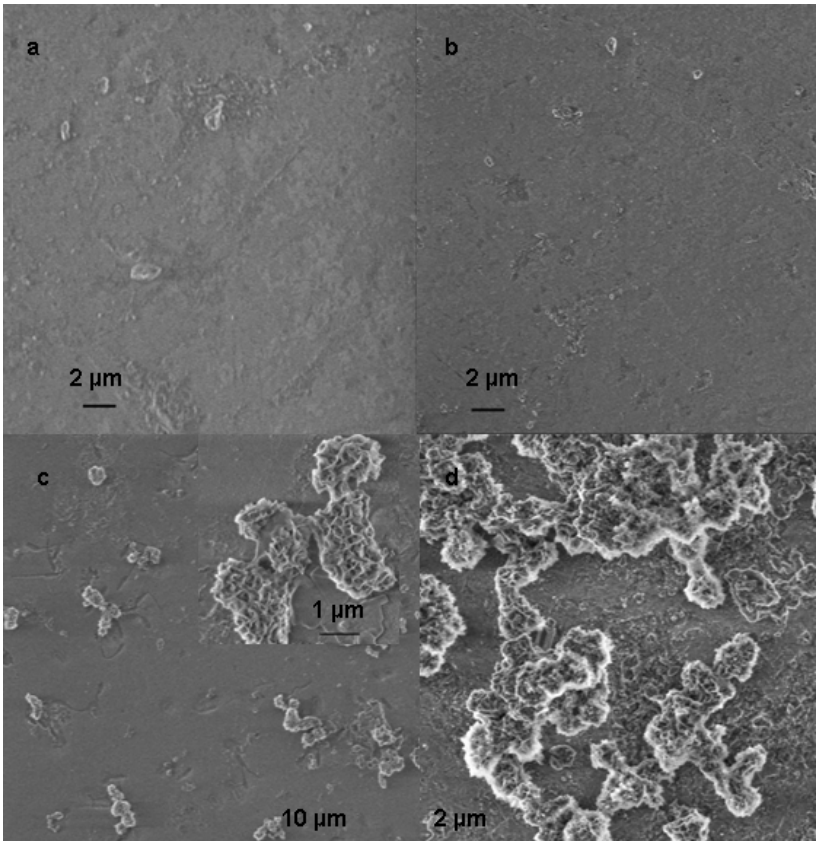

Figure 3.2.5: High resolution scanning electron migrographs of the natural apatite crystal a) without treatment, b) after one day, and c) seven days of treatment in presence of Nacrein, and d) after one day of treatment in the absence of Nacrein. (All: room temperature, pH 8)

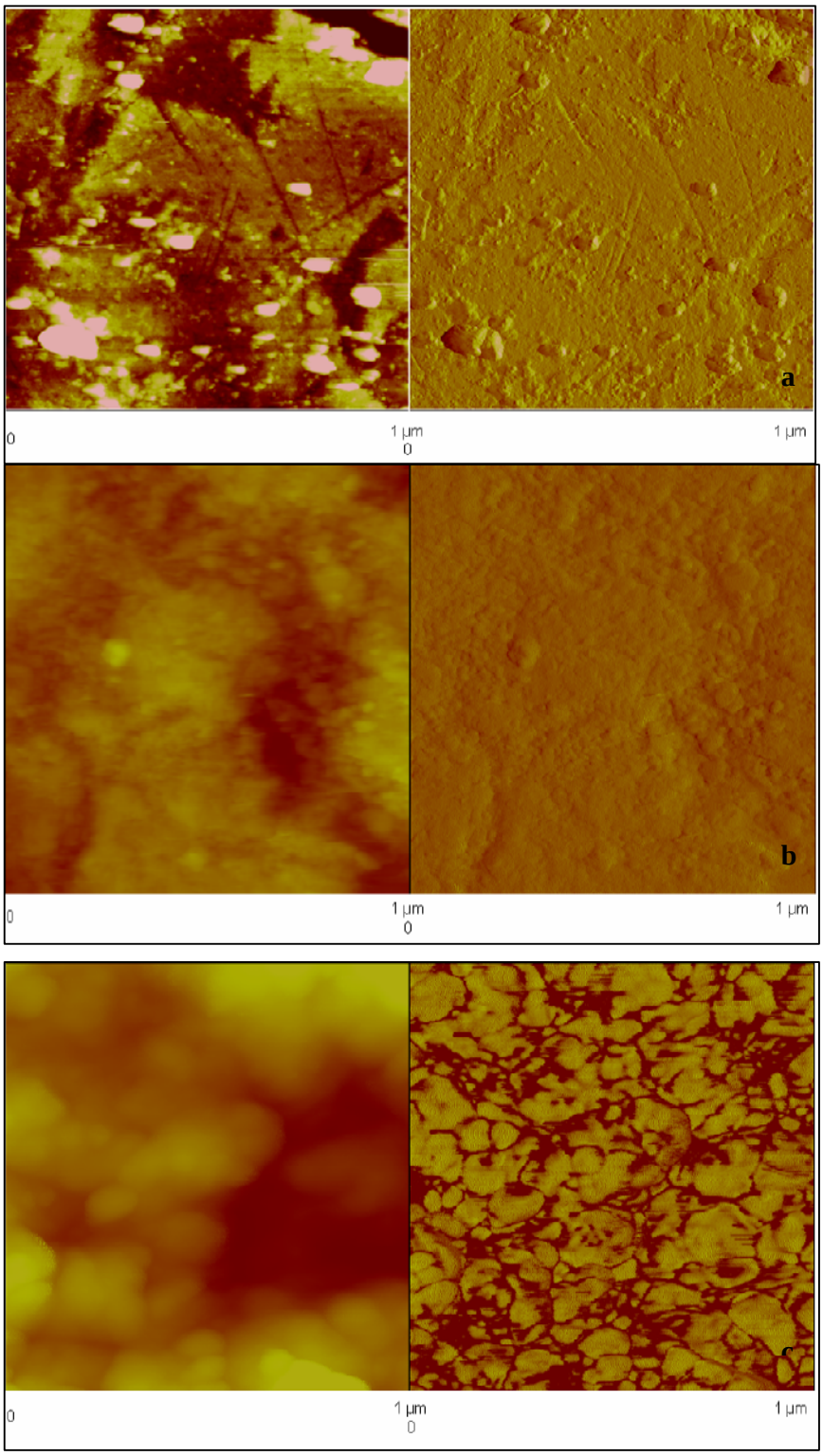

Figure 3.2.6: AFM height and phase images of the natural apatite crystal a) without any treatment, b) one day, and c) seven days of treatment in presence of Nacrein, and c) at room temperature and pH 8.

3.2.6 References

1) a) L. Addadi, S. Weiner, *Angew. Chem.* **1992**, *104*, 159-176; *Angew.Chem. Int. Ed. Engl.* **1992**, *31*, 153-170. (b) S. Mann, D.D. Archibald, J.M. Didymus, T. Doughlas, B.R. Heywood, F. Meldrum, N.J. Reeves, *Science* **1993**, *261*, 1286-1292.
2) H. A. Lowenstam, S. Weiner: *On Biomineralization,* Oxford University Press: New York, **1989**.
3) a) R. J. Levy, J. Wolfrum, F. J. Schoen, M. A. Hawley, S. A. Lund, R. Langer, *Science,* **1985**, *228*, 190-192 b) F. J. Schoen, J. W. Tsao, R. J. Levy, *Am. J. Pathol.* **1986,** *123*, 134-144. c) F. J. H. Schoen, H. K. H. Kim, H. C. Anderson, R. J. Levy, *Biomed. Mater. Res. Appl. Biomater.* **1988**, *22*, 11-36.
4) a) M. Epple, P. Lanzer, *Z. Kardiol.* **2001**, *90 S3*, 2-5. b) P. Peters, M. Epple, *Z. Kardiol.* **2001**, *90 S3*, 81-85. c) T. Kokubo, H.-M. Kim, M. Kawashita, T. Nakamura, *Z. Kardiol.* **2001**, *90 S3*, 86-91. d) R. Z. LeGeros, *Z. Kardiol.* **2001**, *90 S3*, 116-124. e) I. B. Rosanova, B. P. Mischenko, V. V. Zaitsev, S. L. Vasin, V. I. Sevastianov, *J. Biomed. Mater. Res.* **1991**, *25*, 277-280.
5) M. J. Glimcher in: *Handbook of Physiology-Endocrinology;* E. B. Astwook (Ed.), Williams & Wilkins, Baltimore, **1976**.
6) a) G. K. Hunter in: B. K. Hall (Ed.): *Bone Metabolism and Mineralization,* CRC Press: Boca Raton, Fl, **1992**, pp 225-247. b) H. I. Roach, *Cell Biol. Int.* **1994**, *18*, 617-628.
7) H. C. Anderson: *Bone and Mineral Research, Excerpta Medica,* Amssterdam, **1985**, Vol. 109.
8) a) L. W. Fisher, S. W. Whitson, L. V. Avioli, J. D. Termine, *J. Biol. Chem.* **1983**, *248*, 12723-12727. b) H. S. Shapiro, J. Chen, J. L. Wrana, Q. Zhang, M. Blum, J. Sodek, *Matrix* **1993**, ***13***, 431-441.
9) J. D. Termine, H. K. Kleinman, S. W. Whitson, K. M. Conn, M. L. McGarvey, G. R. Martin, *Cell* **1981**, *26*, 99-105.
10) A. Franzen, D. Heinegard, *Biochem. J.* **1985**, *232*, 715-724.
11) J. P. Gorski, K. Simizu, *J. Biol. Chem.* **1988**, *263*, 15938-15945.
12) A. L. Boskey, *J. Cellular Biochem. Suppl.* **1998**, *30/31*, 83-91.

13) E. Dalas, J. K. Kallitsis, P. G. Koutsoukos, *Langmuir*, **1991**, *7*, 1822-1826. b) B. C. Bunker, P. C. Rieke, B. J. Tarasevich, A. A. Camell, G. E. Fryxell, G. L. Graff, L. Song, J. Liu, J. W. Vifden, G. L. McVay, *Science*, **1994**, *264*, 48-55.

14) (a) E. Baeuerlein, (Edt.): *Biomineralization - Progress in Biology, Molecular Biology and Application*, 2nd ed,. Wiley-VCH, Weinheim **2004.** b) S. Mann: *Biomineralization - Principles and Concepts in Bioinorganic Materials Chemistry*, Oxford University Press, New York, **2002**. c) Lowenstam, S. Weiner (Eds.), *On Biomineralisation* Oxford University Press, New York, **1989**. d) S. Mann, J. Webb, R.J.P. Williams, *Biomineralization: Chemical and Biochemical Perspectives*, VCH Publishers, New York, **1989**.

15) L. Addadi, S. Weiner, *Proc. Natl. Acad. Sci. U.S.A.* **1985**, *82*, 4110-4114.

16) A. L. Oliveira, J. F. Mano, R. L. Reis, *Curr. Opinion Solid State Mater. Sci.* **2003**, *7*, 309-318.

17) a) T. Kokubo, S. Ito, Z. T. Huang, T. Hayashi, S. Sakka, *J. Biomed. Mater. Res.* **1990**, *24*, 331-343. b) M. Tanashi, T. Kokubo, T. Matsuda, *J. Biomed. Mater. Res.* **1996**, *31*, 243-249. c) O. N. Tretinnikov, K. Kato, Y. Ikada, *J. Biomed. Mater. Res.* **1994**, *28*, 1365-1373. d) M. M. Pereria, A. E. Clark, L. L. Hench, J. *Biomed. Mater. Res.* **1994**, *28*, 693-698. e) R. L. Reis, A. M. Cunha, M. H. Fernandes, R. N. Correia, *J. Mater. Sci.: Mater. Med.* **1997**, *8*, 897-905. f) T. Kokubo, *Acta Mater.* **1998**, *46*, 2519-2527. g) H. M. Kim, Y. Kim, S. J. Park, C. Rey, H. M. Lee, M. J. Glimcher, J. S. Ko, *Biomaterials* **2000**, *21*, 1129-1134. h) M. G. Nooney, A. Campbell, T. S. Murrell, X.-F. Lin, L. R. Hossner, C. C. Chusuei, D. W. Goodman, *Langmuir*, **1998**, *14*, 2750-2755.

18) a) J. Chen, C. Burger, S. C. Krishnan, B. Chu, B. S. Hsiao. M. J. Glimcher, *Macromol. Chem. Phys.* **2005**, *206*, 43-51. b) E. L. Mertz, S. Leikin, *Biochemistry*, **2004**, *43*, 14901-14912. c) L. J. Zhang, X. S. Feng, H. G. Liu, D.J. Qian, L. Zhang, X. L. Yu, F. Z. Cui, *Mater. Let.* **2004**, *58*, 719-722. d) J.-H. Bradt, M. Mertig, A. Teresiak, W. Pompe, *Chem. Mater.* **1999**, *11*, 2694-2701.

19) a) W. Wu, G. H. Nancollas, *Langmuir* **1997**, *13*, 861-865. b) P. G. Koutsoukos, G. H. Nancollas, *Colloids Surf.* **1987**, *28*, 95-108. c) E. Dalas, J. K. Kallitsis, P. G. Koutsoukos, *Langmuir*, **1991**, *7*, 1822-1826. d) N. Spanos, P. G. Koutsoukos, *J. Mater. Sci.* **2001**, *36*, 573-578. e) S. Koutsopoulos, P. C. Paschlakis, E. Dalas, *Langmuir* **1994**, *10*, 2423-2428.

20) W. Wu, G. H. Nancollas, *J. Colloid Interface Sci.* **1998**, *199*, 206-211.

21) D. Rautaray, S. Mandal, M. Sastry, *Langmuir* **2005**, *21*, 5185-5191.

22) C. Deng, J.Chen, H. Fan, X. Zhang, *J. Mater. Sci.* **2005**, *40*, 1809-1812.

23) a) M. M. Pereria, A. E. Clark, L. L. Hench, *J. Biomed. Mater. Res.* **1994**, *28*, 693-698. b) A. Sáenz, M. L. Montero, G. Mondragón, V. Rodríguez-Lugo, V. M. Castagno, *Mat. Res. Innovat.* **2003**, *7*, 68-73.

24) a) E. Dalas, *J. Mater. Chem.* **1991**, *1*, 473-474. b) O. N. Tretinnikov, K. Kato, Y. Ikada, *J. Biomed. Mater. Res.* **1994**, *28*, 1365-1373. c) E. Dalas, *J. Mater. Sci. Lett.* **1992**, *11*, 1408-1410. d) T. Miyazaki, C. Ohtsuki, Y. Akioka, M. Tanihara, J. Nakao, Y. Sakaguchi, S. Konagaya, *J. Mater. Sci.: Mater. Medicine*, **2003**, *12*, 569-574. e) I. B. Leonor, R. L. Reis, *J. Mater. Sci.: Mater. Medicine* **2003**, *14*, 435-441.

25) E. Dalas, J. K. Kallitsis, P. G. Koutsoukos, *Langmuir 1991*, *7*, 1822-1826.

26) a) B. Derfus, S. Kranendonk, N. Camacho, N. Mande, V. Kushnaryov, K. Lynch, L. Ryan, *Calcif. Tissue Int.* **1998**, *63*, 258-262 b) W. L. Murphy, P. B. Messersmith, *Polyhedron*, **2000**, *19*, 357-363. c) P. B. Messersmith, S. Starke, *Chem. Mater.* **1998**, *10*, 117-124. d) P. B. Messersmith, S. Vallabhaneni, V. Nguyen, *Chem. Mater.* **1998**, *10*, 109-116. e) M. Michel, M. Winterhalter, L. Darbois, J. Hemmerle, J. C. Voegel, P. Schaaf, V. Ball, *Langmuir*, **2004**, *20*, 6127-6133. f) H. T. Schmidt, A. E. Ostafin, *Adv. Mater.* **2004**, *14*, 532-535.

27) M. Sauer, T. Haefele, A. Graff, C. Nardin, W. Meier, *Chem. Commun.* **2001**, 2452-2453.

28) A. Taubert, E. Furrer, W. Meier, *Chem. Commun.* **2004**, 2170-2171.

29) P. A. Ngankam, P. Lavalle, J. C. Voegel, L. Szyk, G. Decher, P. Schaaft, F. J. G. Cuisinier, *J. Am. Chem. Soc.* **2000**, *122*, 8998-9005.

30) a) K. Schwarz, M. Epple, *Chem. Eur. J.* **1998,** *4*, 1898-1903. b) R. Kniep, S. Busch, *Angew. Chem.* **1996**, *108*, 2788-2791. c) S. Busch, U. Schwarz, R. Kniep, *Chem. Mater.* **2001**, *13*, 3260-3271. d) S. Busch, U. Schwarz, R. Kniep, *Adv. Funct. Mater.* **2003**, *13*, 189-198.

31) J. J. J. M. Donnersl, R. J. M. Nolte, N. A. J. M. Sommerdijk, *Adv. Mater.* **2003**, *15*, 313-316.

32) a) Y. Li, W. Wenig, K. Cheng, P. Du, G. Shen, J. Wang, G. Han, *J. Mater. Sci. Lett.* **2003**, *22*, 1015-1016. b) A. Peytcheva, H. Cölfen, H. Schnablegger, M. Antonietti, *Colloid Polym. Sci.* **2002**, *280*, 218-227. c) A. Zieba, G. Sethuraman, F. Perez, G. H.

Nancollas, D. Cameron, *Langmuir,* **1996**, *12*, 2853-2858. d) K. Flade, C. Lau, M. Mertig, W. Pompe, *Chem. Mater.* **2001**, *13*, 3596-3602. e) M. Iijima, Y. Moriwaki, T. Takagi, J. Moradian-Oldak, *J. Cryst. Growth*, **2001**, *222*, 615-626. e) H. Furedi-Milhofer, P. B. Y. Ofir, M. Sikiric, N. Garti, *Bioceramics,* **2004**, Vol. 16: Key *Engin. Mater.* 254-2, 11-14. f) S. Eiden-Assmann, M. Viertelhaus, A. Heiss, K. A. Hoetzer, J. Felsche, *J. Inorg. Biochem.* **2002**, *91*, 481-486.

33) a) R. I. Martin, P. W. Brown, *Calcif. Tissue Int.* **1997**, *60*, 538-546. b) H. E. Lundager Madsen, F. Abbona, E. Barrese, *Cryst. Res. Technol.* **2004**, *39*, 235-239.

34) L. J. Zhang, H. G. Liu, R. J. Zhang , L. Zhang, D. J. Qian, Y. D. Mu, X. L. Yu, X. S. Feng, *Colloids Surf. A – Physiochem. Engin. Aspects* **2005**, *257-58*, 307-312. b) Y. J. Zhang, P. He, X. D. Xu, J. H. Li, *Thin Solid Films,* **2004**, *468*, 273-279. c) F. A. Muller, L. Jonasova, P. Cromme, C. Zollfrank, P. Greil, *Bioceramics*, **2004**, Vol. 16: *Key Engin. Mater. 254-2*, 1111-1114. d) N. Costa, P. M. Maquis, *Medical Engin. & Phys.* **1998**, *20*, 602-606.

35) a) J. Küther, W. Tremel, *Chem. Commun.* **1997**, 2029-2030. b) J. Küther, G. Nelles, R. Seshadri, M. Schaub, H.-J. Butt, W. Tremel, *Chem. Eur. J.* **1998**, *4*, 1834-1842. c) J. Küther, R. Seshadri, W. Knoll, W. Tremel, *J. Mater. Chem.* **1998**, *8*, 641-650.

36) a) M. Balz, E. Barriau, H. Frey, W. Tremel, *Langmuir*, **2005**, *21*, 3987-3991. b) M. Balz, H. A. Therese, M. Kappl, L. Nasdala, W. Hofmeister, H. J. Butt, W. Tremel, *Langmuir,* **2005**, *21*, 3981-3986. c) M. Balz, H. A. Therese, J. X. Li, J. S. Gutmann, M. Kappl, L. Nasdala, W. Hofmeister, H. J. Butt, W. Tremel, *Adv. Funct. Mater.* **2005**, *15*, 683-688.

37) a) B. J. Tarasevich, C. C. Chusuei, D. L. Allara, *J. Phys. Chem. B* **2003**, *107*, 10367-10377. b) P. Zhu, Y. Masuda, T. Yonezawa, K. Koumoto, *J. Am. Ceram. Soc.* **2003**, *86*, 782-790. c) K. Onuma, A. Oyane, T. Kokubo, G. Treboux, N. Kanzaki, A. Ito, *J. Phys. Chem. B* **2000**, *104*, 11950-11956. d) M. Tanahashi, T. Matsuda, *J. Biomed. Mater. Res.* **1997**, *34*, 305-315. e) S.-P. Huang, K.-C. Zhou, Y. Liu, B.-Y. Huang, *Trans. Nonferrous Metals Soc. China*, **2003**, *13*, 595-599.

38) a) E. K. Girija, Y. Yokogawa, F. Nagata, *J. Mater. Sci.: Mater. Med.*, **2004**, *15*, 593-599. b) K. Onuma, *J. Phys. Chem. B* **2005**, *109*, 8257-8262.

39) a) I. M. Weiss, S. Kaufmann, K. Mann, M. Fritz, *Biochem. Biophys. Res. Commun.* **2000**, *267*, 17-21. b) K. Mann, I. M. Weiss, S. Andre. H.-J. Gabius, M. Fritz, *Eur. J.*

Biochem. **2000**, **267**, 5257-5264. c) S. Blank, M. Arnoldi, S. Khoshnavaz, L. Treccani, M. Kuntz, K. Mann, G. Grathwohl, M. Fritz, *J. Microsc.* **2003**, *212*, 280-291.

40) A. Reiber, L. Treccani, M. Fritz, L. Nasdala, W. Tremel, G. Glasser, in preparation

41) a) H. Miyamoto, T. Miyashita, M. Okushima, S. Nakano, T. Moritas, A. Matsushiro, *Proc. Natl. Acad. Sci. USA,* **1996**, *93*, 9657-9660. b) M. Kono, N. Hayashi, T. Samata, *Biochem. Biophys. Res. Commun.* **2000**, *269*, 213-218.

42) M. Markovic, B. O. Fowler, W. E. Brown, *Chem. Mater.* **1993**, *5*, 1406-1416.

43) a) M. Rodahl, F. Höök, A. Krozer, P. Brzezinski, B. Kasemoa, *Rev. Sci. Instrum.* **1995**, *66*, 3924-3939. b) M. Rodahl, F. Höök, B. Kasemo, *Anal. Chem.* **1996,** *68*, 2219-2227.

44) L. Nasdala, A. Banerjee, T. Häger, W. Hofmeister, *Microscopy and Analysis, Eur. Ed.* **2001**, *70*, 7-9.

4. Conclusion

In the present study a new method is introduced to realize the synthesis of nanowires in a chemical laboratory under convenient and simple conditions instead of using tedious procedures in a clean room. This method is based on the employment of different templates and colloids.

It could be demonstrated that granular gold nanochains consisting of individual gold colloid particles linked by a flexible α,ω-dithiol spacer can be synthesized from colloidal gold by making use of V_2O_5 nanotubes as templates. The diameter of the resulting nanochains reflects the inner diameter of the template nanotubes, while the chain lengths may vary from 200 nm to 1100 nm. These chains may be considered models of 1D-granular metals. The unique structural features could make them interesting objects for structuring and assembling in the nanoscale range.

Moreover it was shown, that collagen fibres can be used as template for the synthesis of nanometer-sized gold wires with high aspect ratio. The spontaneous immobilization of gold colloids onto the collagen fibres allowed to control the reduction of gold tetrachloride acid from solution to form a defined mantle of gold on the collagen fibre surface. Even though reduction conditions have to be carefully monitored in order to avoid aggregation of the discrete wires, it was possible to develop a new valid method for the synthesis of gold nanowires.

To gain a deeper insight into the process of biomineralization it is indispensable to account for cooperative interactions between a self-assembled monolayer, ions and a soluble component like Perlucin and Nacrein were accomplished.

It was possible to demonstrate that there is existent a cooperative effect between a hydrophobic self-assembled monolayer and Perlucin, a soluble protein, which acts as a promoter for the process of biomineralization. By kinetic measurements such as surface plasmon resonance spectroscopy and quartz crystal microbalance measurements it could be revealed that the Perlucin molecule is a very flexible molecule when it is adsorbed onto a CH_3 terminated SAM surface. It was shows the capability of the protein to accelerate the nucleation by unfolding the active side of the protein. This kind of behaviour was also found on a phospholipid monolayer. However this activation is not observed on other modified and more hydrophilic self-assembled monolayers. Thus it can be speculated if the protein must be

activated in vivo by the cell double membrane which mainly consists of lipid molecules but future work is necessary to understand the crystallization size of the Perlucin molecule.

On the other hand the second protein used in this study, Nacrein, shows only a less explicit cooperative effect with self-assembled monolayers. It can be stated that Nacrein is capable of covering hydroxoapatite crystals and probably also crystals of octacalcium phosphate due to its structural relationship. If Nacrein is present as additive in the crystallization solution it seems to interact with the surface of the primarily formed octacalcium phosphate stabilizing the crystals for a long period at a temperature of 34 °C on polar as well as nonpolar SAMs. However at room temperature the stabilization of the crystals could be accomplished only on the COOH terminated surface. This can be ascribed to a cooperative effect between substrate and soluble component. By using less polar or nonpolar self-assembled monolayers at room temperature Nacrein is not able to inhibit the transformation of octacalcium phosphate to the thermodynamically more stable hydroxyapatite which suggests that a less intensive cooperative effect is existent.

5. Methods and instrumentation

5.1 Surface Plasmon Resonance Spectroscopy (SPR)

The Surface Plasmon Resonance spectroscopy [1] is a versatile tool to measure the thickness of thin films adsorbed onto a metal surface. The method is based on electrons which have the ability to move nearly free as electron gas and thus they are completely disconnected from the atomic nuclei. This property is related to metals with a complete d-shell, having valence electrons in s- or p-orbitals like gold or silver. Under these circumstances the electrons are able to pass on vibrations, i. e. the charge density like the gas particles in air. These fluctuations of the charge density are called plasmon. They show characteristic vibration energies:

$$E_p = \hbar \cdot \omega_P = \hbar \cdot \sqrt{\frac{4\pi\eta e^2}{\varepsilon\varepsilon_0 m_e}}$$

η = electron concentration

m_e = electron mass

ε, ε_0 = dielectric constants

As the vibrational energy acts as an electromagnetic wave the electrons can be excited by radiation.

The excitation of the plasmon is possible at a metal-dielectric interface by a monochromatic light beam, normally by a Helium-Neon laser and can be understood as a longitudinal propagation of the surface plasmon at the interface. Therefore, it is surface selective as well as a surface sensitive method. It is observed as a deep minimum

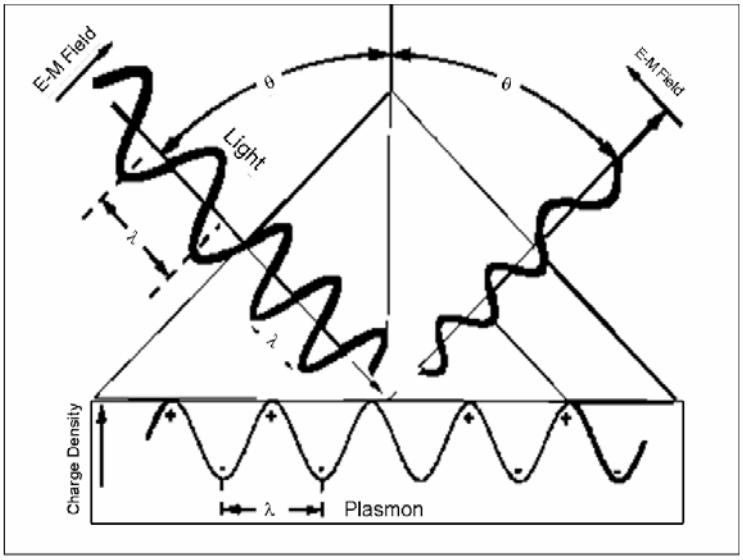

Figure 5.1.1: Kretschmann configuration of the plasmon resoncance

in the p-polarised reflected light as the angle-of-incidence is incremented. The amplitude of the vibration is exponentially attenuated into the interior of the metal with a penetration depth of about ~ 100 nm. To measure the film thickness at a gold surface the most convenient configuration for plasmon resonance is the Kretschmann configuration (Figure 5.1.1) [2].

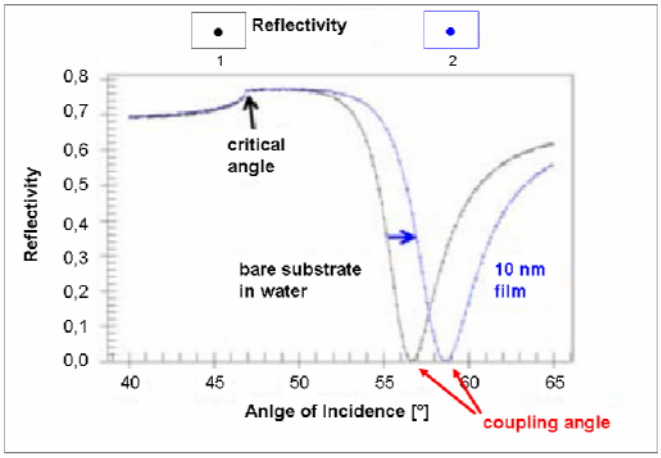

Figure 5.1.2: Plasmon spectrum from bare gold (black line) and with a substrate on the gold surface (blue line)

The plasmon is measured at the interface between a dielectric material and the gold, where the light comes from a medium with a higher refractive index to penetrate a material with a lower refractive index. The Snellius equation of refraction is valid (Figure 5.1.1):

$$\frac{\sin\alpha}{\sin\beta} = \frac{n_2}{n_1}$$

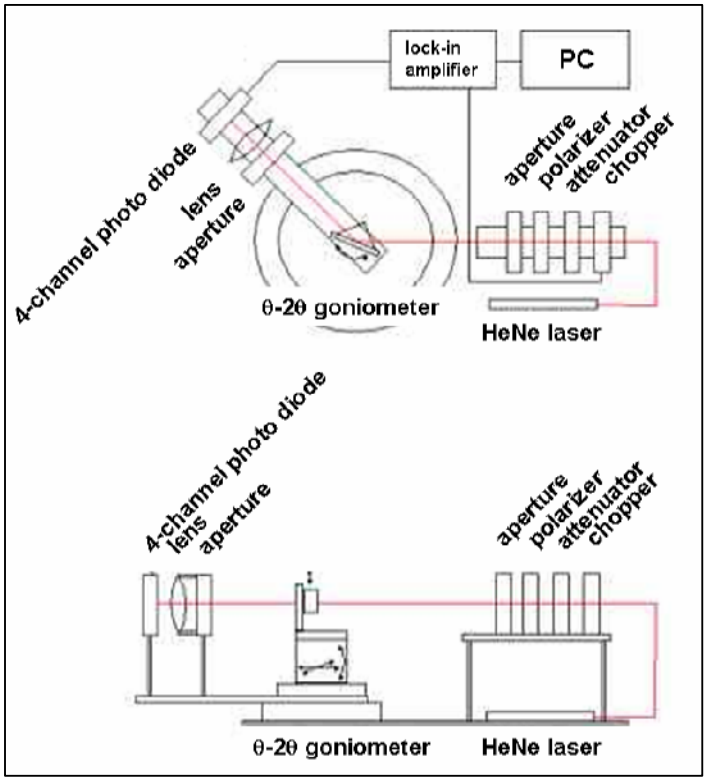

Figure 5.1.3: Kretschmann set-up of a surface plasmon spectrometer

The phenomen of total reflection is observed by the transition of light from an optically dense material to a less dense material. In this case β is > 90°. At a critical angle of $\alpha_T = \alpha$, β is 90° and thus $\sin\beta = 1$. The refraction equation results in:

$$\sin\alpha_T = \frac{n_2}{n_1}$$

At this critical angle total reflections of the light beam occurs. Thus the plasmon spectra show a maximum (Figure 5.1.2). If α increases more, a small part of the incident light beam energy

passes through the boundary layer between glass and gold. This so-called evanescent wave couples with the plasmon and at a certain angle a maximum of energy is absorbed resulting in a minimum in the spectrum. This coupling angle indicates the point of the highest light absorption by the plasmon, i. e. the collective oscillation of the electrons with the light. The value of the experiment is that the exact angle for the plasmon resonance peak is extremely sensitive to any thin film on the metal surface even for a monolayer consisting of organic molecules. So the minimum position of the peek can be used to determine the thickness and density. The theoretical characterization of these phenomena is completely understood and the thickness of the layer can be inferred from the angle shift between spectra taken from the clean gold surface and from the gold surface with an absorbed layer by simulation with programs like WINSPALL [3].

One of the important advantages of the SPR analysis is the good time resolution since the surface plasmon can be generated and measured in a short time. Thus real time analysis can be made as in kinetic measurements of the absorption of a solute like proteins.

For this PhD thesis all measurements were done using a spectrometer in the Kretschmann-configuration purchased from Resonant Probes GmbH (Goslar) [4]. A graphical description of the complete equipment is shown in figure 5.1.3.

5.2 Atomic Force Microscopy (AFM) [5]

All scanning techniques which use a sharp tip moving over the surface of a sample in a raster scan are summarized under the name scanning probe microscopy (SPM) [6]. In 1982 Binnig, Rohrer, and Gerber invented the scanning tunnelling microscope (STM), the first type of SPM. They won the Nobel Prize in 1986. This method based on electron tunnelling, i.e. an electrical current that flows between two conductors that are separated by very short distances at Angstrom scale. This tunnelling current depends exponentially on the distance between the two conductors. By monitoring the current over each point of the surface of the sample, the electronic topography of the surface is recorded. Thus there are two distinguishable modes of operation:

i) **Constant Height Mode**: When the distance between tip and samples is kept constant, the current is recorded over each point giving the electronic properties of the sample;

ii) **Constant Current Mode**: When the current is kept constant during the scan, the topography of the substrate surface is recorded.

This microscopic method is restricted to conductive substrates but permits atomic information not from an average over many atoms, but rather atom by atom.

The complementary technique to the STM is the atomic force microscopy (AFM). With this instrument also non-conducting materials can be investigated. It was invented by Binnig, Quate and Gerber in 1986. The AFM uses a cantilever with a sharp tip moving over the surface of the sample in a raster scan. The cantilever bends in response to the force

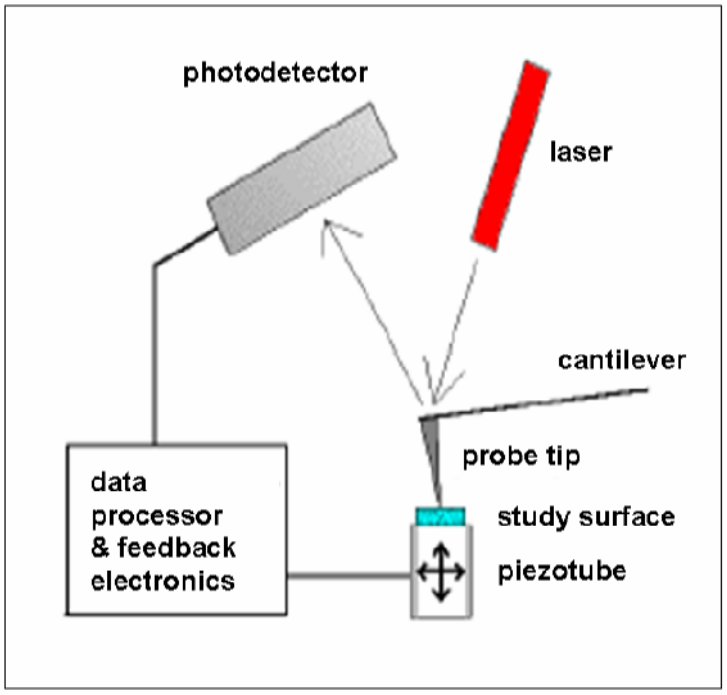

Figure 5.2.1: Schematic illustration of the measurement technique by an Atomic Force Microscope

between the tip and the sample surface. Most of the AFMs employ an optical lever technique for detecting the bending of the cantilever. The light from a laser is reflected from the cantilever onto a split photo-diode. By measuring the aberration of the signal, and changes in the bending of the cantilever, (as the cantilever obeys Hooke´s Law for small displacements,) the interaction force between the tip and the sample can be determined (Figure 5.2.1). The displacement of the tip or sample is performed by an extremely precise positioning device made from piezo-electric ceramics with a resolution of sub-angstrom.

There are principally three different classes of interaction between tip and sample: contact mode, tapping mode, and non-contact mode.

1) Contact mode signifies a close contact between tip and sample during scanning progress. Close contact means that the tip approaches the surface resulting in a positive inter-molecular repulsive force and large lateral forces on the sample. The tip is dragged over the surface.(Figure 5.2.2)
2) The tapping mode is used for poorly immobilised or soft samples. By operating in air or other gases, the cantilever oscillates at its resonant frequency and is positioned above the surface. It only taps the surface for a very small part of its oscillation period. Thus it has a short time contact with sample surface. This leads to a dramatical decrease of the lateral force during the scan process.
3) The third mode of measuring is the non-contact mode. The cantilever oscillates above the surface at such a distance that there is no lateral force which means that it is no longer in the repulsive regime of the inter-molecular force curve.

Apart from the study of topography with high resolution and interactions between the tip and the surface of nearly every material, AFM can also be applied for nanomechanic studies employing the AFM tip to produce indents in a specimen, or for friction measurements by scratching the tip over the surface.

The great advantage of all SPM techniques is the ability to do time-

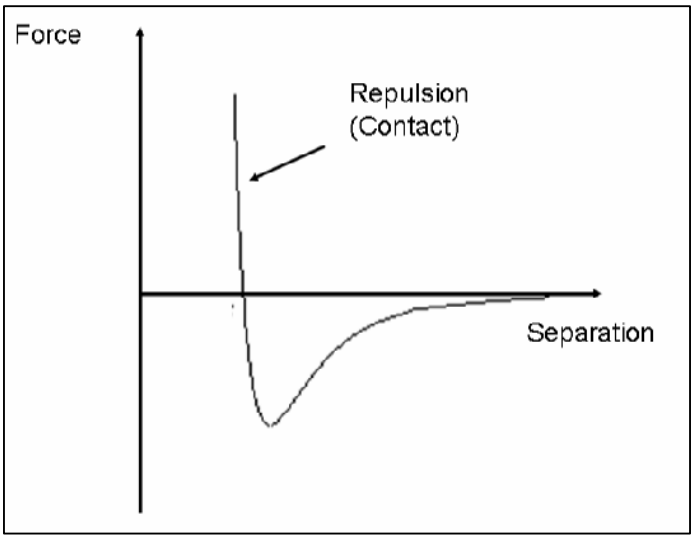

Figure 5.2.2: Inter-molecular force curve

resolved investigations down to atomic or near-atomic processes in all materials.

In this Ph.D. thesis all measurements were performed using a Nanoscope III Multimode from Digital Instruments or a Dimension 3000 von Digital Instruments in the tapping mode with an Olympus tapping mode cantilever (Type OMCL-AC160TN-W2).

5.3 Quartz Crystal Microbalance [7] (QCM)

A quartz crystal microbalance (QCM) is an instrument used for monitoring the adsorption of small amounts (5 ng/cm^2) of materials, like proteins, polymers or gases, onto surfaces in liquid or gaseous environment. The central component of the microbalance is a quartz crystal. It consists of an AT-cut quartz plate, typically coated from both sides with a gold layer which acts as electrodes (Figure 5.3.1). By applying an alternating electric field to the quartz crystal, a mechanical shear oscillation in the crystal in a direction perpendicular to the applied electric field with a frequency in an order of MHz is induced. This phenomenon is related to the piezoelectric properties of the quartz crystal. The oscillation frequency of the quartz crystal decreases when a molecule adsorbs onto one of the electrodes. The kinetic of an adsorption process can be monitored by tracking the frequency over time. If the film is thin and rigid the decrease in frequency is proportional to the mass adsorbed onto the surface of the crystal. The mass of the layer is calculated by using the Sauerbrey relation:

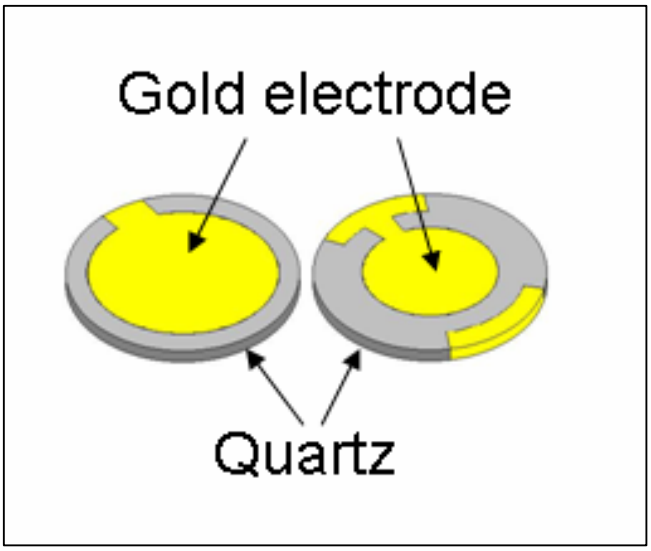

Figure 5.3.1: Illustration of a QCM sensor

$$\Delta m = -\frac{C \cdot \Delta f}{n}$$

C = 17.7 ng Hz^{-1} cm^{-2} for a 5 MHz quartz crystal

n = 1,3,5,7 is the overtone number

It is also possible to estimate the thickness (d) of the adhering layer:

$$d_{eff} = \frac{\Delta m}{\rho_{eff}}$$

ρ_{eff} is the effective density of the adsorbed layer

If the layer is not rigid then the Sauerbrey relation becomes invalid. A soft overlayer will not fully couple to the oscillation of the crystal which will mute the oscillation. Thus the dissipation of the oscillation is a rate for softness of the film, i. e. the viscoelasticity. The dissipation D is defined as:

$$D = \frac{E_{lost}}{2\pi E_{stored}}$$

E_{lost} is the energy dissipated during one oscillation cycle, and

E_{stored} is the total energy stored in the oscillator

When QCM is operated in pulse mode, i. e. the alternating field has been turned off, the dissipation of the crystal is determined by monitoring the damping of the amplitude of the crystal vibration over time and it can be detected how much energy of the adsorbed layer is consumed. If the signal comes from a rigid adlayer, the damping will be weak; i. e. the adlayer has a small dissipation factor. It means the adlayer has only few degrees of freedom into which energy can be lost. On the other hand a soft adlayer has many degrees of motional freedom and thus a large dissipation factor. The amplitude of the signal from a crystal with a soft adlayer will decay very quickly (Figure 5.3.2). At the same time it is possible to jump between the fundamental frequency and overtones (e. g. 15, 25, 35 MHz). If the multiple frequencies are known, a viscoelastic model can be used to characterize in detail the properties of the adsorbed film. The viscosity, elasticity and correct thickness may be derived even for soft films by applying certain assumptions.

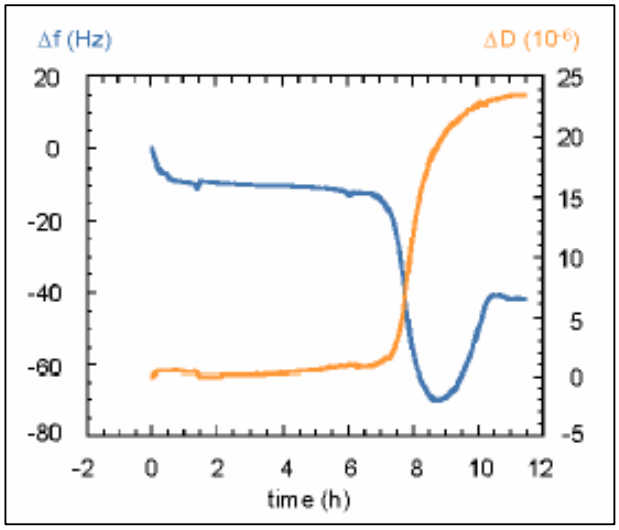

Figure 5.3.2: Example of a kinetic measurement: the frequency shift indicates mass attachment and the dissipation shift indicates the softness of the adsorbed material by a high dissipation

Measurements of the frequency shift and changes in the dissipation factor are called “QCM-D”-measurements and are realized by the equipment used in this Ph.D. thesis. The system was provided by Q-Sense AB, Göteborg, SE.

5.4 References

1. a) W. Knoll, *MRS Bulletin*, **1991**, **16**, 29-39. b) A. Janshoff, H.-J. Galla, C. Steinem, *Angew. Chem.* **2000**, *112*, 4164-4195. c) H. Raether, *"Surface Plasmons on Smooth and Rough Surfaces and on Gratings"*, Tracts in Modern Physics, Springer Verlag, Berlin, **1988**. d) E. Burstein, W. P. Chen, Y. J. Chen, A. Hartstein, *J. Vac. Sci. Technol.*, **1974**, *11*, 1004-1019. e) B. Rothenhäusler, C. Duschl, W. Knoll, *Thin Solid Films*, **1988**, *159***,** 323-330.
2. E. Kretschmann, *Z. Physik.* **1971**, *241*, 313-324.
3. http://www.mpip-mainz.mpg.de/documents/akkn/index.html.
4. http://www.resonant-probes.de
5. D. Sarid: *Scanning Force Microscopy*, Oxford Series in Optical and Imaging Sciences, Oxford University Press, New York, **1994**.
6. R. Wiesendanger (ed.): *Scanning probe microscopy: analytical Methods*, Springer, Berlin, **1998**.
7. a) M. Rodahl, F. Höök, A. Krozer, P. Brzezinski, B. Kasemoa, *Rev. Sci. Instrum.* **1995**, *66*, 3924-3939. b) M. Rodahl, F. Höök, B. Kasemo, *Anal. Chem.* **1996,** *68*, 2219-2227. c) M. Rodahl, F. Höök, C. Fredriksson, C. A. Keller, A. Krozer, P. Brzezinski, M. Voinova, B. Kasemo, *Faraday Discussions* **1997**, *107*, 229-246. d) F. Höök, M. Rodahl, P. Brzezinski, B. Kasemo, *Langmuir* **1998,** *14*, 729-734. e) F. Höök, M. Rodahl, P. Brzezinski, B. Kasemo, *J Coll. Interf. Sci.* **1998**, *208***,** 63–67. f) F.Höök, M. Rodahl, B. Kasemo, P. Brzezinski, *Proc. Natl. Acad. Sci.* **1998**, *95*, 12271-12276. g) F. Höök, J. Vörös, M. Rodahl, R. Kurrat, P. Böni, J. J. Ramsden, M. Textor, N. D Spencer, P. Tengvall, J. Gold, B. Kasemo, *Coll. Surf. B: Biointerfaces*, **2002**, *24*,155-170. h) M. V. Voinova, M. Rodahl, M. Jonson B. Kasemo, *Phys. Scripta* **1999,** *59*, 391-396. i) R. Schumacher, *Chemie in unserer Zeit* **1999**, *33*, 268-278. j) F. L. Dickert, O. Schuster, *Chem. unserer Zeit* **1994**, *28*, 147-152. k) C. K. O`Sullivan, G. G. Guilbault, *Biosensors Bioelectron.* **1999**, 663-670.